ROADVIEW

Robust Automated Driving in Extreme Weather

Project No. 101069576

Deliverable D3.6
Vehicle dynamics modelling methodology

WP3 – Validated sensor and sensor noise models for synthetic environments

Authors	Maikol Funk Drechsler (THI), Yuri Poledna (THI), Mattias Hjort (VTI) and Sogol Kharrazi (VTI)
Lead participant	THI
Delivery date	21 May 2024
Dissemination level	Public
Type	Report

Version 02

Deliverable No. D3.6
Version 02
Project no. 101069576

Title
Vehicle dynamics modelling methodology

ROADVIEW

Revision history

Author(s)	Description	Date
Maikol Funk Drechsler (THI), Yuri Poledna (THI), Mattias Hjort (VTI) and Sogol Kharrazi (VTI)	Draft deliverable	04/09/2023
Maikol Funk Drechsler (THI), Yuri Poledna (THI), Mattias Hjort (VTI) and Sogol Kharrazi (VTI)	First deliverable Version	02/02/2024
Ipek Alptekin (Ford) and Mert Sever (Ford)	Revision 1	14/02/2024
Tuomas Herraren (LUA)	Revision 2	27/02/2024
Maikol Funk Drechsler (THI), Yuri Poledna (THI), Mattias Hjort (VTI) and Sogol Kharrazi (VTI), Eren Aksoy (HH)	Final version	28/02/2024
Andreia Cruz (accelCH)	Formatting and formal check	29/02/2024
Mario Ceccarelli (accelCH)	Logo & acknowledgement update	21/05/2024

Deliverable No. D3.6
Version 02
Project no. 101069576

Title
Vehicle dynamics modelling methodology

ROADVIEW

Contents

Deliverable No. D3.6
Version 02
Project no. 101069576

Title
Vehicle dynamics modelling methodology

ROADVIEW

List of Figures

Deliverable No. D3.6
Version 02
Project no. 101069576

Title
Vehicle dynamics modelling methodology

ROADVIEW

Deliverable No. D3.6
Version 02
Project no. 101069576

Title
Vehicle dynamics modelling methodology

ROADVIEW

List of Tables

Deliverable No. D3.6
Version 02
Project no. 101069576

Title
Vehicle dynamics modelling methodology

ROADVIEW

Table of Symbols

Symbol	Description	Units
a	Longitudinal position of the wheel in relation to the CG	$[m]$
A_0	Drag area of the vehicle	$[m^2]$
a_x	Longitudinal acceleration of the vehicle	$[m/s^2]$
a_y	Lateral acceleration of the vehicle	$[m/s^2]$
B	Stifness factor of the tires MF	$-$
b	Lateral position of the wheel in relation to the CG	$[m]$
b_B	Brake Bias Vector	-
b_P	Vector of percentage of torque being forwarded to each wheel	$[\%]$
$b_{P_{xx}}$	Percentage of torque being forwarded on specific wheel	$[\%]$
C	Shape factor of the tires MF	$-$
C_0	Center of curve rotation	-
CC	Cornering coefficient	$[1/rad]$
C_{Ax}	Drag coefficient	$-$
CC_y	Load dependence for the cornering coefficient	$[1/rad]$
CC_{yg}	Cornering coefficient gradient	$-$
CC_{y0}	Nominal cornering coefficient	$[1/rad]$
C_D	Damping coefficient of the suspension	$[Ns/m]$
CS	Cornering stiffness of the front and rear tires	
C_z	Vertical tire stifness	$[N/m]$
$C_{F\kappa}$	Longitudinal slip stiffness	$[N]$
$C_{F\propto}$	Cornering stiffness	$[N/rad]$
D	Peak friction of the tires MF	$[N]$
dfz	Normalized change in vertical load	-
d_S	Suspension displacement for each wheel	$[m]$
d_S^t	Displacement of the suspension in each wheel for the current time	$[m]$

Deliverable No. D3.6
Version 02
Project no. 101069576

Title
Vehicle dynamics modelling methodology

ROADVIEW

Symbol	Description	Units
d_S^{t-1}	Displacement of the suspension in each wheel for the last time	$[m]$
$\dot{d}_S$	Vector of velocity of the displacement in each wheel	$[m/s]$
E	Curvature factor of the tires MF	$-$
$F_{Z_{static}}$	Static forces acting on each wheel	$[N]$
F_S	Forces acting on the suspension	$[N]$
$F_{Y,SS}$	Steady state lateral force	$[N]$
F_x	Longitudinal Forces acting on the tire-road interaction in the body coordinate systems	$[N]$
F_{W_x}	Longitudinal Forces acting on the tire-road interaction in the wheels coordinate systems	$[N]$
F_y	Lateral Forces acting on the tire-road interaction in the body coordinate systems	$[N]$
F_{W_y}	Lateral Forces acting on the tire-road interaction in the wheels coordinate systems	$[N]$
F_z	Vertical load acting on each wheel	$[N]$
F_{z0}	Standard load of the tire	$[N]$
$\Delta F_{Z_{lat}}$	Lateral load transfer acting on each wheel	$[N]$
$\Delta F_{Z_{lon}}$	Longitudinal load transfer acting on each wheel	$[N]$
h	Height of the CG	$[m]$
h_p	Height of the pitch centre	$[m]$
h_{pc}	Distance between the pitch centre and the centre of gravity	$[m]$
h_r	Roll centre height	$[m]$
h_{rc}	Distance between the roll centre and the centre of gravity	$[m]$
I_D	Inertia of the driveshaft	$[kg \cdot m^2]$
I_E	Engine inertia	$[kg \cdot m^2]$
I_G	Inertia of the gearbox	$[kg \cdot m^2]$
I_W	Inertia of the wheels and axles	$[kg \cdot m^2]$
I_θ	Pitch inertia	$[kg \cdot m^2]$
I_φ	Roll Inertia	$[kg \cdot m^2]$
I_ψ	Yaw inertia	$[kg \cdot m^2]$

Deliverable No. D3.6
Version 02
Project no. 101069576

Title
Vehicle dynamics modelling methodology

ROADVIEW

Symbol	Description	Units
i_D	Gear ratio from the differential	$-$
i_F	Final ratio	$-$
i_G	Gear ratio from the gearbox	$-$
i_S	Steering ratio	$-$
K_{ARB}	Stiffness of the anti-roll bar	$[Nm/rad]$
K_S	Stiffness of the spring	$[N/m]$
K_{in}	Converter factor	-
κ	Longitudinal slip angle of the tires	$-$
l	Wheel base	$[m]$
l_f	Front axel of the vehicle	$[m]$
l_r	Rear axel of the vehicle	$[m]$
m	Vehicle mass	$[kg]$
m'_{FL}	Mass measured on the front left wheels of the vehicle	$[kg]$
m'_{FR}	Mass measured on the front right wheels of the vehicle	$[kg]$
m_s	Sprung mass of the vehicle in each wheel	$[kg]$
$\mathrm{m}_{unsprung}$	Unsprung mass of the vehicle in each wheel	$[kg]$
$Pedal_B$	Normalised brake pedal input	$[\%]$
$Pedal_{Gas}$	Gas Pedal Position	$[\%]$
R	Loaded tire radius	$[m]$
R_0	Unloaded tire radius	$[m]$
R_R	Rolling resistance factor	-
r_d	Dynamic rolling radius	$[m]$
S	Steering wheel angle	$[rad]$
s	Velocity ratio of the torque converter	-
T_B	Vector containing the brake torque in each one of the wheels	$[Nm]$
$T_{B_{XX}}$	Brake Torque on a specific wheel	$[Nm]$

Deliverable No. D3.6
Version 02
Project no. 101069576

Title
Vehicle dynamics modelling methodology

ROADVIEW

Symbol	Description	Units
$T_{B_{max}}$	Sum of the Maximum Brake Torque for all wheels	$[Nm]$
T_E	Engine Torque	$[Nm]$
$T_{E_{max}}$	Maximum Engine Torque for a specific Engine Rotation	$[Nm]$
T_I	Impeller torque	$[Nm]$
T_T	Turbine torque	$[Nm]$
T_W	Total wheel torque on all wheels	$[Nm]$
$\overline{T_W}$	Average wheel torque	$[Nm]$
t	Current time step	$[s]$
t_0	Initial time	$[s]$
Δt	Time step	$[s]$
$V_{minslip}$	Minimal angular velocity of the wheels	$[m/s]$
V_x	The tire speed along the tire longitudinal direction	$[m/s]$
V_y	The tire speed along the tire lateral direction	$[m/s]$
w	Track width	$[m]$
W_d	Weight distribution in each wheel considering the CG position	$[\%]$
w_l	Left wheel of the vehicle	-
w_r	Right wheel of the vehicle	-
X	Map frame from x coordinate system of the vehicle	$[m]$
x	Longitudinal displacement of the vehicle	$[m]$
$\ddot{x}$	Longitudinal acceleration of the vehicle in the vehicle coordinate system	$[m/s^2]$
$\dot{x}$	Vehicle longitudinal velocity of the vehicle	$[m/s]$
$\dot{x}_0$	Initial speed of the vehicle	$[m/s]$
Y	Map frame from y coordinate system of the vehicle	$[m]$
$\dot{y}$	Lateral velocity of the vehicle	$[m/s]$
$\ddot{y}$	Lateral acceleration of the vehicle	$[m/s^2]$
$\ddot{z}$	Vertical acceleration of the vehicle	$[m/s^2]$

Deliverable No. D3.6
Version 02
Project no. 101069576

Title
Vehicle dynamics modelling methodology

ROADVIEW

Symbol	Description	Units
z_W	Respective high of the road	$[m]$
Δz_{CG}	Longitudinal movement of the CG	$[m]$
α	Lateral slip angle of the tires	$[rad]$
α'	Relaxed tire slip angle	$[rad]$
α_{peak}	Slip angle at peak friction	$[rad]$
$\boldsymbol{\alpha}$	Vector of the slip angle of all wheel	$[rad]$
γ	Vehicle inclination angle	$[rad]$
δ	Wheel steering angle	$[rad]$
δ_I	Internal wheel steering angle	$[rad]$
δ_O	External wheel steering angle	$[rad]$
η_P	Powertrain efficiency	-
θ	Pitch angle	$[rad]$
$\ddot{\theta}$	Variation of the pitch rate of the vehicle	$[rad/s^2]$
μ	Torque ratio	-
μ_{asym}	Asymptotic friction value at infinitely large slip angles	-
μ_y	Normalized tire friction	-
μ_{yg}	Peak lateral friction gradient	-
μ_{y0}	Nominal peak lateral friction	-
$\boldsymbol{\kappa}$	Vector of the longitudinal slip of all wheels	−
v_{XT}	Tire longitudinal velocity	$[m/s]$
$\xi_{Z_{lat}}$	Vector that defines if the load is being added or removed from each wheel	-
$\xi_{Z_{long}}$	Vector that describes addition or removal of the load from the specific axle	-
ρ	Radial tire deflection	$[m]$
ρ_A	Density of the air	$[kg/m^3]$
σ_y	Tire lateral relaxation length	$[m]$
φ	Roll angle	$[rad]$

Deliverable No. D3.6
Version 02
Project no. 101069576

Title
Vehicle dynamics modelling methodology

ROADVIEW

Symbol	Description	Units
$\ddot{\varphi}$	Roll rate variation	$[rad/s^2]$
$\dot{\psi}$	Yaw rate	$[rad/s]$
$\ddot{\psi}$	Variation of the yaw rate	$[rad/s^2]$
ω_E	Engine's angular velocity	$[rad/s]$
ω_T	Angular velocity of the torque converter turbine	$[rad/s]$
ω_w	Angular velocity of the wheel	$[rad/s]$
ω_w	Angular velocity of all wheels	$[rad/s]$
$\dot{\omega}_E$	Engine's angular acceleration	$[rad/s^2]$
$\dot{\omega}_W$	Acceleration of the wheels	$[rad/s^2]$
$\overline{\omega_W}$	Average of the wheel angular velocity	$[rad/s]$
$\overline{\dot{\omega}_W}$	Average of the wheels acceleration	$[rad/s^2]$
∇f	Gradient of the f function	_
$\mathcal{R}^n$	Set of the real numbers n dimensional	_
$H_{i,j}$	Hessian of the function f(n) at i,j	_

Partner short names

FORD	Ford Otomotiv Sanayi Anonim Sirketi
LUA	Lapin Ammattikorkeakoulu Oy
THI	Technische Hochschule Ingolstadt
VTI	Statens Vag- och Transportforskningsinstitut

Deliverable No. D3.6
Version 02
Project no. 101069576

Title
Vehicle dynamics modelling methodology

ROADVIEW

Abbreviations

ABS	Anti-lock Braking System
CG	Center of Gravity
C-IAD	CARISSMA Institute of Automated Driving
CM	IPG CarMaker
D	Deliverable
DoF	Degrees of Freedom
EC	European Commission
EU	European Union
HEU	Horizon Europe
M	Month
MF	Magic Formula
MS	Milestone
RMSE	Root Mean Square Error
WP	Work Package

Deliverable No. D3.6
Version 02
Project no. 101069576

Title
Vehicle dynamics modelling methodology

ROADVIEW

Executive summary

Objectives

The use of virtual testing and respective comprehensive models is important for the testing of automated driving systems. The parametrisation of these models is, however, usually expensive, and time-consuming. The estimation of parameters for vehicle dynamics has been conducted for a long time by the automotive industry, but the research lacks publicly available methods which can estimate the parameters of the vehicle. The main objective of this work is the development of a method for the estimation of vehicle dynamics parameters directly from dynamic manoeuvres conducted in test tracks. Furthermore, the implemented model shall address the effect of adverse weather conditions on vehicle behaviour. For this purpose, a comprehensive vehicle dynamics model is implemented, which is used as the basis for running the optimisation algorithms and real tests are conducted at the test track of the CARISSMA Institute of Automated Driving at THI.

Methodology and implementation

The initial work consists of the implementation of a vehicle dynamics model of 11 Degrees of Freedom (DoF), including the engine rotation, rotation of the wheels and Euler movement of the chassis, with separate models for the tires. The model is implemented in Python, to enable higher modularity of the system and easy integration with the optimization algorithms. The implemented model is then validated against the vehicle model available in the commercial software IPG CarMaker. Based on the literature a methodology for the data collection, including required measurements and manoeuvres as well as the method for the parameter estimation are proposed. The data is gathered in different steps, including static measurements, tire test rig measurements at VTI and dynamic data collection on the test track of the CARISSMA Institute of Automated Driving on dry and wet road conditions. Finally, the vehicle dynamics parameters are optimised aiming to match the results obtained by the vehicle model with the behaviour of the real vehicle. Novel tire models for use on snow and ice has been developed using extensive tire measurements conducted by VTI in an earlier project, but never before used for this purpose.

Outcomes

The outcomes of this task/report include the publication of an open-source vehicle dynamics models and the parameters from the test vehicle from CARISSMA Institute of Automated Driving, as well as the definition of a methodology for the estimation of the vehicle dynamics parameters on different weather conditions. The algorithms and the parameters will be made available to the research community, supporting the virtualization of automated driving testing. Furthermore, the dissemination of the ROADVIEW project and work developed in this task is planned to be conducted as a conference publication planned for the summer 2024.

Next steps

The next steps include the integration of the vehicle dynamics model in the XiL test system from WP7. Furthermore, together with WP6 the controls can be tested and other test vehicles from the ROADVIEW project can be modelled to support the testing of the decision-making and control algorithms.

Deliverable No. D3.6
Version 02
Project no. 101069576

Title
Vehicle dynamics modelling methodology

ROADVIEW

1   Introduction

As the global automotive landscape continues to evolve, the surge in the number of vehicles on the road poses multifaceted challenges and opportunities. The ever-expanding European Union passenger car fleet, as reported by the European Automobile Manufacturers' Association (ACEA), underlines the need for innovative approaches to address the optimization of highway utilization, fuel efficiency, and overall vehicular performance. As of 2021, the EU witnessed a 1.2% growth in its passenger car fleet, totalling nearly 250 million vehicles, a trend reflective of the worldwide escalation in motorization [1].

This escalating trend necessitates comprehensive research to not only accommodate the growing vehicle population but also to enhance aspects of safety, comfort, and environmental sustainability. As underscored by [2], the imperative to optimize high/way and fuel resources while minimizing environmental impact has driven a surge in research endeavours. In this context, the study of vehicle dynamics, offers indispensable insights for addressing the complexities of modern transportation challenges in virtual testing.

The testing of automated driving systems requires the evaluation of a comprehensive number of scenarios, which cannot be tested only in real conditions, due to the complexity and costs involve in real testing. Due to that, the virtualization of testing plays an important role in the verification and validation of automated driving systems. The testing of decision-making and control systems requires a detailed vehicle model, able to reproduce the vehicle in the virtual environment, however, the parametrisation of the model requires extensive data collection in different test rigs. This expensive process limits the visualisation of vehicle dynamics in small research centres and companies.

To minimise the costs and time required for the vehicle dynamics parameter estimation, this work proposes a methodology for optimizing the parameters by the comparison with dynamic manoeuvres conducted on the test track. The development consists of the implementation of a vehicle dynamics model with 11 DoF, the definition of the methodology for the parameter estimation and the implementation of the optimization process. Furthermore, the model as well as the parameter estimation focuses on the adaptation of the vehicle to different weather conditions.

This work is separated in 7 chapters, the first one is the introduction where concepts are discussed, it is followed by a literature review on the topic. The implementation of the proposed vehicle dynamics model is explained in the third chapter. Followed by a discussion on data collection and the implemented parameter estimation method. The sixth chapter discusses the main results of the implemented method. Finally, the seventh chapter finishes of the work with a gathering of results and outlook of future works.

2   Literature Review

Previous researches [3] provide a comprehensive framework for understanding vehicle dynamics by emphasising its intrinsic connection to the intricate movements of vehicles navigating road surfaces. The dynamics of a vehicle involve a complex interplay of various factors, including acceleration and braking, ride quality, and turning dynamics. This intricate dance of motions is a result of dynamic behaviours shaped by the forces acting upon the vehicle, originating from the interaction with tires, gravitational forces, and aerodynamic effects.

Building upon the foundation of the vehicle's mathematical model, it is imperative to delve into the pivotal components that shape the dynamics of the system. In the intricate world of vehicle dynamics, the vehicle body, suspension components, and tires play indispensable roles, collectively contributing to the overall performance and behaviour of the vehicle, as addressed by [4]. A representation of a vehicle model can be seen in Figure 1.

The vehicle body, often referred to as the sprung mass, constitutes a substantial portion of the dynamic system [3, 4]. This mass encompasses not only the vehicle's chassis but also elements such as the engine, passengers, and cargo. The behaviour of the sprung mass is intricately linked to its motion in response to external forces, making it a central focus in the study of vehicle dynamics.

Complementing the sprung mass, the suspension components, comprising springs and dampers, serve as the critical interface between the vehicle body and the wheels [5]. The springs absorb and distribute forces stemming from uneven road surfaces, while dampers regulate the rate of motion, ensuring controlled and comfortable ride quality. Together, these components significantly influence the vehicle's handling, stability, and overall ride comfort.

Deliverable No. D3.6
Version 02
Project no. 101069576

Title
Vehicle dynamics modelling methodology

ROADVIEW
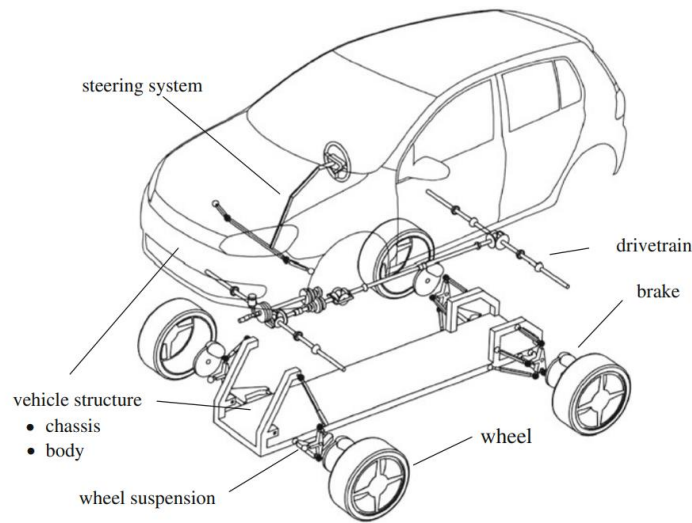
Figure 1. Example of a complex vehicle model [6]

Conversely, the tires, considered as the unsprung mass, directly connect with the road surface and are pivotal for transmitting forces and providing traction. Tire characteristics, such as grip, rolling resistance, and compliance, play a paramount role in determining the vehicle's response to acceleration, braking, and steering inputs, as shown in Figure 2, which represents the wheel seen from the top. (a) represents the wheel when the travelling direction is inline with the rotation plane, and (b) represents the wheel when the travelling direction is not in line with the rotation plane.
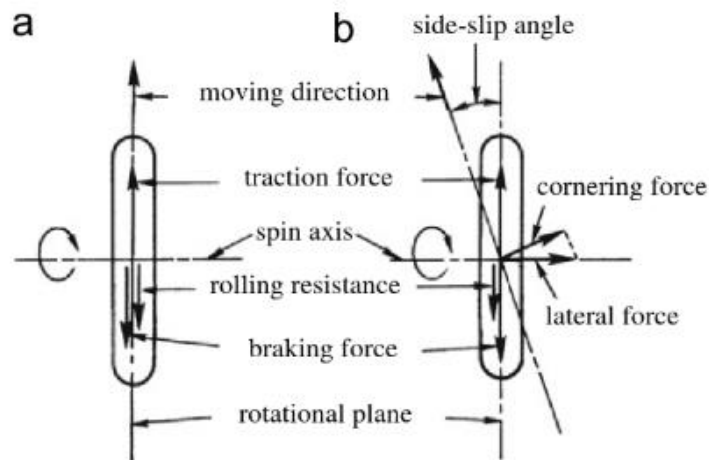
Figure 2. Vehicle tire in motion: Wheel conditions a) strait and b) in curve with rotation plane seen from the top [7]

The integration of these components into the mathematical model facilitates a holistic understanding of the intricate interplay between the sprung and unsprung masses, the suspension system, and the tires [7]. This understanding is fundamental for devising advanced control strategies, optimising vehicle performance, and addressing challenges such as ride comfort, stability, and safety.

Within this mathematical framework, a fixed coordinate system is employed, tethered to the vehicle. The x-axis aligns with the longitudinal direction, the y-axis spans the lateral dimension, and the z-axis extends vertically following the right-hand rule.

As defined by [3, 7], this coordinate system affords a comprehensive understanding of the vehicle's motion, encompassing six independent degrees of freedom. These degrees of freedom delineate the various ways in which a vehicle can move within its environment, and they include:

Deliverable No. D3.6
Version 02
Project no. 101069576

Title
Vehicle dynamics modelling methodology

ROADVIEW
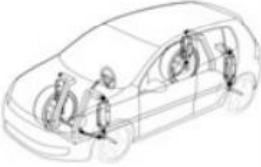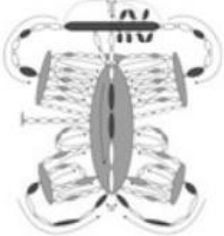
1. Vertical motion in the z-direction: Reflecting the vehicle's capacity for vertical displacement, this degree of freedom accounts for movements such as suspension compression and rebound.

2. Left and right motion in the y-direction: Capturing lateral movements, this degree of freedom signifies the vehicle's ability to traverse sideways, crucial for manoeuvres such as lane changes and lateral stability.

3. Longitudinal motion in the x-direction: Representing the vehicle's forward and backward motion along the longitudinal axis, this degree of freedom is vital for understanding acceleration, deceleration, and overall longitudinal dynamics.

4. Rolling motion around the x-axis: Describing the rotation of the vehicle around its longitudinal axis, this degree of freedom is associated with movements akin to a ship's rolling motion.

5. Pitching motion around the y-axis: Pertaining to the rotation of the vehicle around its lateral axis, this degree of freedom is analogous to the nodding motion experienced during acceleration or deceleration.

6. Yawing motion around the z-axis: Signifying the rotation of the vehicle around its vertical axis, this degree of freedom encapsulates the pivotal turning motions that vehicles undergo during steering manoeuvres.

That said, vehicle dynamics is proving to be an extremely important element in the development of the automotive sector [4], such as in the automotive aerodynamics [8]. This also implies in the relevance of vehicle dynamics in the field of simulation. As pointed by [6], different models can be used, depending on the approach and desired level of detail. [6] also emphasises three key approaches for modelling and simulating the mechanical components in vehicle dynamics:

1. Multibody Systems (MBS): A multibody system usually consists of rigid bodies with mass – connected via bearings and joints –, which are subject to concentrated forces and moments at discrete points. Characteristic points of a rigid body are the centre of gravity CG as well as a finite number of node-points at which concentrated forces and moments act or other bodies are connected via corresponding joints. Elasticity and damping are represented as massless force elements. The mathematical description of the kinematics and kinetics of the multibody system results, depending on the modelling and formalization, in ordinary differential or differential algebraic systems of equations with relatively small degrees of freedom. Multibody systems are ideally suited for complex models that help describe vehicle dynamics.

2. Finite-Element-Method (FEM): Primarily employed to mathematically describe the elastic and, where applicable, plastic characteristics of mechanical systems. FEM involves a model with many finite elements, each with a simple geometry, whose principle deformation options are constrained by so-called elementary functions, leading to ordinary differential equations with many degrees of freedom.

3. Continuous Systems (COS): Utilised to depict the elastic characteristics of mechanical systems with continuous mass, elasticity, and sometimes plasticity. The mathematical formulation of continuous systems leads to descriptions using partial differential equations with an infinite number of degrees of freedom. The method of finite elements and the continuous systems are primarily suitable for mechanical systems or bodies with evenly distributed elasticity.

According to the required level of complexity and performance of the required models, the multibody models can even be simplified by two track models and single track models. In the two track models each wheel are considered separately from the unsprung mass, being usually implemented in simulation environments, in order to enable the description of movement of the main components of the vehicle, including wheels and chassis. In the single track models, on the other hand, the rear wheels as well as the front wheels are combined in two wheels and the vehicle is simplified by a mass without springs and dampers. The single track models are usually applied in controllers and optimization algorithms which requires a low runtime. Table 1 shows the differences among the single, two track models and the multibody system model regarding the frequencies which are modelled, the degrees of freedom and the type of motion that these models describe.

Deliverable No. D3.6
Version 02
Project no. 101069576

Title
Vehicle dynamics modelling methodology

ROADVIEW

Table 1. Overview of vehicle models [6]

Single track model		Two track model		Multibody systems model		
linear	nonlinear	without kinematics	with kinematics	reduced	complex	combined with finite-element method

Type of motion		planar translation, yaw				
			roll-, pitch-, vertical dynamics			
				Component motion		
				Special Applications, Rollover, Accident, Crash		
Degrees of freedom	2	3– 7	14– 25		20– …		20– …
Frequency spectrum	0–2 Hz		0–5 Hz		0–30 Hz		0–200 Hz

The models are usually divided in different modules which describe separately the longitudinal and lateral movement of the vehicle. Furthermore, submodules on the component level as tires or engine can be implemented according to the method being evaluated. The next subchapters describe the longitudinal and lateral modules as well as the tire module which is the most important module for the integration of harsh weather conditions in the vehicle model.

2.1 Longitudinal dynamics

Encompassing the previous concepts, longitudinal dynamics in vehicles refers to the study of movement along the direction of travel, i.e., along the length of the vehicle. This includes the analysis of behaviour during acceleration, deceleration, braking and other interactions that affect the longitudinal movement of a vehicle.

In this respect, the powertrain of a vehicle – which includes the engine, transmission, driveshaft, axles, and differential, as shown in Figure 3 – is responsible for generating and transmitting power to the vehicle's wheels, thus influencing acceleration and braking characteristics. Important research in this area [9] highlights the significant impact of powertrain technology on vehicle performance, fuel efficiency and emissions control. In the same vein, [10] proposes a discussion about how the landscape of hybrid and electric powertrains has further complicated this dynamic, reaffirming the importance of this topic in current research. These developments required a deeper understanding of how the different powertrain configurations affect the vehicle's longitudinal dynamics, especially in terms of energy efficiency and drivability.

Deliverable No. D3.6
Version 02
Project no. 101069576

Title
Vehicle dynamics modelling methodology

ROADVIEW
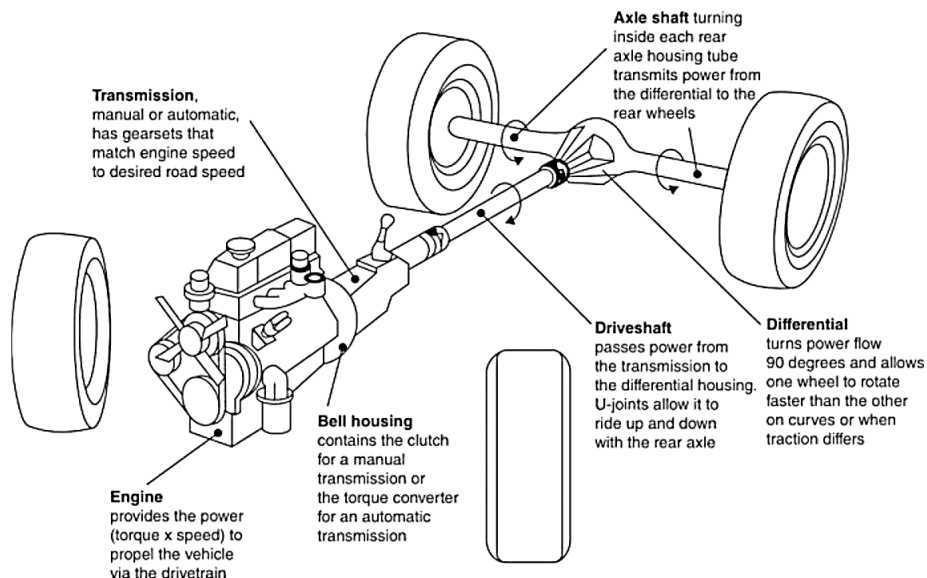
Figure 3. Primary elements in the powertrain [3]

Powertrain capabilities, as well as the vehicle's mass, directly influence the acceleration. The work of [11] offers a deep dive into the principles governing acceleration, focusing on how power is translated into forward motion. This work discusses the impact of various factors like engine torque, transmission gear ratios, and vehicle weight on acceleration performance.

Involving the interaction between the vehicle's brake system and tire-road friction, the braking dynamics is dealt with by [3], providing insights into the physics of braking, including the distribution of braking forces among the wheels and the role of anti-lock braking systems (ABS) in maintaining vehicle stability and reducing stopping distances.

In addition, drivability and ride comfort are influenced by the vehicle's suspension system, as well as its powertrain characteristics. The suspension system, particularly its damping and spring characteristics, plays a crucial role in absorbing shocks and vibrations during acceleration and braking, as detailed in [12].

Furthermore, vehicle aerodynamics significantly impacts longitudinal dynamics, especially at higher speeds where air resistance becomes more pronounced. [8] work on automotive aerodynamics explores how aerodynamic design influences vehicle performance, fuel efficiency, and stability.

2.2 Lateral dynamics

Lateral dynamics in vehicles focuses on the study of movement along the lateral direction, i.e., changes in direction and inclination of the vehicle around the vertical axis.

Most passenger vehicles use the rack pinion steering system. This system consists of the rack, two tie rods and two steering arms of the wheel knuckle. Steering mechanisms are restricted positioning due to engine compartment, suspension linkages and other vehicular systems.

The Ackermann principle, particularly in terms of steering and stability during cornering, ensures that during a turn, the inner wheels turn at a sharper angle compared to the outer wheels, providing optimal cornering efficiency and reducing tire wear. The work of [13] on tire dynamics investigates the intricate aspects of how steering geometry and tire characteristics interact to influence vehicle handling. In addition, [14] provides an exhaustive analysis of tire behaviour under various conditions, a key aspect of understanding the lateral dynamics of vehicles.

The Ackermann principle is shown in Figure 4, in which δ_O is the steering angle of the outer wheel, δ_I is the inner wheel steer angle, w is the track and l is the wheelbase of the vehicle [21]. This condition confirms that the inner wheel has a bigger steer angle than the outer wheel, because it is closer to the center of rotation C_0 as exemplified. For model simplifications, an average steering wheel angle δ can be implemented and the Ackermann effects can be disconcerted.

Deliverable No. D3.6
Version 02
Project no. 101069576

Title
Vehicle dynamics modelling methodology

ROADVIEW
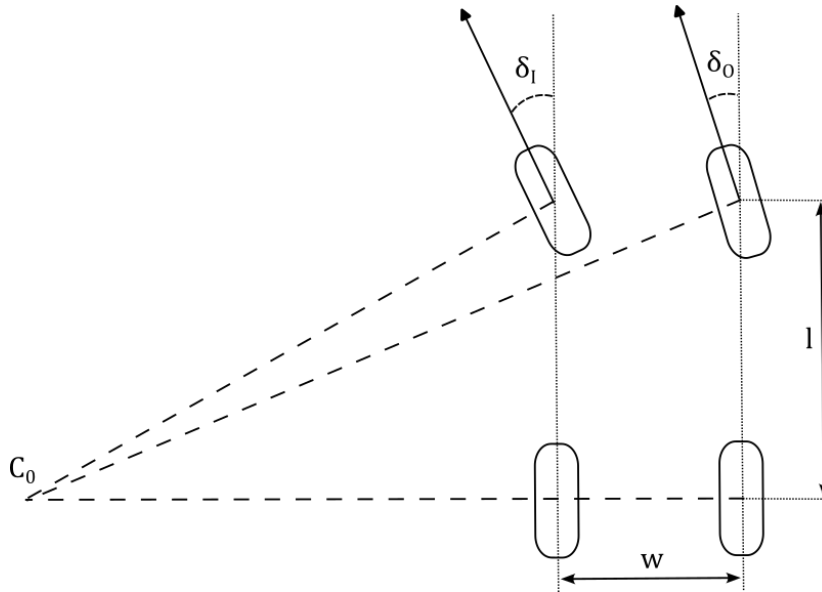
Figure 4. Ackermann steering [8]

Additionally, advanced steering systems like Electronic Power Steering (EPS) have revolutionized the field of vehicle lateral dynamics. [15] elaborates on how these systems not only enhance energy efficiency but also provide better feedback and control, crucial for vehicle stability and handling.

2.3 Tires and harsh weather

To understand the vehicle behaviour, it is essential to know the forces created in the interaction between the tire and the ground. The vehicle wheels must withstand the vertical, longitudinal and lateral forces, as well as move and control the vehicle path [10]. The tire can be compared to an elastic deformation structure with internal damping. Thus, the loaded tire radius R will assume a value smaller than the unloaded value R_0, because of the applied vertical force. The radial tire deflection $\rho = R_0 - R = F_z/C_z$ where F_z is the vertical force and C_z is the vertical tire stiffness. The effective rolling radius R_E is the relation between the rolling speed Ω and the forward speed V_x for a free rolling tire. As illustrated by Figure 5, $R < R_E < R_0$. The rolling radius needs to be measured using a rolling tire. The loaded radius relates the longitudinal friction force to the torque applied on the wheel due to this force, and is not identical to the effective rolling radius as stated above. It is however common in vehicle dynamic models to assume that these two entities are the same. This assumption is made also in the vehicle dynamics model developed in this report. To make this clear the expression dynamic radius, R_d has been used in the vehicle dynamics model formulation, where $R_d = R_e = R$.

The force transmission between tire and road surface takes place through the tire contact patch. Force components in the longitudinal and lateral directions which are parallel to the road surface are generally transmitted through friction [25]. The friction forces originate from a slip between the contact patch and the road surface. The slip speed V_s is usually divided into its longitudinal and lateral components V_{sx} and V_{sy} as illustrated by Figure 5. The longitudinal and lateral slip speeds are defined through:

$$V_{sx} = V_x - \Omega R_e \tag{1}$$

$$V_{sy} = V_y \tag{2}$$

Deliverable No. D3.6
Version 02
Project no. 101069576

Title
Vehicle dynamics modelling methodology

ROADVIEW

(a)   **(b)**
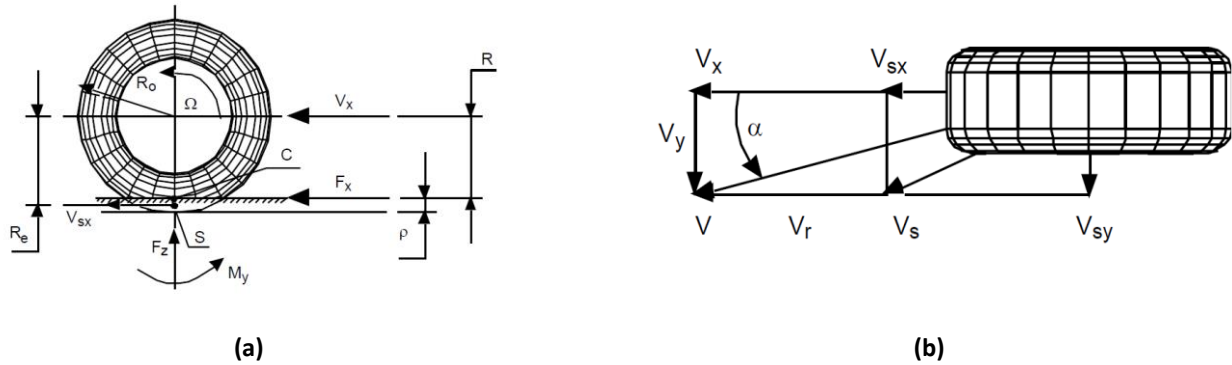
Figure 5. Illustration of various tire radiuses (a), slip angle and slip speeds (b) [16]

Usually, the practical slip quantities κ (longitudinal slip) and α (slip angle) are used. They are defined as:

$$\kappa = -\frac{V_{sx}}{V_x} \tag{3}$$

$$\tan\alpha = \frac{V_{sy}}{|V_x|} \tag{4}$$

The slip angle is thus the angle between the tire forward direction and the tire speed vector.

The friction forces that are generated at different slip can be mostly summarized by the so-called slip curves for pure cornering (steering) and pure braking. Examples of such curves are shown in Figure 6, and give the relation between slip and friction force at steady state conditions. It is often convenient to use normalized friction force, i.e. the friction force divided by the vertical force. Both curves are typically symmetrical around origo, with a linear region for small slip values. At higher slip values the friction reaches a peak value, and then diminishes somewhat at slip values beyond the peak. Only the braking part of the longitudinal friction force is shown in the figure, but the traction force due to acceleration slip is generally very similar in shape, but with an opposite sign.
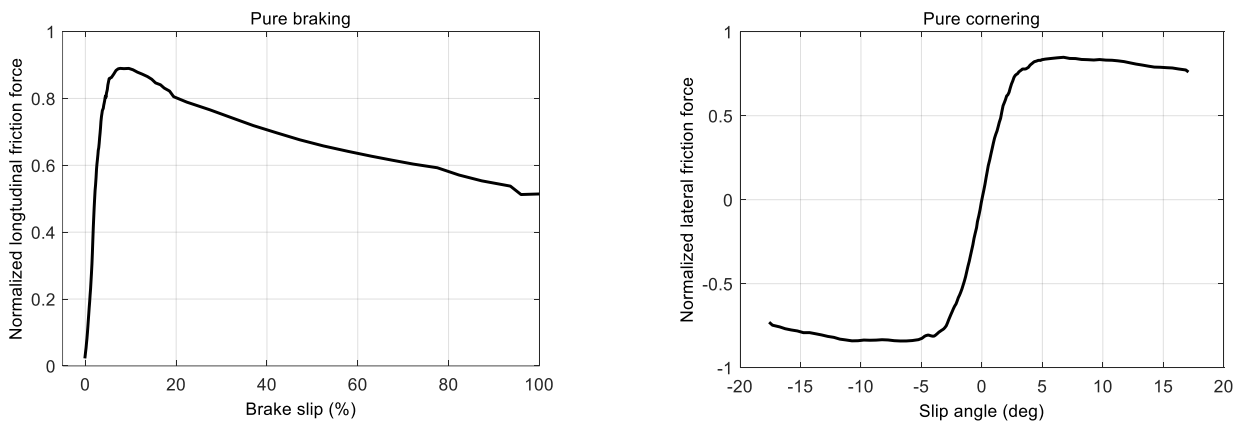
Figure 6. Examples of pure braking (longitudinal force) and pure cornering (lateral force) slip curves for a passenger car tire on wet asphalt, measured by VTI.

The shapes of the slip curves for a specific tire are very dependent on the road surface conditions as illustrated by Figure 7. On wet asphalt and smooth ice the brake slip curve peak is marked and typically occurs within 10-15 % brake slip on asphalt, and 5-10 % on ice for a passenger car tire. On snow there is no peak, and maximum friction typically occurs for locked wheel, where loose snow is being pushed in front of the tire. The cornering slip curves show similar behaviour as the brake slip curves. The lateral peak friction occurs at a few degrees slip angle on smooth ice, and typically between 5-10 degrees on wet asphalt. It is evident that the maximum attainable friction differs substantially between various road conditions. But also for the same kind of road surface, different weather

Deliverable No. D3.6
Version 02
Project no. 101069576

Title
Vehicle dynamics modelling methodology

ROADVIEW

conditions can have a large impact as indicated in Figure 8, with a substantial variation of the peak friction on smooth ice due to varying ice temperature. In this example, the braking distance on ice at -1°C would be almost 3 times longer than the braking distance at -15°C.
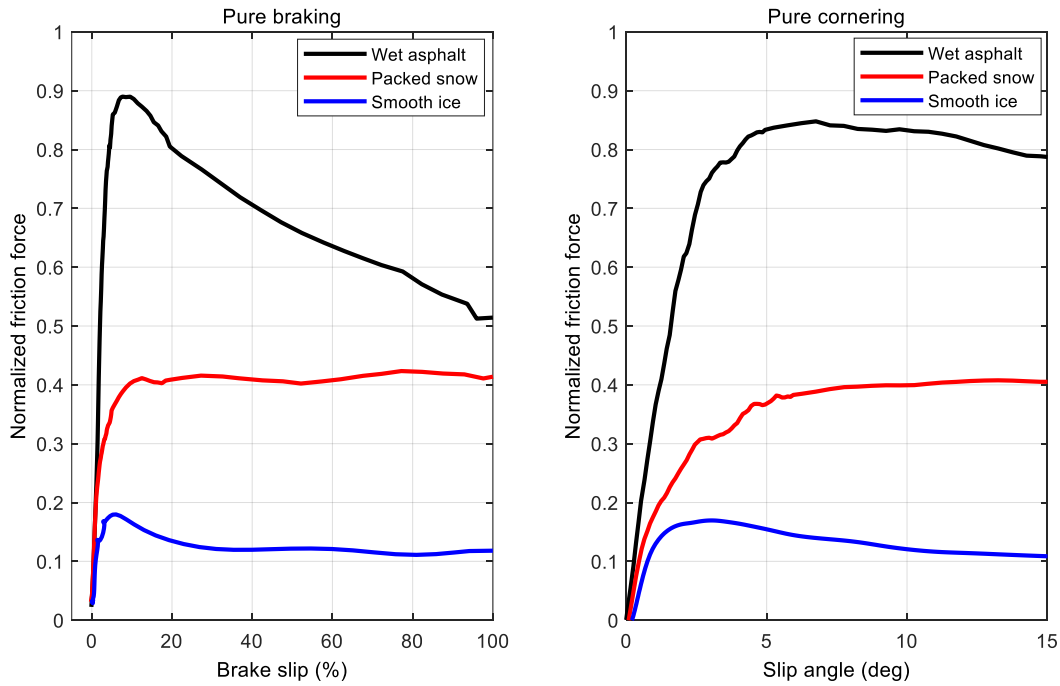
Figure 7. Slip curves for a passenger car tire on different surfaces. All measurements conducted by VTI.
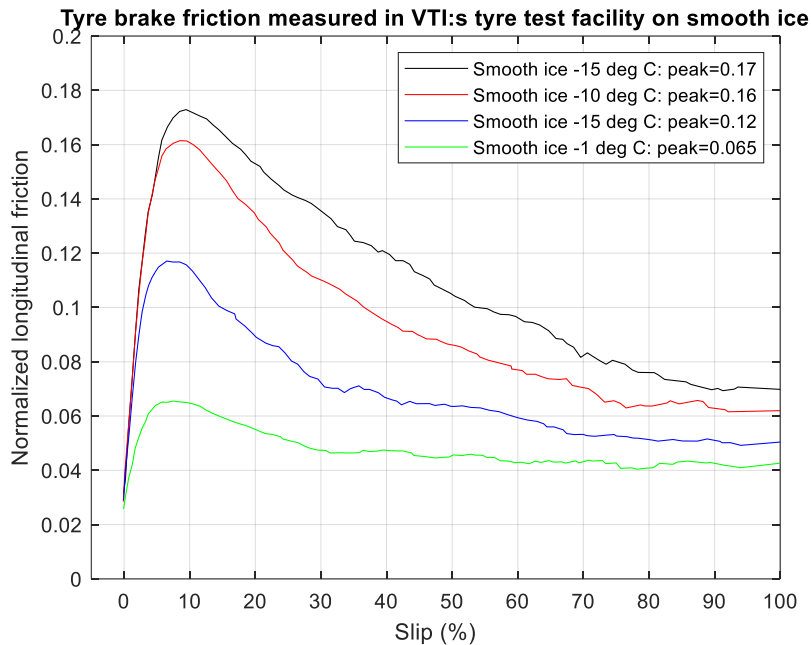
Figure 8. Brake slip curves for a tire on smooth ice at different ice temperatures. All measurements conducted by VTI.

Since the friction forces are due to a complex interaction between the tire and the road, it is generally very difficult to separate the pure tire properties from the road properties. Thus, a specific tire model parameterization is only valid for a specified road surface condition.

Deliverable No. D3.6
Version 02
Project no. 101069576

Title
Vehicle dynamics modelling methodology

ROADVIEW

During real driving the tires will mostly operate in the linear region, so the simplest tire model is just a linear one with respect to brake slip and slip angle, with limit value of the attainable force. The constant of proportionality of the linear model is denoted cornering stiffness, $C_{F\alpha}$, for the lateral force, and longitudinal slip stiffness, $C_{F\kappa}$, for the longitudinal force.

$$F_x = \begin{cases} C_{F\kappa} \cdot \kappa & (\kappa \leq F_{xmax}/C_{F\kappa}) \\ F_{xmax} & (\kappa > F_{xmax}/C_{F\kappa}) \end{cases} \tag{5}$$

$$F_y = \begin{cases} C_{F\alpha} \cdot \alpha & (\alpha \leq F_{ymax}/C_{F\alpha}) \\ F_{ymax} & (\alpha > F_{ymax}/C_{F\alpha}) \end{cases} \tag{6}$$

For simulations on high friction conditions (wet or dry asphalt) a linear model force would be sufficient for non-extreme driving. Also, for vehicle dynamics models that do not explicitly include an ABS system, the linear model will be the best choice, and will implicitly function as an ABS system with respect to the generated braking force. The cornering stiffness is one of the most important property parameters of the tire and is crucial for the vehicle's handling and stability performance [14]. On hard road surfaces, like dry or wet asphalt, the cornering stiffness is a pure tire property, related to the stiffness of the rubber and the size of the contact patch. On loose surfaces, like gravel roads or snow-covered roads, the softness of the road will to a large extent affect the cornering stiffness.

For slippery conditions like ice and snow, the non-linear region will become increasingly important. This is also the case on high friction roads when driving at higher speeds with manoeuvres involving fast steering inputs. Accurate simulations then require non-linear tire models. In addition, the fact that the normalized friction force typically is load dependent is usually also accounted for. Another refinement is the introduction of a transient model which describes the build-up of the forces over time. There exist plenty of different tire models in the literature. Accurate models for describing specific tires are predominantly empirical, or semiempirical. A commonly used model for the complex behaviour of the tires is a semi-empirical equation, named the magic formula (MF) [14]. In this report we propose to use a simplified version of the MF, jointly developed by Volvo Trucks and VTI [16]. That model is described in chapter 3.5. As a background, for a better understanding of that model, the MF tire model is described below.

2.3.1   The Magic Formula tire model

The full MF model contains over a hundred parameters and can describe the tire behaviour in many different situations. The simplest form considers the longitudinal and lateral slips of the wheels separately to define the respective forces acting between the tires and the road. Eq. (7) and Eq. (8) represent respectively the magic formula applied for the calculation of the longitudinal F_x and lateral F_y forces acting on the tire-road interaction. These equations describe the steady state force at a given input and is complemented by a transient model.

$$\boldsymbol{F_x} = \boldsymbol{F_z} * D_x * \sin\{C_x * \text{atan}[B_x * \boldsymbol{\kappa} - E_x * (B_x * \boldsymbol{\kappa} - \text{atan}(B_x * \boldsymbol{\kappa}))]\} \tag{7}$$

$$\boldsymbol{F_y} = \boldsymbol{F_z} * D_y * \sin\{C_y * \text{atan}[B_y * \boldsymbol{\alpha} - E_y * (B_y * \boldsymbol{\alpha} - \text{atan}(B_y * \boldsymbol{\alpha}))]\} \tag{8}$$

In Eq. (51) and Eq. (52) $\boldsymbol{F_z}$ is the vertical load acting on each wheel, B, C, D and E are the empirical parameters that describe the behaviour of the road-tire interaction, finally $\boldsymbol{\kappa}$ and $\boldsymbol{\alpha}$ are respectively the longitudinal slip and the lateral slip angle of the tires.

Deliverable No. D3.6
Version 02
Project no. 101069576

Title
Vehicle dynamics modelling methodology

ROADVIEW
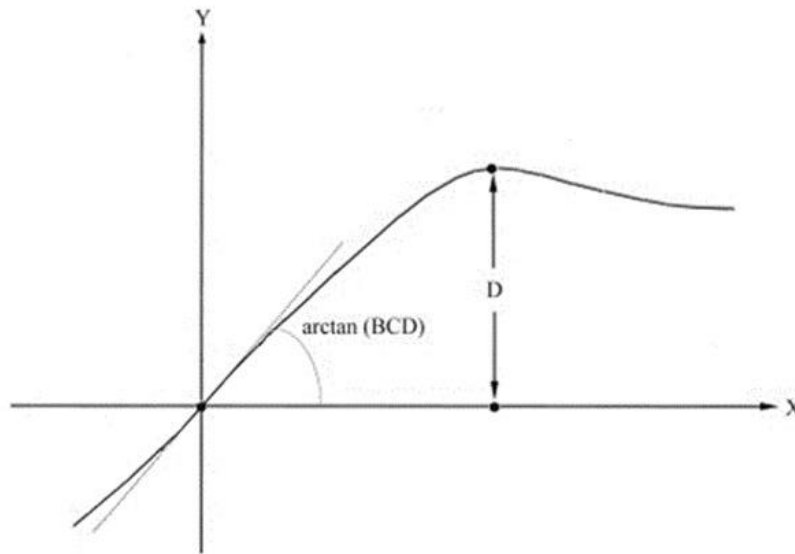
Figure 9. Magic Formula tire model – adapted from [17]

The basic equation is the same for both longitudinal and lateral force. At small slip values the corresponding force is linear, while for higher slip the force relation becomes non- linear where the force reaches as peak value and then diminishes somewhat for even higher slip. The simplest MF model thus has 4 parameters. The equations will be similar for lateral and longitudinal forces, where the lateral case is exemplified below:

D : peak friction
C : shape factor
E : curvature factor (E≤1)
B : stiffness factor. Defined by the cornering stiffness (for the lateral case) $K = B \cdot C \cdot D$

The cornering stiffness is

$$\frac{dF_y}{d\alpha}\bigg|_{\alpha=0} = B \cdot C \cdot D \tag{9}$$

It is often useful to use normalized friction force in the models.

Corresponding functions for the normalized friction:

$$\mu_y = u_y \cdot \sin\left(C \cdot atan\left(B \cdot \alpha - E \cdot \left(B \cdot \alpha - atan(B \cdot \alpha)\right)\right)\right) \tag{10}$$

with $u_y = D/F_z.$

The cornering stiffness normalized by the vertical load is denoted cornering coefficient:

$$\frac{d\mu_y}{d\alpha}\bigg|_{\alpha=0} = K/F_z = B \cdot C \cdot u_y \tag{11}$$

If C>1, the curve will have a peak. The E parameter can then be used for specifying the position of the peak value, without affecting the other parameters:

Deliverable No. D3.6
Version 02
Project no. 101069576

Title
Vehicle dynamics modelling methodology

ROADVIEW

$$E = \frac{B\alpha_{\text{peak}} - tan(\pi/2C)}{B\alpha_{\text{peak}} - \arctan(B\alpha_{\text{peak}})} \tag{12}$$

A positive value of E will shift the peak position toward higher slip angles compared to the peak position with E=0, while a negative E shifts the peak toward smaller angles.

In the simplest friction models, friction is proportional to the vertical load. However, for more accurate description this is not the case. Hence the MF parameters are not load independent. The load dependence is described in relation to the normalized change in vertical load, defined as

$$dfz = (F_z - F_{z0})/F_{z0} \tag{13}$$

where F_{z0} is the standard load of the tire. The choice of standard load has no effect on the load dependence with respect to F_z, but only affect the resulting parameter values. Thus, F_{z0} can be chosen arbitrarily, but it is common to use the nominal load, i.e., the rated load of the tire.

Load dependence for the parameters according to MF-Tire Model 5.2:

The load dependence of the parameters according to MF are described below, where p_{Dy1}, p_{Dy2} etc are constants.

$$u_y = p_{Dy1} + p_{Dy2} \cdot dfz \qquad \text{(linear dependence)} \tag{14}$$

$$C \quad : \text{constant} \qquad \text{(no load dependence)} \tag{15}$$

$$E = p_{Ey1} + p_{Ey2} \cdot dfz \qquad \text{(linear dependence)} \tag{16}$$

$$K = p_{Ky1} \cdot F_{z0} \cdot sin\left(2atan\left(F_z/(p_{Ky2} \cdot F_{z0})\right)\right) \quad \text{(non-linear dependence)} \tag{17}$$

Using that $F_z/F_{z0} = 1 + dfz$, the load dependence for the cornering coefficient can be written as:

$$CC_y = K/F_z = p_{Ky1}/(1 + dfz) \cdot sin\left(2atan\left((1 + dfz)/p_{Ky2}\right)\right) \tag{18}$$

Transient properties

Applying a longitudinal or lateral slip will not produce the steady state force instantaneously. Forces will be gradually developed as the tire rolls on the ground, and the travelled distance at which the forces reach 63% of the steady state value is denoted the relaxation length. The longitudinal relaxation length is much smaller than the lateral one, and may often be neglected. The MF transient model is described for the lateral case below, but the longitudinal model is practically identical.

The tire model transient properties are represented by the tire lateral relaxation length which divided with the tire longitudinal velocity results in a time constant used in a first order low-pass filter applied to the steady state calculation above. Thus, the tire lateral force can be calculated by the differential equation:

$$\frac{\sigma_y}{V_x}\dot{F}_Y + F_Y = F_{Y,SS} \tag{19}$$

where σ_y is the lateral relaxation length and $F_{Y,SS}$ is the steady state lateral force.

In simulations, a practical way of solving this differential equation is to low pass filtering the tire slip angle rather than the tire lateral force, which has the advantage that the tire lateral force directly becomes zero when the tire

Deliverable No. D3.6
Version 02
Project no. 101069576

Title
Vehicle dynamics modelling methodology

ROADVIEW

normal force vanishes. The steady state equation of the lateral force can then still be used, where the relaxed tire slip angle α' is replacing the actual slip angle. The relaxed tire slip angle is calculated from:

$$\frac{\sigma_y}{V_x}\dot{\alpha}' + \alpha' = \qquad (20)$$

Tire lateral relaxation length is linearly dependent on the vertical load as

$$\sigma_y K = p_{Ty1} \cdot F_{z0} \cdot sin\left(2atan\left(F_z/(p_{Ty2} \cdot F_{z0})\right)\right) \cdot R_0 \qquad (21)$$

which is the same equation form as for the cornering stiffness. The nominal lateral relaxation length value is approximately equal to the unloaded radius of the tire, R_0.

Deliverable No. D3.6
Version 02
Project no. 101069576

Title
Vehicle dynamics modelling methodology

ROADVIEW

3 Proposed Vehicle Dynamics Model

The vehicle dynamics model implemented in the ROADVIEW project requires a detailed mathematical model of the systems that directly influence the perception and decision-making algorithms, enabling the virtual testing of the ROADVIEW algorithms. In these circumstances, the control of the engine, brake, and steering systems as well as the movement of the whole vehicle and coupled sensors have the main influence on the behaviour of the implemented automated driving algorithms under test. In ROADVIEW, the weather conditions were also considered for the vehicle dynamics model, which is considered in the road-tire interaction. Due to the integration with the Hardware-in-the-Loop systems, the model must have a great performance to enable soft real-time testing.

The integrated model shall consider the driver/controller inputs (gas pedal, brake, and steering) and calculate the chassis movement (x, y, z, pitch, roll, yaw) as well as wheels and engine rotations with a total of 11 Degrees of Freedom (DoF). Figure 10 shows the coordinate system used in the vehicle used in the vehicle, as well as part of the DoF of the model. In this implementation, the coordinate system follows the ISO 8855:2011 [18] which uses the right-hand rule with z pointing up and y pointing to the left side of the vehicle.
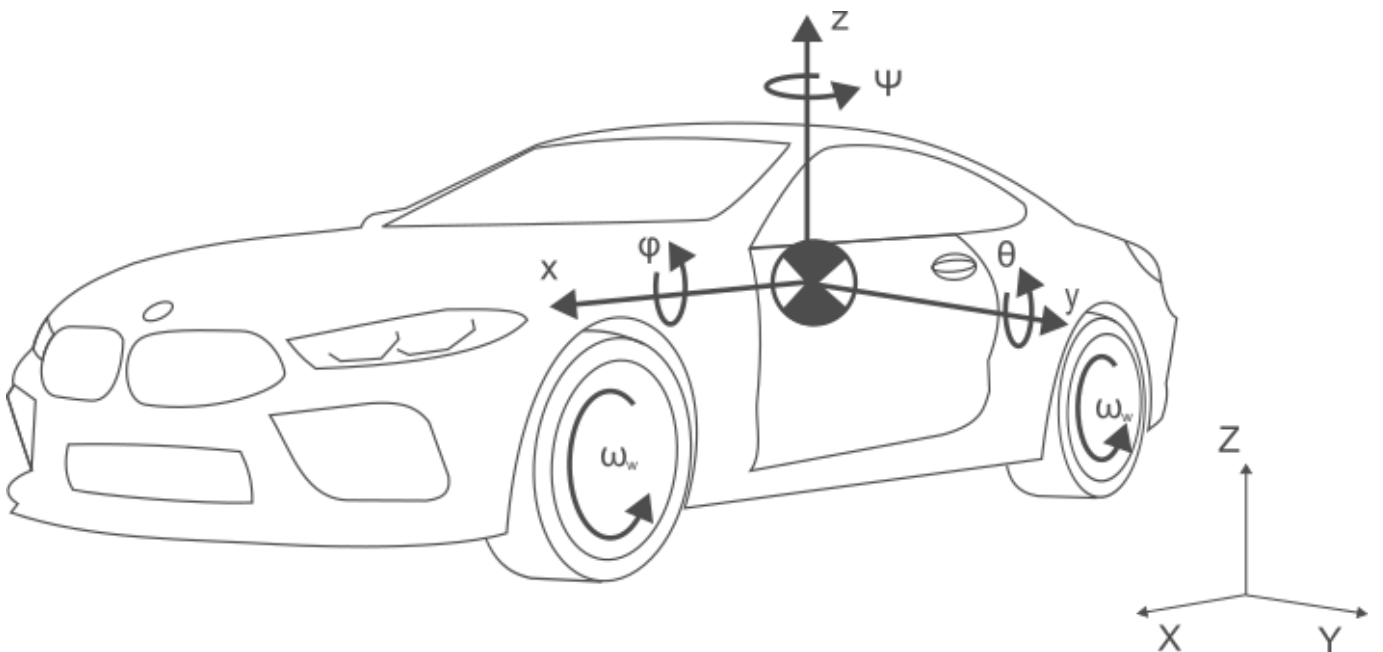
Figure 10. Vehicle coordinate system

A simplification is applied to the model, considering that only flat test tracks will be used in the X-in-the-Loop environment and the wheels are always in contact with the ground. With this simplification, the spring and damping of the tires can be integrated with the suspension and the vertical position of the tires are ignored.

The implemented model is divided into 3 modules to facilitate debugging and parameter optimization. The modules are further divided into logical modules which represent different physical characteristics of the whole vehicle. Figure 11 shows in orange the implemented modules and in green are indicated the logical sub-modules in each script. The blue arrows indicate the variables exchanged between the modules while the black arrows indicate the variables obtained from the last time step.

ROADVIEW
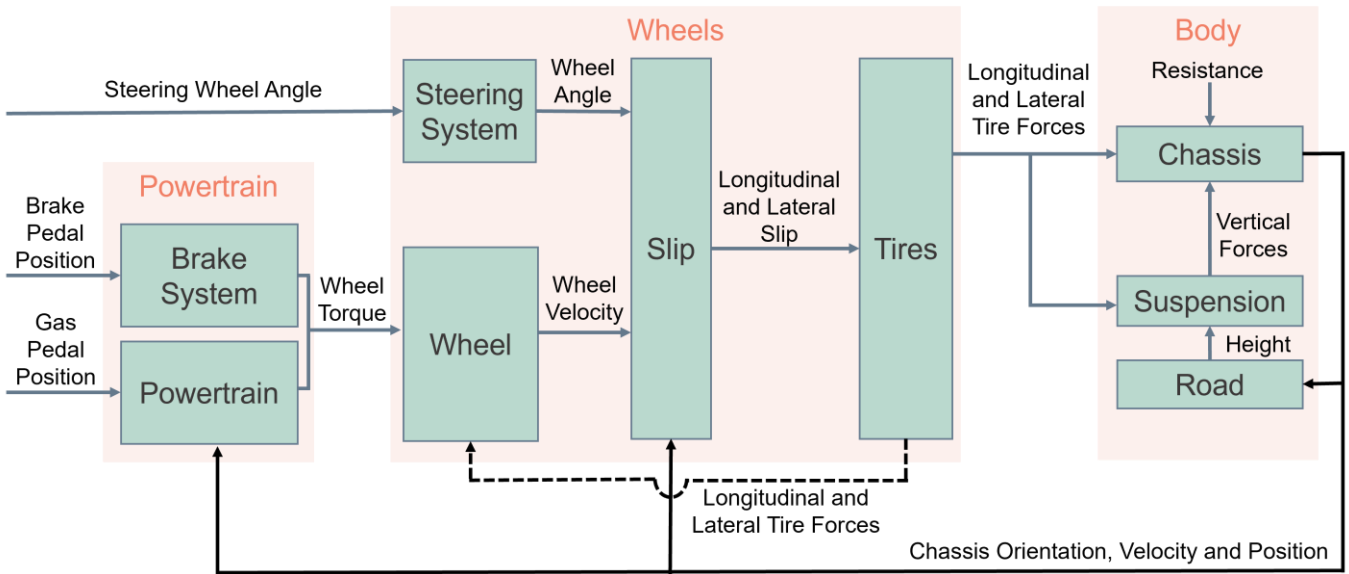
Figure 11. Vehicle dynamics modules

In the next subsection, the physical models implemented in the logical sub-modules from Figure 11 are presented, including the correspondent simplifications and assumptions.

3.1 Brake System

The fluid behaviour as well as the friction between the disk and pad are simplified through a linear correlation between the brake pedal position and the braking torque on the wheel. Eq. (22) shows the implemented brake torque calculation.

$$\boldsymbol{T_B} = Pedal_B * T_{B_{max}} * \boldsymbol{b_B} \tag{22}$$

In Eq. (22) $\boldsymbol{T_B}$ is a vector containing the brake torque in each one of the wheels, $Pedal_B$ is the normalised brake pedal input, $T_{B_{max}}$ is the sum of the maximal brake torque on the vehicle wheels and $\boldsymbol{b_B}$ is a brake bias vector, which indicates the percentage of brake torque to each one of the wheels. In all vectors containing values for all wheels, the vector positions correspond to front left, rear left, front right, and rear right as exemplified for the brake torque in Eq. (23).

$$\boldsymbol{T_B} = \begin{bmatrix} T_{B_{FL}} & T_{B_{RL}} & T_{B_{FR}} & T_{B_{RR}} \end{bmatrix} \tag{23}$$

3.2 Powertrain

The powertrain model implemented in ROADVIEW consists of an automatic transmission with torque converter. The principle of the torque converter operation requires a relation between engine and transmission rotation to define torque and efficiency ratios. Consequently, a DoF respected to the engine rotation shall be included in the model [19]. Figure 12 shows the implementation in which the blue arrows indicate the variables exchanged between the components while the black arrows indicate the variables obtained from the last time step.

Deliverable No. D3.6
Version 02
Project no. 101069576

Title
Vehicle dynamics modelling methodology

ROADVIEW
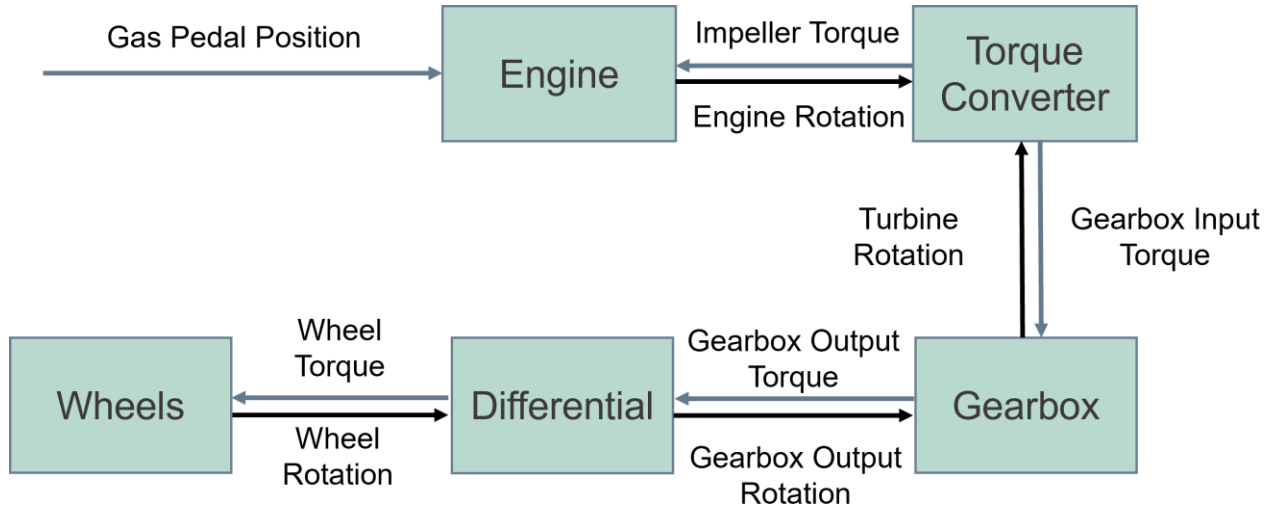
Figure 12. Powertrain architecture

The engine is empirically modelled and the maximum torque available is collected from a look-up table which takes into consideration the rotation calculated at the past time step. The engine torque is simplified as directly proportional to the gas pedal position as shown Eq. (24). In Eq. (24) T_E is the engine torque, $Pedal_{Gas}$ is the gas pedal position in percentage and $T_{E_{max}}$ is function of the engine RPM.

$$T_E = Pedal_{Gas} * T_{E_{max}} \tag{24}$$

Figure 13 demonstrates an example of an engine torque curve, including different gas pedal positions. In the implemented model, a linear interpolation is used to obtain the engine toque in engine rotation points not available at the look-up table.
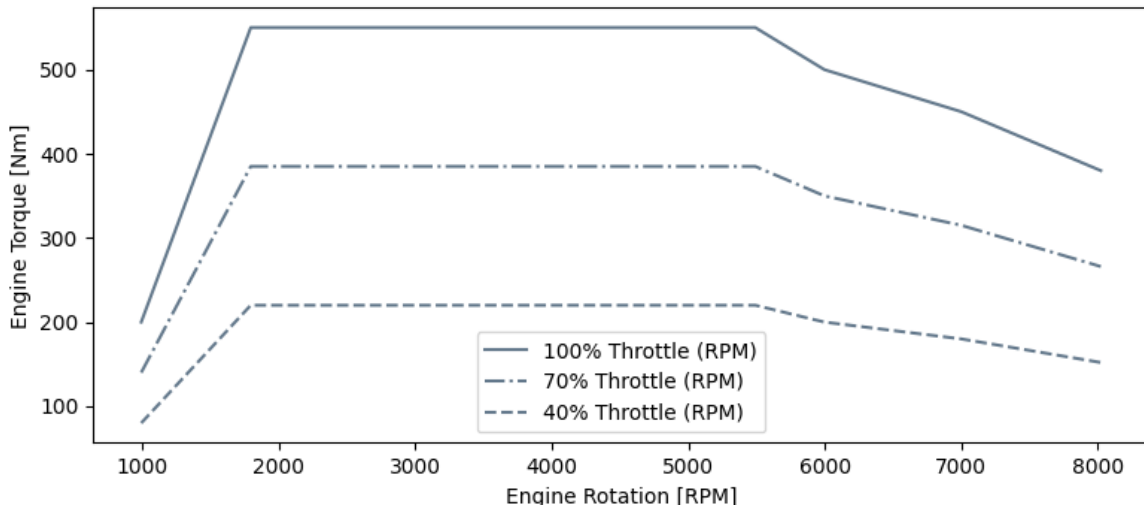
Figure 13. Engine Torque

Based on the engine angular velocity ω_E and the angular velocity of the torque converter turbine ω_T obtained from the last time step, the velocity ratio of the torque converter s can be calculated by Eq. (25). In this

Deliverable No. D3.6
Version 02
Project no. 101069576

Title
Vehicle dynamics modelling methodology

ROADVIEW

implementation, the transmission is considered rigid and the angular velocity of the turbine ω_T is directly calculated from the average of the wheel angular velocity $\overline{\omega_W}$ using the gear ratio from the differential i_D and from the gearbox i_G, which can be combined in a final ratio i_F as shown in Eq. (26) and Eq. (27).

$$s = \frac{\omega_T}{\omega_E} \tag{25}$$

$$\omega_T = i_F * \overline{\omega_W} \tag{26}$$

$$i_F = i_D * i_G \tag{27}$$

Using the velocity ratio s, the impeller torque T_I, as well as the turbine torque T_T can be estimated using Eq. (28) and Eq. (29) respectively [19].

$$T_I = K_{in} * {\omega_E}^2 \tag{28}$$

$$T_T = \mu * T_I \tag{29}$$

In which, K_{in} is the converter factor and μ torque ratio, both functions of the velocity ratio, empirically obtained. Figure 14 shows an example of the converter factor and torque ratio. In case of velocity ratio higher than a lock up value, usually around 0,9, the system is considered as locked and the engine angular velocity ω_E and the turbine angular velocity ω_T are considered the same.
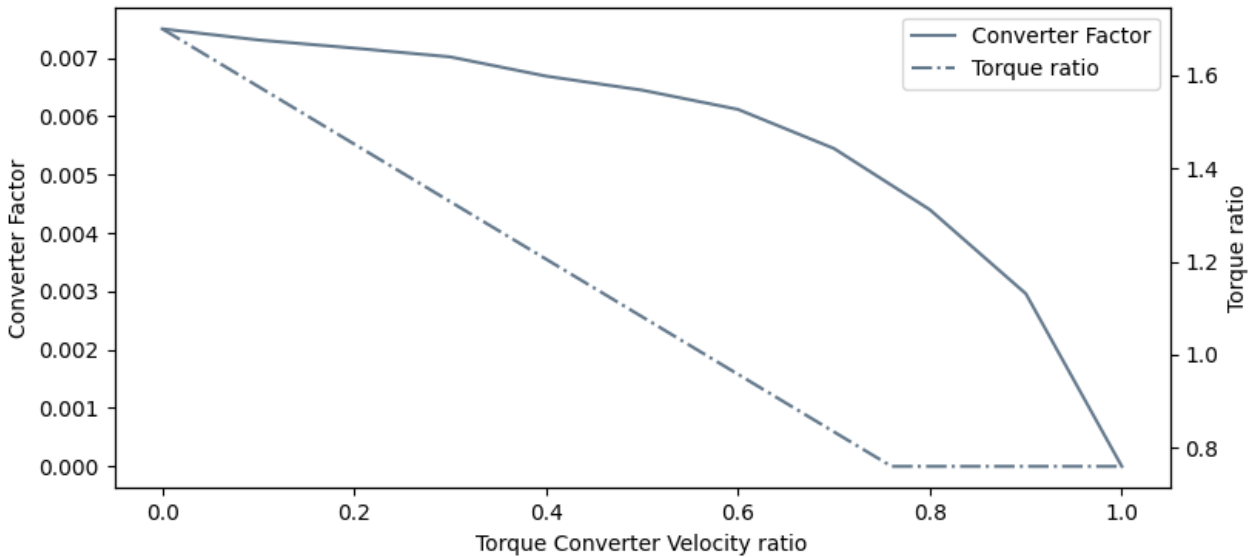
Figure 14. Torque Converter Parameters.

To calculate the changes in the angular velocity of the engine ω_E in each iteration, the engine's angular acceleration $\dot{\omega}_E$ can be obtained by the Eq. (30), in which I_E is the engine inertia. Integrating the angular acceleration, the engine's angular velocity can be directly obtained [3].

Deliverable No. D3.6
Version 02
Project no. 101069576

Title
Vehicle dynamics modelling methodology

ROADVIEW

$$\dot{\omega}_E = \frac{(T_E - T_I)}{I_E} \tag{30}$$

To establish the final speed ratio between the torque converter turbine and the vehicle's wheels, the appropriate transmission gear needs to be selected. Gear selection is based on engine speed rotation and throttle position. A lookup table is used to establish the upper and lower limits of the engine rpm that trigger the shifting of gears. Figure 15 shows an example of a gear-shifting strategy for a four gears transmission system, every time the engine rpm passes the maximum engine rpm to a specific gear, the gear is changed up and changed down in case the engine rpm is lower than the minimum limits.
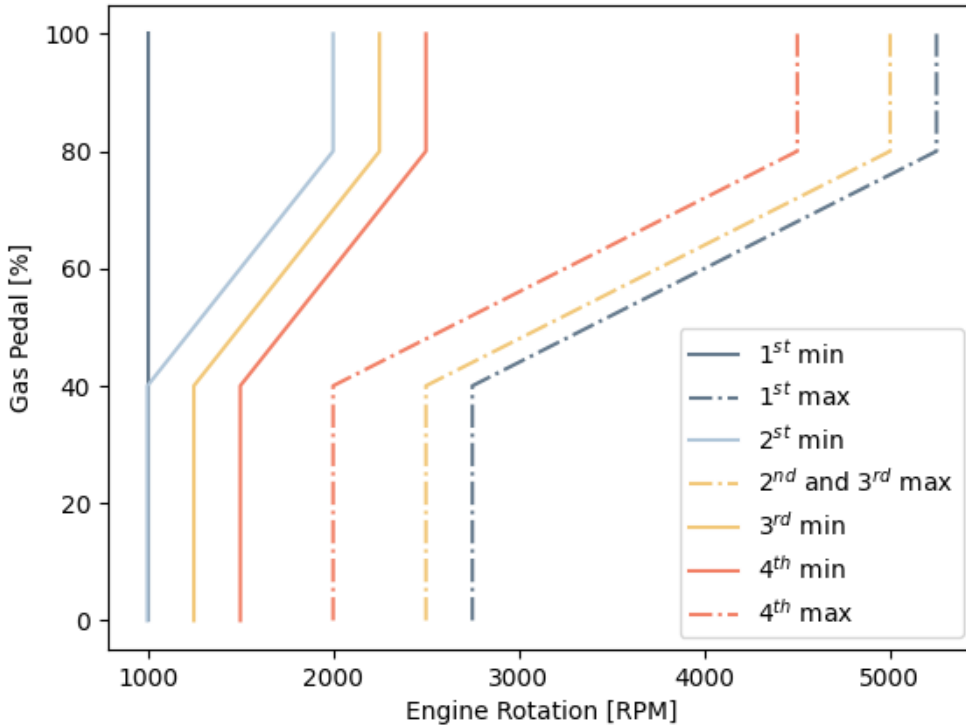
Figure 15. Gear Selection strategy

Once the gear ratio of the transmission is updated, the torque of the turbine can be forwarded to the wheels and added to the brake torque resulting on the total wheel torque $\boldsymbol{T_W}$ as shown in Eq. (31) [3]. To calculate the losses caused by the inertia, the average of the wheels acceleration $\overline{\dot{\omega}_W}$ is considered from last time step and the whole efficiency of the system is simplified by the powertrain efficiency η_P.

$$\boldsymbol{T_W} = \left(T_T * i_F * \eta_P - I_G * i_F{}^2 * \overline{\dot{\omega}_W} - I_D * i_D{}^2 * \overline{\dot{\omega}_W}\right) * \boldsymbol{b_P} - \boldsymbol{T_B} \tag{31}$$

In Eq. (31) I_G represents the inertia of the gearbox, I_D the inertia of the driveshaft and $\boldsymbol{b_P}$ is a vector which indicates the percentage of torque being forwarded to each wheel following the order indicated in the Eq. (32).

$$\boldsymbol{b_P} = \begin{bmatrix} b_{P_{FL}} & b_{P_{RL}} & b_{P_{FR}} & b_{P_{RR}} \end{bmatrix} \tag{32}$$

Deliverable No. D3.6
Version 02
Project no. 101069576

Title
Vehicle dynamics modelling methodology

ROADVIEW

3.3 Steering System

Most of the steering systems available in the market attend to the Ackermann steering geometry, in which both front wheels steer with radius with radius on the same common centre point, and consequently with different steering angles. To simplify the implementation, however, the steering angle from both wheels is considered the same and directly proportional to the steering wheel angle as shown in Eq. (33). The factor i_S is the steering ratio, which linearly converts the steering wheel angle S to the front wheel angle δ.

$$\delta = \frac{S}{i_S} \tag{33}$$

3.4 Slip Calculation

To obtain the forces being transferred to the ground, the longitudinal and lateral slip of the wheels shall be estimated. The longitudinal slip consists of the difference between the wheel velocity and the vehicle longitudinal velocity $\dot{x}$ as shown in Eq. (34) [6]. The speed difference is then normalized by dividing the obtained value by the absolute value of the wheel velocity in acceleration scenario and by the body longitudinal velocity in braking scenarios. The $V_{minslip}$ is a minimal velocity implemented to avoid misbehaviour of the slip calculation in low velocities.

$$\kappa = \frac{r_d * \omega_w - \dot{x}}{max(|r_d * \omega_w|, |\dot{x}|, V_{minslip})} \tag{34}$$

In Eq. (34) κ is a vector containing the longitudinal slip of all wheels, r_d is the dynamic radius of all wheels and ω_w is the angular velocity of all wheels. The indexation of the wheels in the vector follows the representation from Eq. (23) and Eq. (32).

The tire lateral slip, on the other hand, is the angle between the tire velocity and the tire centreline which is directly correlated with the steering angle δ and the yaw rate $\dot{\psi}$. The lateral slip α can be calculated for each one of the wheels according to Eq. (35) [20].

$$\alpha_{FL} = \delta - atan\left(\frac{\dot{y} + a_i * \dot{\psi}}{\dot{x} - b_i * \dot{\psi}}\right) \tag{35}$$

In which a and b are respectively the longitudinal and lateral position of the wheel in relation to the CG and $\dot{y}$ is the lateral velocity of the vehicle. In the implemented model a_i is and b_i are calculated based on the distances between the wheels and the CG l_F, l_R, w_L and w_R as shown in Eq. (36) and Eq. (37).

$$a = [l_F, -l_R, l_F, -l_R] \tag{36}$$

$$b = [w_L, w_L, -w_R, -w_R] \tag{37}$$

The representation of the distances l_F, l_R, w_L and w_R on the vehicle are shown in Figure 16.

Deliverable No. D3.6
Version 02
Project no. 101069576

Title
Vehicle dynamics modelling methodology

ROADVIEW
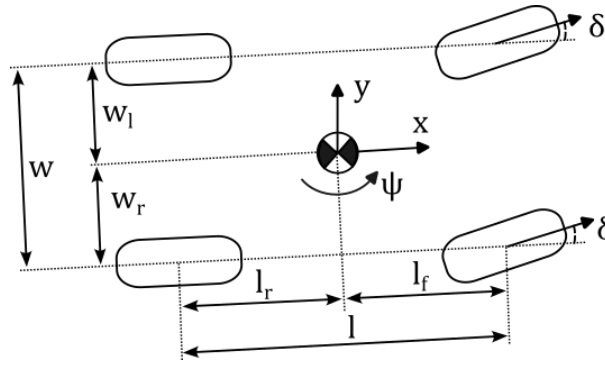
Figure 16. Distances between the Centre of Gravity and the wheels.

3.5 Tires

VTI has together with Volvo Trucks proposed a simplified version of the MF for vehicle dynamics simulation of heavy vehicles. This model, together with suggested parameter values for different standard truck tires, are currently under process to become an ISO standard. I principal it is the MF model with E=0, and with a linear load dependence for the cornering coefficient instead of the more complicated MF assumption. The so-called ISO-model is described below for the lateral tire force. For the longitudinal case the linear model described by eq. 5 would be the preferred model, since the vehicle dynamics model does not include and ABS system.

Steady state conditions:

$$F_Y = F_Z\, \mu_y\, \sin\left[C\, \mathrm{atan}\left(\frac{CC_y}{C\,\mu_y}\,\alpha\right)\right] \tag{38}$$

with
μ_y : normalized peak friction
C : shape factor
CC_y : cornering coefficient

The cornering stiffness is

$$\left.\frac{\mathrm{d}F_{Wy}}{\mathrm{d}\alpha}\right|_{\alpha=0} = F_z \cdot CC_y \tag{39}$$

Corresponding functions for the normalized friction:

$$\mu_y = u_y \cdot \sin\left(C \cdot atan\left(CC_y \cdot \alpha/(C \cdot u_y)\right)\right) \tag{40}$$

and cornering coefficient:

$$\left.\frac{\mathrm{d}\mu_y}{\mathrm{d}\alpha}\right|_{\alpha=0} = CC_y \tag{41}$$

The shape factor C determines the limits of the range of the sine function, and therefore also the shape of the resulting curve. The shape factor is related to the ratio between the peak friction and the asymptotic friction value at infinitely large slip angles, μ_{asym}, in the following way:

Deliverable No. D3.6
Version 02
Project no. 101069576

Title
Vehicle dynamics modelling methodology

ROADVIEW

$$C = 2 - \frac{2}{\pi} \arcsin\left(\frac{\mu_{\text{asym}}}{u_y}\right) \tag{42}$$

$C \leq 1$ results in a slip curve without a peak, approaching the asymptotic value at infinitely large slip angles. C>1 will result in a peak, getting more pronounced with increasing values of C. Setting C=2 results in a curve that approaches zero at large slip angles. Since slip angles can never be above 90 degrees, the asymptotic value may in some cases be of less importance, and values of C > 2 (with negative asymptotic friction) can still be of use. It should be noted that in such case the curve will have more than one peak with respect to infinitely large slip angles, but for modelling a slip curve within a smaller slip angle range such artefacts will not be present.

For C>1 the peak value will occur at

$$\alpha_{\text{peak}} = \frac{C \cdot \mu_y}{CC_y} \tan\left(\frac{\pi}{2C}\right) \tag{43}$$

The overall curve shape and position of the peak will be strongly influenced also by the peak friction value and the cornering coefficient, as illustrated in Figure 17, Figure 18 and Figure 19. In these figures, the inclination of the curve at zero slip angle (cornering coefficient) is indicated by a red line, the peak position by a blue marker, and the asymptotic friction value by a dashed line.
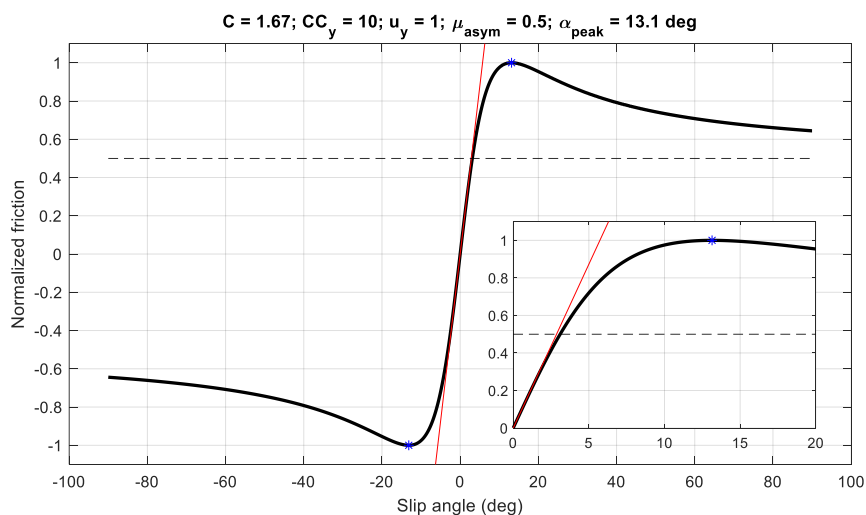
Figure 17 – ISO-model: a slip curve for high friction ($u_y = 1.0$), high cornering coefficient ($CC_y = 10$), and C=1.67.

Deliverable No. D3.6
Version 02
Project no. 101069576

Title
Vehicle dynamics modelling methodology

ROADVIEW
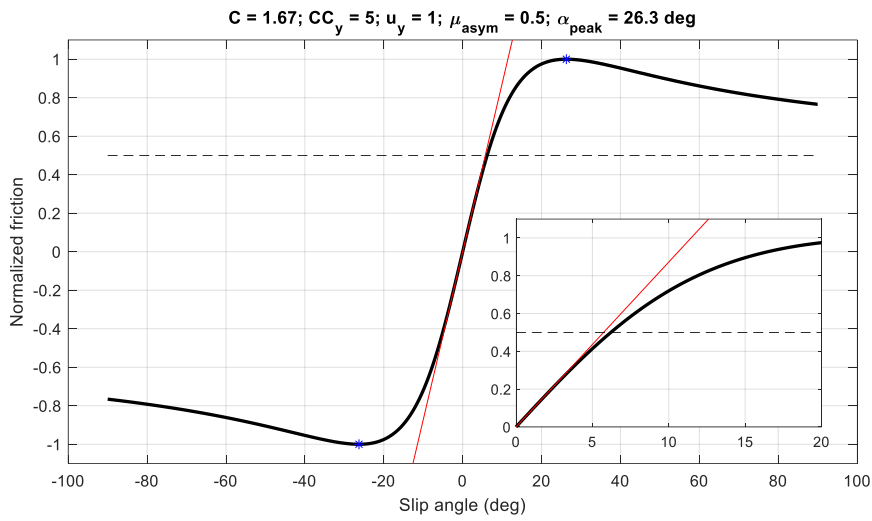
Figure 18 – ISO-model: same conditions as Figure 17, but with lower cornering coefficient ($CC_y = 5$).
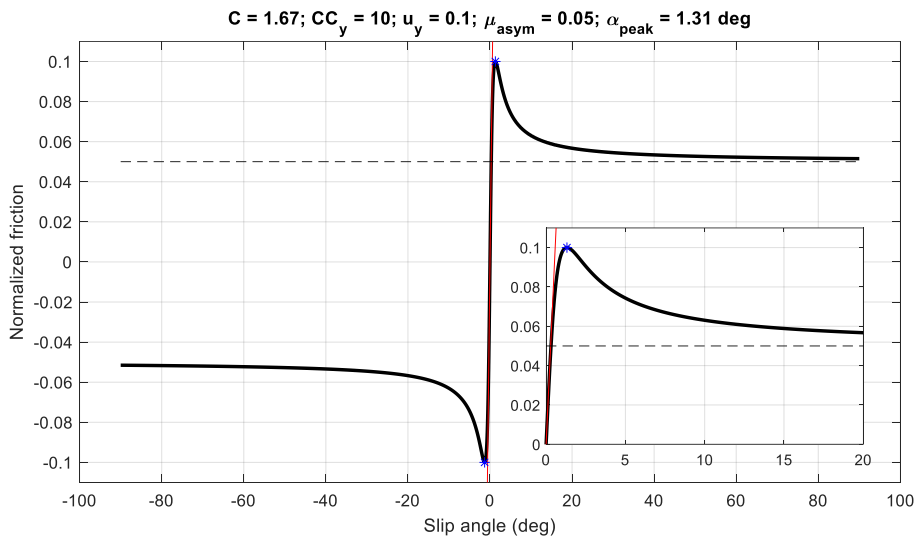
Figure 19 – ISO candidate model: same conditions as Figure 17, but with lower peak friction ($u_y = 0.1$).

Load dependence for the parameters

The tire peak lateral friction at a given tire normal force is calculated using the nominal peak lateral friction and the peak lateral friction gradient, as:

$$\mu_y = \mu_{y0} \left(1 + \mu_{yg} \cdot dfz\right) \tag{44}$$

The tire cornering coefficient at a given tire normal force is calculated using the nominal cornering coefficient and the cornering coefficient gradient, as:

$$CC_y = CC_{y0} \left(1 + CC_{yg} \cdot \text{dfz}\right) \tag{45}$$

Deliverable No. D3.6
Version 02
Project no. 101069576

Title
Vehicle dynamics modelling methodology

ROADVIEW

The shape factor C can be obtained numerically by solving the equation describing the relation between the tire peak lateral friction, the peak position, and the tire cornering coefficient with the nominal values of peak friction and cornering coefficients:

$$\alpha_{\text{peak}} = \frac{C \, \mu_{y0}}{CC_{y0}} \tan\left(\frac{\pi}{2C}\right) \tag{46}$$

However, the tire lateral force will exhibit a peak only if C >1. Another requirement is that $\frac{\mu_y}{c_n} < \frac{\pi}{2}$, so that the peak occurs before a tire slip angle of 90°. If C ≤1, the tire force-slip curve will not have a peak; in that case the shape factor C can be obtained by fitting a curve to the tire measurement data.

Transient properties

The transient ISO-model is similar to that of the Magic Formula. The only difference is a simplification of the load dependence of the lateral relaxation length, which is now linear with load:

$$\sigma_y = \sigma_{y0} \left(1 + \sigma_{yg} \cdot \text{dfz}\right) R_0 \tag{47}$$

The Eq. (38) can also be applied for the longitudinal forces on the wheels F_{W_x} and the forces acting to each one of the wheels in the vehicle coordinate system can be obtained by a rotation matrix shown in Eq.s (48) and (49).

$$\boldsymbol{F_x} = \boldsymbol{F_{W_x}} * \cos(\boldsymbol{\delta}) - \boldsymbol{F_{W_y}} * \sin(\boldsymbol{\delta}) \tag{48}$$

$$\boldsymbol{F_y} = \boldsymbol{F_{W_y}} * \cos(\boldsymbol{\delta}) + \boldsymbol{F_{W_x}} * \sin(\boldsymbol{\delta}) \tag{49}$$

3.6 Wheel

To calculate the acceleration of the wheels $\dot{\omega}_W$, a sum of forces on the longitudinal axle of the wheel leads to Eq. (50) [3]. Using this approach, the total wheel torque T_W and the tire longitudinal force F_X are used to obtain $\dot{\omega}_W$. Furthermore, the rolling resistance R_R is included as a linear factor from the wheel velocity ω_W.

$$\dot{\omega}_W = \frac{(T_W - F_x * r_d)}{I_W} - R_R * \omega_W \tag{50}$$

In Eq. (50) the I_W is the Inertia of the wheels and axels and r_d is a vector with the dynamic radius of the tires. By integrating the wheel acceleration from the initial time t_0 until the current time step t, the wheel velocity ω_W can be obtained as shown in Eq. (51).

$$\omega_W = \int_{t_0}^{t} \dot{\omega}_W \, \mathrm{d}t \tag{51}$$

3.7 Road

The road consists of a function which access the global position of each wheel and return the respective high of the road, enabling a horizontal interaction with the ground as shown in Eq. (52). Since for the purpose of the project ROADVIEW, the vehicle dynamics model will be compared with tests conducted at the CARISSMA outdoor test track, which is a flat road, the function was simplified, returning a null height.

Deliverable No. D3.6
Version 02
Project no. 101069576

Title
Vehicle dynamics modelling methodology

ROADVIEW

$$z_W = f(X_W, Y_W) \tag{52}$$

For future implementations the integration of an OpenCRG® reader can be used to consider the road relief.

3.8 Suspension

The suspension module considers the spring and damper forces, which interact with the ground and directly affects the vertical, lateral, and longitudinal forces interacting with the chassis of the vehicle. The simplifications made in this model consider that the wheels are always in contact with the ground and the stiffness and damping of the tires are neglectable.

The model implemented was adapted from the vehicle model used by VTI in driving simulators [20]. In this case, the suspension displacement for each wheel d_S is calculated from the longitudinal movement of the CG Δz_{CG} as well as the effect of the pitch, roll and the height of the road z_W as shown in Eq. (53). For the calculations of the suspension the positions, velocities and accelerations of the chassis are taken from the past time step.

$$d_S = \Delta z_{CG} - a * \sin(\theta) + b * \sin(\phi) - z_W \tag{53}$$

A vector containing velocity of the displacement in each wheel $\dot{d}_S$ is directly obtained from the discrete derivate of the displacement as shown in Eq. (54), in which Δt represents the time step and the d_S^t and d_S^{t-1} are the displacement of the suspension in each wheel for the current and last time respectively.

$$\dot{d}_S = \frac{d_S^t - d_S^{t-1}}{\Delta t} \tag{54}$$

The suspension forces are calculated based on the Eq. (55) considering the effect of the spring, the damper, and the anti-rollbar. The stiffness of the spring is defined as K_S, the damping coefficient as C_D and the stiffness of the anti-roll bar K_{ARB}.

$$F_S = -K_S * d_S - C_D * \dot{d}_S - \frac{K_{ARB} * \sin(\phi)}{2 * b} \tag{55}$$

The vertical forces acting on the ground depend not only on the suspension forces but also on the lateral $\Delta F_{Z_{lat}}$ and longitudinal load transfer $\Delta F_{Z_{lon}}$ as well as the static forces $F_{Z_{static}}$. The static force $F_{Z_{static}}$ acting on each wheel is calculated based the whole vehicle mass m and the weigh distribution W_d as shown in Eq. (56).

$$F_{Z_{static}} = m * W_d * g \tag{56}$$

The weight distribution W_d describes the percentage of the total weight in each wheel considering the CG position. The weight distribution is calculated by the Eq. (57).

Deliverable No. D3.6
Version 02
Project no. 101069576

Title
Vehicle dynamics modelling methodology

ROADVIEW

$$W_d = \frac{(l - |a|) * (w - |b|)}{w * l} \tag{57}$$

The lateral load transfer $\Delta F_{Z_{lat}}$ generated by lateral accelerations is calculated by the torque equilibrium around the roll centre as shown in Eq. (58).

$$\Delta F_{Z_{lat}} = \xi_{Z_{lat}} \frac{m * a_y * h_r}{w} \tag{58}$$

In Eq. (58) a_y is the lateral acceleration, h_r is the roll centre height, m, the mass of the vehicle and $\xi_{Z_{lat}}$ is a vector that defines the load distribution being added or removed from each wheel taking into account the division of load on the front and the rear axles as shown in Eq . (59).

$$\xi_{Z_{lat}} = \begin{bmatrix} \dfrac{-l_R}{l} & \dfrac{-l_F}{l} & \dfrac{l_R}{l} & \dfrac{l_F}{l} \end{bmatrix} \tag{59}$$

Similarly, the load transfer generated by the longitudinal acceleration is calculated by the torque equilibrium around the pitch centre as shown in Eq. (60) which h_p is the height of the pitch centre, a_x is the longitudinal acceleration and $\xi_{Z_{long}}$ describes load distribution being added or removed from the axles taking into account that the weight is divided between both wheels of each axle.

$$\Delta F_{Z_{long}} = \xi_{Z_{long}} \frac{m * a_x * h_p}{l} \tag{60}$$

$\xi_{Z_{long}}$ is positive for front axle and negative for rear axle and is defined as the vector shown in Eq. (61).

$$\xi_{Z_{long}} = \begin{bmatrix} -\dfrac{1}{2}, & \dfrac{1}{2}, & -\dfrac{1}{2}, & \dfrac{1}{2} \end{bmatrix} \tag{61}$$

Finally, the vertical forces actuating on the ground can be calculated by the Eq. (62).

$$F_Z = F_{Z_{static}} + F_S + \Delta F_{Z_{lat}} + \Delta F_{Z_{lon}} \tag{62}$$

3.9 Chassis

The calculation of the vehicle movement is based on the second law of motion applied to the longitudinal and lateral movement of the vehicle as implemented in the simulators from VTI [20]. Slope forces are not considered in this model, since only manoeuvres on the flat test tracks will be considered for the evaluations inside the ROADVIEW project.

Considering the effect of the aerodynamics the longitudinal acceleration $\ddot{x}$ in vehicle coordinate system can be calculated by the Eq. (63).

Deliverable No. D3.6
Version 02
Project no. 101069576

Title
Vehicle dynamics modelling methodology

ROADVIEW

$$\ddot{x} = \frac{\sum \boldsymbol{F_x} - 0.5 * C_{Ax}\, \rho_A\, A_0\, \dot{x}^2}{m} - \dot{y} * \dot{\psi} \tag{63}$$

In Eq. (63) the $\sum \boldsymbol{F_x}$ is the sum of the longitudinal forces from all tires in the vehicle coordinate system. C_{Ax}, ρ_A and A_0 represent the drag coefficient, the density of the air and the drag area of the vehicle respectively. The aerodynamic drag is proportional to the square of the longitudinal velocity $\dot{x}$. The multiplication of the lateral velocity $\dot{y}$ and the yaw rate $\dot{\psi}$ are added to consider the effect of the orientation change on the vehicle.

The lateral acceleration $\ddot{y}$ in the vehicle coordinate is calculated similarly to the longitudinal acceleration as shown in Eq. (64), however aerodynamic effects are neglected on the lateral acceleration.

$$\ddot{y} = \frac{\sum \boldsymbol{F_y}}{m} + \dot{x} * \dot{\psi} \tag{64}$$

In Eq. (64) the $\sum \boldsymbol{F_y}$ is the sum of the lateral forces from all tires in the vehicle coordinate system and $\dot{x}$ the longitudinal velocity of the vehicle. In Eqs. (63) and (64) the vehicle velocity and yaw rate are taken from the previous time step.

The vertical acceleration $\ddot{z}$ is directly calculated by the sum of the forces acting on the suspension $\sum \boldsymbol{F_S}$ divided by the vehicle mass m as shown in the Eq. (65).

$$\ddot{z} = \frac{\sum \boldsymbol{F_S}}{m} \tag{65}$$

The orientation of the vehicle is calculated considering the forces acting on the suspension $\boldsymbol{F_S}$ and the load transfer generated by the accelerations and vehicle inclination. Eq. (66) shows the calculation of the roll rate variation $\ddot{\varphi}$ in which h_{rc} is the distance between the roll centre and the centre of gravity, φ is the roll angle and I_φ is the roll inertia.

$$\ddot{\varphi} = \sum \frac{\boldsymbol{b} * \boldsymbol{F_S} + \boldsymbol{m_s} * h_{rc} * \left(\ddot{y} + \boldsymbol{g} * sin(\varphi)\right)}{I_\varphi} \tag{66}$$

The sprung mass $\mathbf{m}_s$ is obtained in this implementation from weight distribution $\boldsymbol{W_d}$, and the unsprung mass $\mathbf{m}_{unsprung}$ as shown in Eq. (67).

$$\mathbf{m}_s = m * \boldsymbol{W_d} - \mathbf{m}_{unsprung} \tag{67}$$

In a similar way the variation of the pitch rate $\ddot{\theta}$ of the vehicle can be calculated by the Eq. (82) in which h_{pc} is the height of pitch centre and the centre of gravity, θ is the pitch angle and I_θ is the pitch inertia. Eqs. (66) and (68) do not consider the inclination of the road since this step was simplified in the implementation of this project.

$$\ddot{\theta} = \sum \frac{\boldsymbol{a} * \boldsymbol{F_S} + \boldsymbol{m_s} * h_{pc} * \left(\ddot{x} + \boldsymbol{g} * sin(\theta)\right)}{I_\theta} \tag{68}$$

Deliverable No. D3.6
Version 02
Project no. 101069576

Title
Vehicle dynamics modelling methodology

ROADVIEW

For the planar motion the variation of the yaw rate $\ddot{\psi}$ is calculated based on the distances between the wheels and the centre of gravity as well as the forces acting on the tires on the orientation of the vehicle frame as shown in Eq. (69). The I_ψ indicates the yaw inertia.

$$\ddot{\psi} = \sum \frac{\boldsymbol{F_y * a - F_x * b}}{I_\psi} \tag{69}$$

To obtain the velocities, positions, angle rates and orientations Eqs. (63) to (69) are integrated from the initial until the current time as exemplified for the longitudinal velocity $\dot{x}$ and longitudinal displacement x in Eq. (70) ans (71) respectively. In Eq. (70) $\dot{x}_0$ indicates the initial speed of the vehicle. In the implemented algorithm the integration is conducted by using the left Riemann sum with a time step of 10 ms.

$$\dot{x} = \int_{t_0}^{t} \ddot{x} \, dt + \dot{x}_0 \tag{70}$$

$$x = \int_{t_0}^{t} \dot{x} \, dt \tag{71}$$

For the orientations, the initial value is added in the Eq. (71). It is also important to highlight that pitch and roll are referred to the vehicle frame, while the yaw is related to the map frame. To convert the longitudinal and lateral displacements from the coordinate system of the vehicle (x and y) to the map frame (X and Y) Eqs. (72) and (73) are applied.

$$X = x * \cos(\psi) - y \sin * (\psi) \tag{72}$$

$$Y = y * \cos(\psi) + x \sin * (\psi) \tag{73}$$

3.10 Vehicle model validation

IPG CarMaker 12.0 (CM) is an advanced software that allows to build virtual prototypes for vehicles [21]. It has an extensive comprehension of vehicular dynamics. In this work CM is utilised as a benchmark of vehicular dynamics, in the preceding testing phase of the algorithm that is developed in this work.

To use CM, it is necessary to define which scenes will be performed under this simulated environment. In this context, this scene must be described with parameters such as ego target speed and steering angle position. With the simulation environment ready it is important to record data simulated by CM, to properly test the proposed algorithm, for this purpose a Matlab API is applied, and the data is stored as a binary file. The main collected parameters can be seen in Appendix A. The utilised vehicle in CM is the Audi R8 as shown in Figure 20.

Deliverable No. D3.6
Version 02
Project no. 101069576

Title
Vehicle dynamics modelling methodology

ROADVIEW
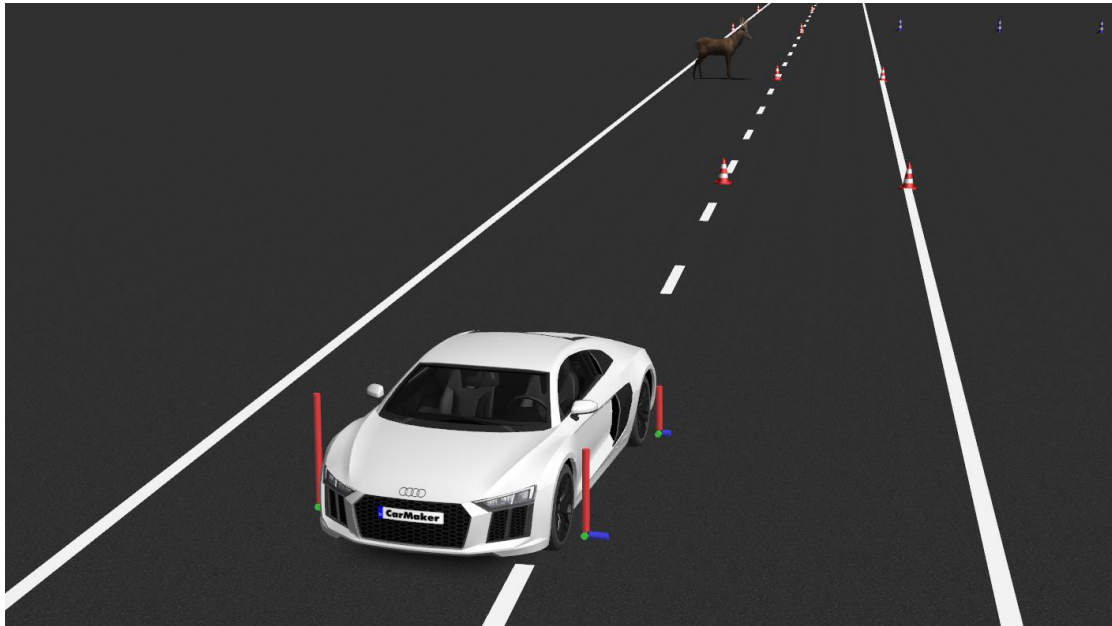
Figure 20. Simulated Audi R8 in IPG CarMaker 12.0 - Double Lane change manoeuvre.

4 Data collection

This chapter describes how data collection is performed to obtain the required parameters of the vehicle dynamics model. Parameter that could be obtained from the documentation of the vehicle, measured on static tests and test benches are conducted separately to simplify the optimization process.

In order to demonstrate the implementation of the proposed parameter estimation method, the test vehicle from the CARISSMA institute of automated driving is applied as test case. The test vehicle is a BMW M8 competition with access to the CAN-bus system, enabling the measurement of data directly from the sensors embedded on the vehicle as the gas pedal, brake pedal, steering wheel angle and wheel torque. The next subchapters describe the steps conducted for the definition of the parameters.

4.1 Documentation research

The required parameters available on the technical data from the OEM are directly obtained from the documentation. Common parameters available include the gear ratio of all gears and differential, steering ratio, wheelbase, track width and drag coefficient. Furthermore, the engine torque curve is obtained from online sources.

4.2 Static Measurements

The parameters related to the vehicle mass and centre of gravity were obtained using four scales and a vehicle lifter. The scales applied in this test are from the Dini Argeo GmbH and are specific for vehicle weighting. The four scales are wired to a central unit, which displays the weight of the vehicle in each one of the wheels. The measurement is conducted with the vehicle fully fuelled and without the driver, since in preliminary tests the influence of the driver weight on the vehicle do not have considerable influence on the final position of the CG. Figure 21 shown the data collection conducted at THI.

Deliverable No. D3.6
Version 02
Project no. 101069576

Title
Vehicle dynamics modelling methodology

ROADVIEW

Figure 21. Measurement of the longitudinal and lateral position of the CG.

For the calculation of the CG position the sum of the moments are applied separately for the longitudinal and lateral calculations. Applying this method, the longitudinal distance between CG and front axel l_f , CG and rear axle l_r as well as the lateral distances to the left wheel w_l and right wheel w_r can be directly obtained as shown in Eqs. (74) to (77) [22].

$$l_f = \frac{m_{RL} + m_{RR}}{m} * l \tag{74}$$

$$l_r = \frac{m_{FL} + m_{FR}}{m} * l \tag{75}$$

$$w_l = \frac{m_{RR} + m_{FR}}{m} * w \tag{76}$$

$$w_r = \frac{m_{RL} + m_{FL}}{m} * w \tag{77}$$

To obtain the height of the CG, the vehicle is tilted to evaluate the load transfer to the front axle. Due to the limited ground distance of the test vehicle an inclination γ of 12.8° was implemented as shown in the Figure 22.

Deliverable No. D3.6
Version 02
Project no. 101069576

Title
Vehicle dynamics modelling methodology

ROADVIEW

Figure 22. Measurement of vertical position of the CG.

$$h = \frac{l}{m} * cot(\gamma) * (m_{FL} + m_{FR} - m'_{FL} - m'_{FR}) \tag{78}$$

Based on the inclination angle γ, the wheel base l and the mass of the vehicle in a flat surface and inclined the height of the CG h can be calculated as by the Eq. (78) in which m'_{FL} and m'_{FR} are the mass measured on the front left and front right wheels with the vehicle inclined [22].

4.3 Tire Test Rig

The purpose of the tests in the VTI tire test facility has been to determine the cornering stiffness of the front and rear tires for the THI test vehicle. The cornering stiffness (CS) is defined according to Eq. (39) and is the derivative of the lateral force with respect to slip angle, taken at zero slip angle.

For measurements and modelling, a more useful entity however is the cornering coefficient (CC), which is the cornering stiffness normalized by the wheel load, as defined in Eq. (41).

Typically, the lateral force is linear with respect to slip angle for small angles. The cornering coefficient can thus be determined by measuring the lateral force at a few fixed small slip angles, and via a line fit estimate the derivative. The slip angle range where the force is linear is limited by the available static friction. Low friction means a smaller slip angle range. For the same friction level, a higher cornering coefficient also leads to a smaller slip angle range. The type of road surface used in the measurements is not that important as long as it is a hard surface. High friction level is an advantage since that increases the linear region, and higher slip angles can be used, but the measurements can also be carried out at lower friction like smooth ice.

From previous investigations on heavy truck tires, we found that the cornering coefficient typically decreases with increasing inflation pressure, or/and. higher rubber temperature. The cornering coefficient also decreases with wheel load, although a low load threshold exists. Reducing the wheel load below that point will not further increase the CC, which may actually drop off instead. For the investigated truck tires, a linear relationship between the CC and wheel load was observed for nominal loads and above.

The measurements were carried out on a steel surface on the VTI flat track machine, depicted in Figure 23. It consists of a stationary but steerable tire test rig and a moving 55-meter-long flat steel bar that can be covered with ice or asphalt cassettes. The bar representing the road surface is moved back and forth under the tire at maximum speed of 30 km/h. Tire forces in all directions are measured by piezoelectric force sensors.

Deliverable No. D3.6
Version 02
Project no. 101069576

Title
Vehicle dynamics modelling methodology

ROADVIEW
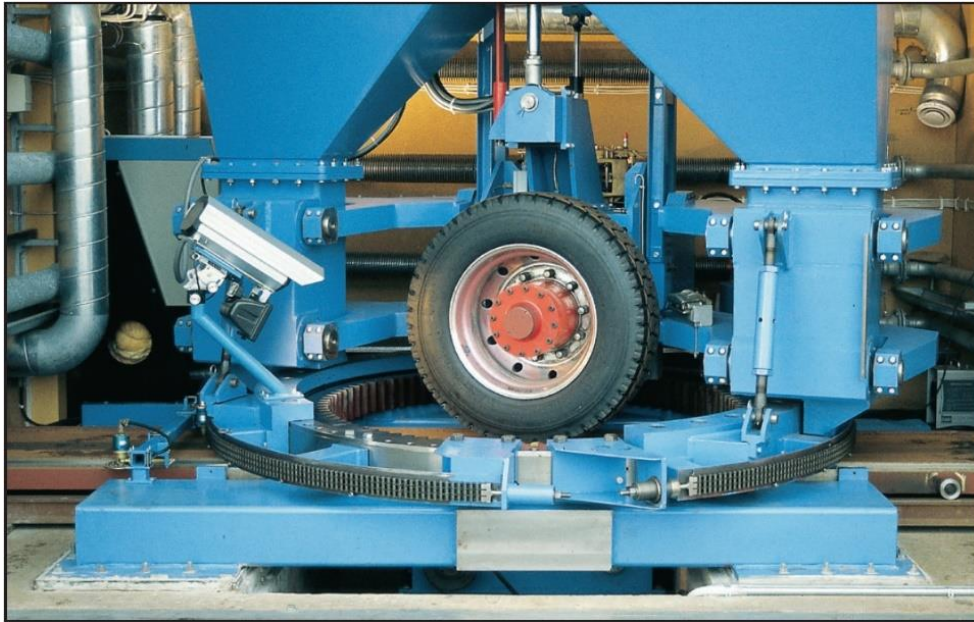
Figure 23. The VTI tire test facility.

Test vehicle: BMW M8 competition. Static wheel loads with a driver (90 kg) were measured to be 561 kg (front left), 545 kg (front right), 525 kg (rear left), and 500 kg (rear right).

The wheel loads are quite similar, so it makes sense to use the same wheel loads for the measurements for both tires. A suitable nominal weight for the measurements would be 525 kg, which corresponds to 5150 N. The measurements should also be carried out at higher and lower loads to obtain a load dependent model of the cornering coefficient. Here we have used 50% and 150% of the nominal load, with translates into 2575 and 7725 N respectively.

Table 2. Specified nominal loads and inflation pressure for the test vehicle.

Tire	Model	Rated inflation pressure	Specified nominal load
Front	Pirelli P Zero 275/35 ZR20 102Y XL	3.2 bar	5150 N
Rear	Pirelli P Zero 285/35 ZR20 104Y XL	3.2 bar	5150 N

For modelling purposes is it convenient to describe the load dependence in terms of the normalized change in vertical load, defined according to Eq. (13).

Since measurements with the test vehicle on the test track was carried out with an inflation pressure of 2.6 bar it was decided to use that pressure together with the noted internal tire temperatures. In addition, to find out the influence of different inflation pressures it was also decided to measure the two tires cold, which corresponds to ca 20°C, at both 2.6 and 3.2 bar. The different measurements are summarized in Table 3.

Table 3. Measurement matrix for VTI tire measurement

Tire	Tire temp	Inflation pressure	Wheel load
Front	Cold (ca. 20°C)	2.6 bar, 3.2 bar	2575, 5150, 7725 N

Deliverable No. D3.6
Version 02
Project no. 101069576

Title
Vehicle dynamics modelling methodology

ROADVIEW

Front	Heated (50°C)	2.6 bar	2575, 5150, 7725 N
Rear	Cold (ca. 20°C)	2.6 bar, 3.2 bar	2575, 5150, 7725 N
Rear	Heated (40°C)	2.6 bar	2575, 5150, 7725 N

For each test condition, three separate measurements will be carried out: measurements of the lateral force at the fixed slip angles -1,.0 and +1 degrees. The cornering coefficient would then be calculated from a linear fit of the normalized lateral force at the different slip angles.

In addition, the vertical stiffness and the loaded tire radius, as well as the effective rolling radius at low speed can be measured.

To obtain the load dependence of the cornering coefficient the data points could be fitted either to the Magic Formula (MF) description of CC load dependence described by Eq. (18), or the linear load dependence of the ISO model, as in Eq.(45). For simplicity we have decided to use the ISO model and the results are presented in section 66.

4.4 Dynamic tests

The dynamic tests encompass the generation of a dataset of the vehicle data under specific manoeuvres. These data shall be further processed using the parametrisation method, using the direct calculation of parameters of the iterative optimization of the unknown values. To accelerate the optimization process, manoeuvres that decouple the longitudinal and lateral movements are desired, since it enables a separated optimization of the longitudinal e lateral models.

Isermann [23] indicates different manoeuvres used for the parametrisation and validation of vehicle dynamics models. Similarly, standards as DIN/OSI 4138 [25], DIN/OSI 7401 [26], DIN/OSI 7975 [27] and DIN/OSI 3888 [28] give example of manoeuvres and the required parameters to validate the vehicle dynamics model. Based on the literature three different manoeuvres are selected for the data collection:

- Acceleration and braking: This test case focused on the longitudinal behaviour of the vehicle, including the powertrain and body parameters. The tests are conducted in three different target velocities (30 km/h, 50 km/h and 70 km/h) using the same acceleration area, consequently obtaining different acceleration profiles. Additionally, a free rolling is conducted and after 55 m the vehicle is braked to standstill as shown in the Figure 24. Two deceleration profiles are considered, full brake, and a comfortable deceleration used in normal traffic. The test is also conducted with fixed 1st and 2nd gear to enable the collection of the data without the influence of the gear changing. In 1st gear only tests on 30 km/h are conducted in in 2nd gear tests on 30 km/h and 50 km/h are performed.
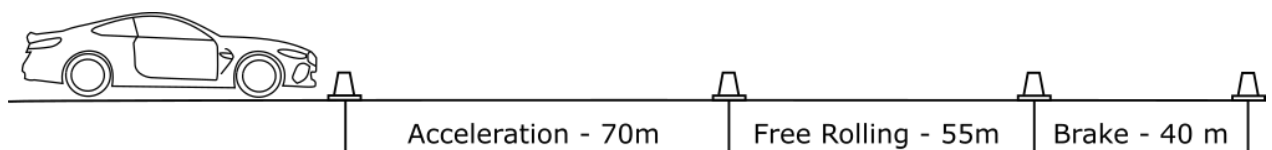
Figure 24. Acceleration and braking testing.

- Step steering: Consist of entering a circle with constant radius, as shown in Figure 25, and maintaining the vehicle with constant velocity and lateral acceleration during three loops. Ideally a step input on the steering wheel is expected when entering the circle, however due to the hardware limitations a ramp behaviour is generated. This enables to evaluate the lateral behaviour with a constant longitudinal and lateral input as well as with a transient behaviour when entering the circle. This test is conducted at 30 km/h, 40 km/h and 50 km/h.

Deliverable No. D3.6
Version 02
Project no. 101069576

Title
Vehicle dynamics modelling methodology

ROADVIEW
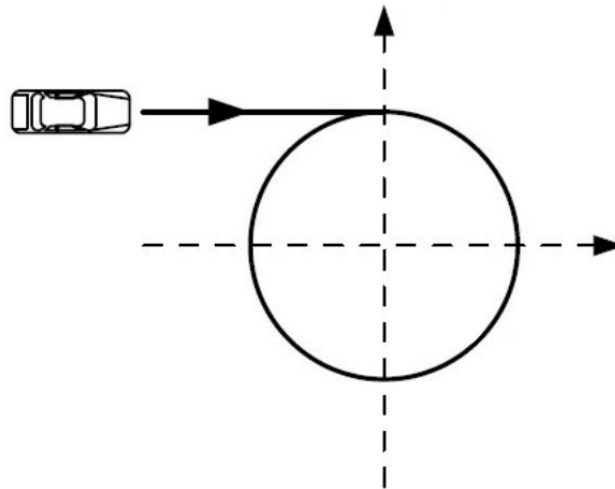
Figure 25. Step steering manoeuvre [23].

- Double lane change: This manoeuvre comprehends the lateral transient behaviour of the vehicle and consist of a lateral change on the vehicle trajectory as shown in Figure 26. This manoeuvre is conducted at 30 km/h, 50 km/h and 70 km/h.
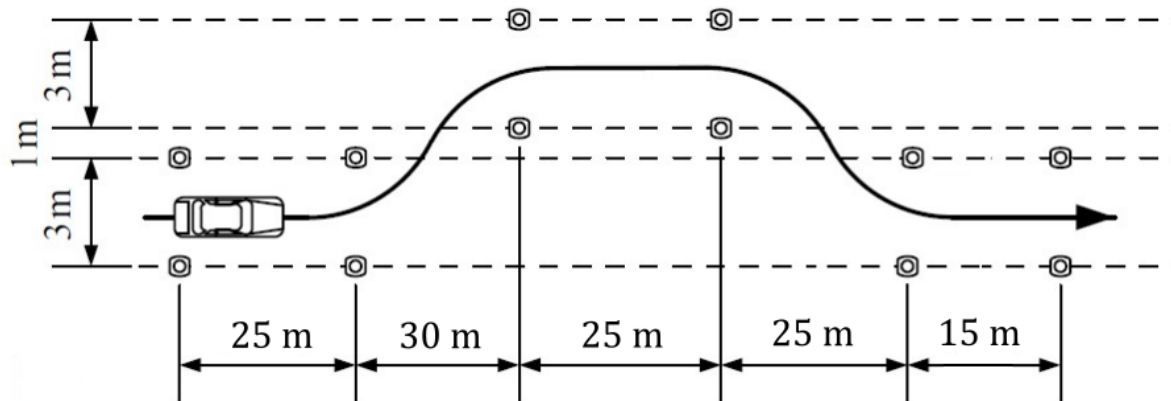
Figure 26. Double lane change manoeuvre [23].

All tests are conducted by the same driver and are repeated three times on both dry and wet surfaces.

The data collection was conducted with the test vehicle from CARISSMA Institute of Automated Driving (C-IAD), a BMW M8 Competition with access to the CAN-bus data. Furthermore, a high precision positioning system from Genesys based on GNSS and IMU are attached to the vehicle, together with a Road Weather Information Sensor from Marwis and an onboarding camera for recording the driver and the conducted tests. Figure 27 shown the test vehicle and the integrated equipment. The tire pressure and temperature are shown in the vehicle dashboard and recorded with the onboard camera as shown in Figure 28. Appendix B present the data measured during the tests.
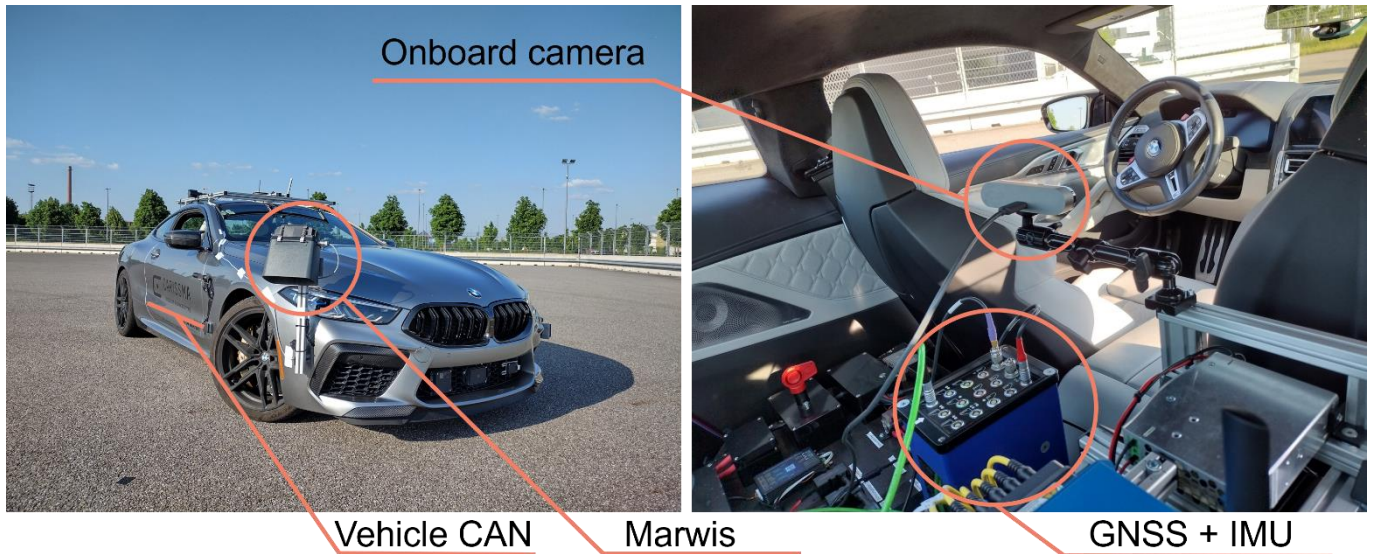
Figure 27. CARISSMA test vehicle and integrated equipment.

Figure 28. Onboard Camera.

All the tests are conducted on the outdoor test track of C-IAD and a sprinkler system is used to wet the road surface. Each sprinkle covers a semicircle with 9 m radius and 180° aperture. A total of 20 sprinkles are positioned with 9 meters between them. Figure 29 shows the double lane change manoeuvre on wet surface and it is possible to identify the location of the sprinkles during the tests. The position of the sprinkles is adapted to each test case to guarantee that the surface is properly wet on the driveable areas.

Deliverable No. D3.6
Version 02
Project no. 101069576

Title
Vehicle dynamics modelling methodology

ROADVIEW

Figure 29. Data collection on wet road surface.

5   Parameter Estimation Method

To obtain the parameters required for the vehicle model, the data collected in the experiments described in the Chapter 4 is processed through the direct calculation/measurement of the values or through the optimization process. This chapter describes the process implemented for obtaining the required parameters.

5.1   Calculated parameters

To reduce the number of parameters to be optimized, parameters that can be directly measured or calculated from the collected data are obtained in a separated process. The implemented methods are presented in the next subchapters according to the correspondent model modules.

5.1.1   Powertrain

The calculations from the powertrain consist of the definition of the torque converter parameters which depends on the velocity ratio between engine and transmission and transmission parameters that are dependent of the gas pedal position and the selected gear. Since these parameters are dynamic, according to the current state, the iterative optimization of them is limited and a separated analysis is conducted.

5.1.1.1   Torque Converter

The converter factor and the torque ratio of the torque converter variate according to the velocity ratio between engine and transmission. To obtain these curves, the manoeuvre of acceleration in 2nd gear with a target velocity of 50 km/h is used. For this approach only the section with positive acceleration is considered. For the definition of the parameters the torque and velocity on the turbine as well as on the impeller are required. Torque and velocity are available in the real vehicle only on the wheels, while the engine rotation is used as the impeller rotation since both systems are mechanically attached. Initially, it is necessary to transpose the wheel velocity and torque to the turbine, based on the gear ratio of the system as shown in Eq. (79) and Eq. (80) respectively.

Deliverable No. D3.6
Version 02
Project no. 101069576

Title
Vehicle dynamics modelling methodology

ROADVIEW

$$\omega_T = \overline{\omega_W} * i_F \tag{79}$$

$$T_T = \frac{\overline{T_W}}{i_F * \eta_P} \tag{80}$$

The engine rotation is directly measured from the real data and the available engine torque is calculated based on the engine torque curve and the gas pedal position. Furthermore, the acceleration of the engine is calculated by the derivation of the engine rotation and the impeller torque is calculated based on the Eq. (30). As an initial guess the engine inertia can be considered as one and optimized during the next steps.

Finally, the converter factor and the torque ratio can be calculated by the Eq. (28) and Eq. (29) respectively. The obtained results are then interpolated and a curve with 11 points with velocity factors from 0 to 1 are stored.

By manually investigating the impeller and turbine rotations of the acceleration and braking manoeuvre at the second gear the luck up ratio can be identified. Similarly, by evaluating the acceleration and braking manoeuvre with automatic transmission and target speed of 70 km/h, the converter sync time is defined.

5.1.1.2   Transmission

The lookup table used for the gear change is obtained by evaluating all the tests conducted with automatic gear change. From this data, the engine rotation in which the gear changes up and down are grouped according to the previous gear and the gas pedal position. The gas pedal position is rounded in a resolution of 10% to split the obtained values in 11 groups for each gear. The average of the engine rotation for each one of the groups is finally calculated and the missing groups are manually fulfilled based on the neighbouring values.

The minimum and maximum engine rotation observed in all evaluated tests are also stored and taken as reference for the model.

5.1.2   Tires

The data collection on the test bench does not enable the calculation of the longitudinal slip stiffness. This parameter is then obtained from the acceleration manoeuvre at the dry asphalt with the target speed of 70 km/h. For this evaluation only the acceleration section of the manoeuvre is considered. To avoid noise derived from the calculation of slip at low speed only data collected at velocity higher than 30 km/h are considered. In Figure 30 the selected data is highlighted with a thicker line.
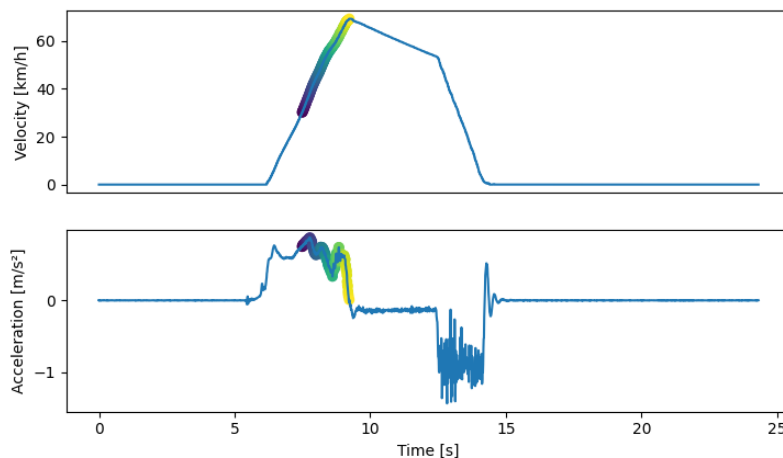
Figure 30. Acceleration and braking manoeuvre, target speed 70 km/h – Selection for longitudinal slip stiffness calculation.

Deliverable No. D3.6
Version 02
Project no. 101069576

Title
Vehicle dynamics modelling methodology

ROADVIEW

Based on this data the longitudinal slip is calculated for each one of the time steps using the Eq. (34). Fitting a linear function of the longitudinal acceleration in gas function of the slip angle enabled the estimation of the longitudinal slip stiffness, using the inclination of the fitted line.

The peak friction of the tire is a parameter that do not depend only on the tire characteristics but is strongly connected to the interaction between ground and the tire. Due to that the peak friction cannot be measured at the test bench and need to be evaluated directly on the proving ground. For this evaluation the full braking manoeuvre at 70 km/h is selected. According to previous results from VTI as well the collected data, the anti-lock brake system (ABS) is more permissive than the traction control, and decelerations nearer to the limit of the tires can be obtained during the braking manoeuvre. The peak friction is the main parameter responsible for the changes of the vehicle behaviour under extreme weather conditions, and due to that an important parameter in the ROADVIEW project.

All three repetitions are used for this evaluation and an average value is obtained in the end. The calculation consists of measuring the average deceleration of the vehicle during the full brake section. The obtained value in g can be directly applied as peak value. To obtain a smooth value, the average deceleration is directly calculated from the difference in the velocity at two different points selected in the deceleration zone.

5.2 Optimized parameters

Some parameters cannot be calculated by the simple observation of the vehicle in steady state or dynamics manoeuvres and require expensive and time intensive test benches. To overcome these limitations these parameters can be optimized by an iterative comparison of the model and the manoeuvres of the real vehicle. This section describes how, and specifically which parameters are optimized in the three main core components of the proposed vehicle dynamics model.

The main optimization methods are the L-BFGS-B [24] [25] and the differential evolution [26]. The BFGS method uses a quasi-Newton method, the name comes from the name of the developers Broyden, Fletcher, Goldfarb, and Shanno, the L-BFGS method is a limited version of the BFGS method which was superseded by the L-BFGS-B [24] [25] with the bounded version of the same algorithm. This is a gradient descent method, which means that given a scalar field defined as

$$f(\mathcal{R}^n) = \mathcal{R}^m, \tag{81}$$

the gradient (∇f) of this scalar field can be defined as

$$(\nabla f)_j = \frac{\partial f}{\partial x_j} \tag{82}$$

and is a vector field. This method is a gradient descent because it minimizes the gradient, but to do that it requires the derivates of the gradient, the Jacobian (J) defined as

$$J_{i,j} = \frac{\partial F_i}{\partial x_j} \tag{83}$$

where F is a singular function from ∇f. This method also requires the Hessian which is defined as

Deliverable No. D3.6
Version 02
Project no. 101069576

Title
Vehicle dynamics modelling methodology

ROADVIEW

$$H_{i,j} = \frac{\partial^2 f}{\partial x_i \partial x_j} \tag{84}$$

remembering that f is the scalar field. To do the gradient descent, the BFGS algorithm starts with an initial guess x_0 and interactively gets closer to a minimum x_k. The interactive method implemented in Fortran to find minimum x_k can be seen in [24]. To increase the temporal efficiency, this algorithm in its parallelized version developed by [27] is utilized.

The L-BFGS-B method is appropriate to find minimums, but in case there are many plateaus the gradient and its derivates will be 0 and this method will not be effective in finding a minimal value. In cases where the minima are surrounded by many plateaus in the answer space, stochastic methods are better suited to find the global minima, because it does not depend on gradients and its derivates. An example of this is the differential evolution (DE) [26]. The main disadvantage of this method is that it requires more function call to find the minima. Though it has a larger answer space than gradient based alternatives. The DE´s process works by assembling a population with agents which evaluate the function in the search space, should an agent have an improvement of the minima, it is added to the population, when the new agent difference to the current population is lower than a predefined threshold, or it hits the limit of iterations, the optimization is concluded. The implemented routines also counts with multiprocessing which allows the faster execution of the optimization by using all CPU cores of the computer.

To improve the convergence of the parameters while working with the data available on the real test vehicle the optimization method is divided into three optimization routines (Powertrain, Longitudinal effect, and Lateral effect). The powertrain routine aims to optimise the parameters of the powertrain module. Since the forces on the wheels are not available in the real data, the wheels and body modules are optimized together, however, to improve the optimisation process the longitudinal and lateral behaviours are evaluated separately in two different routines. The next sub-sections show the implemented optimization routines.

5.2.1   Powertrain optimization routine

The powertrain routine computes the gas pedal and brake inputs and outputs the torque on the wheels of the vehicle. All this information can be measured from the real vehicle and the L-BFGS-B optimization method is implemented to minimise the Root Mean Square Error (RMSE) of the torque on the wheels. The optimization is done using the acceleration manoeuvre with automatic transmission and target velocity of 70 km/h to reach a bigger range of the engine performance. The parameters optimised as well as the initial value and boundaries used in this optimisation are shown in Table 4.

Table 4. Optimization parameters powertrain.

Parameter	Initial Value	Inferior Boundary	Superior Boundary	Unit
Engine Inertia	0.8	0.1	8.0	kgm²
Gearbox Efficiency	0.95	0.7	1.0	%
Gearbox Inertia	1.0	0.01	3.0	kgm²
Front Wheel Inertia	1.0	0.1	3.0	kgm²
Rear Wheel Inertia	1.0	0.1	3.0	kgm²

5.2.2   Longitudinal effect optimization routine

The interaction between the wheels and body modules is done by the forces acting on the wheels, which are not measurable on the available test vehicle. To overcome this limitation, the body and wheel modules are optimized together and to reduce the number of parameters to be optimised in each one of the interactions the optimisation was divided in longitudinal and lateral effects.

Deliverable No. D3.6
Version 02
Project no. 101069576

Title
Vehicle dynamics modelling methodology

ROADVIEW

For the longitudinal effects routine, the torque on the wheels and the steering wheel angle is taken as input and the final output is the movement of the vehicle. The acceleration and braking manoeuvre with target velocity of 70 km/h is used, to avoid the interaction with the lateral movement of the vehicle. The RMSE of the pitch rate and longitudinal acceleration is minimised, and the L-BFGS-B method is implemented to optimise the parameters shown in Table 5.

Table 5. Optimisation parameters longitudinal movement of the chassis.

Parameter	Initial Value	Inferior Boundary	Superior Boundary	Unit
Front Spring Rate	15000.0	10000.0	30000.0	N/m
Rear Spring Rate	20000.0	10000.0	30000.0	N/m
Front Damping Rate	7000.0	3000.0	8000.0	Ns/m
Rear Damping Rate	6000.0	3000.0	8000.0	Ns/m
Pitch Centre height	0.45	0.1	0.7	m
Pitch Inertia	1950.0	1500.0	3000.0	kgm²
Front Unsprung mass	80.0	50.0	100.0	kg
Rear Unspring mass	70.0	50.0	100.0	kg

5.2.3   Lateral effect optimisation routine

The optimisation of the parameter that involves the lateral movement of the vehicle takes the torque on the wheels and the steering wheel angle as input and the final output is the movement of the vehicle. The double lane change manoeuvre with target velocity of 70 km/h is implemented to include the lateral behaviour of the vehicle. The RMSE of the yaw, lateral acceleration and roll are minimised, and the L-BFGS-B method is implemented to optimise the parameters shown in Table 6.

Table 6. Optimisation parameters lateral movement of the chassis.

Parameter	Initial Value	Inferior Boundary	Superior Boundary	Unit
Roll Bar Stiffness	0.8	0.1	8.0	N/m
Roll Centre Height	0.95	0.7	1.0	m
Roll Inertia	1.0	0.01	3.0	kgm²
Yaw Inertia	1.0	0.1	3.0	kgm²

Deliverable No. D3.6
Version 02
Project no. 101069576

Title
Vehicle dynamics modelling methodology

ROADVIEW

6   Results

This chapter discusses the results obtained from the proposed vehicle dynamics as well as the results from the proposed parameters estimation methodology, which are divided in two subsections.

6.1   Validation of the vehicle dynamics model with the simulation

By applying the same input signal in the CM simulator and on the implemented vehicle dynamics model, it is possible to evaluate the obtained results and compare the validity of the implemented model.

To facilitate the debugging process, the 3 modules (powertrain, wheels and body) are validated separately. The input and output variables of each module are exported from CM and compared with the results obtained from each module. The next subsections show the results of the validation according to each one of the modules.

6.1.1   Powertrain module

The powertrain module is stimulated with the following parameters:

- Gas pedal position
- Brake Pedal Position
- Longitudinal Velocity
- Wheel angular velocity

Figure 31 and Figure 32 demonstrate a comparison between the CM model and the results obtained from the vehicle dynamics model implemented in ROADVIEW.
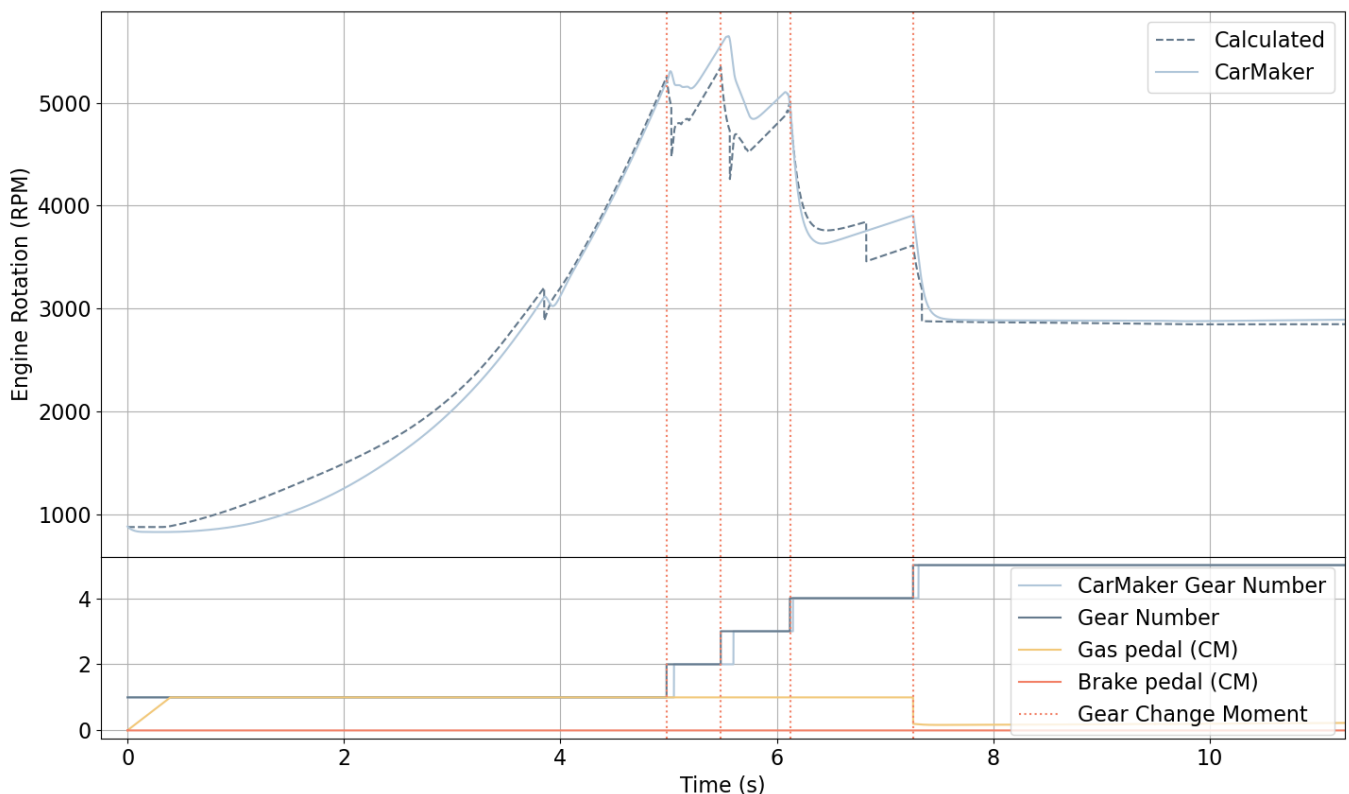
Figure 31. Powertrain engine rotation - CM and ROADVIEW vehicle dynamics model.

Figure 31 shows the engine rotation (revolutions per minute, in dark blue - calculated using CM inputs, light blue – CM calculated) in the main graph and in the auxiliary graph the Gear number (dark blue – calculated using CM inputs, light blue – CM calculated), gas pedal (orange), and brake pedal (red), this last two are inputs from CM also used as inputs in vehicle dynamics model. The vertical lines in red show when the gear changed. It is important to notice that

Deliverable No. D3.6
Version 02
Project no. 101069576

Title
Vehicle dynamics modelling methodology

ROADVIEW

the algorithm that is proposed in this work has a simplified implementation in comparison to the CM model, therefore the outputs will be slightly different. Upon analysis of the data reported on Figure 31, it can be observed that the engine rotation, calculated by the proposed models, follows the CM calculation closely. Also, it is important to notice that the gear shifts, are very close to that of the CM calculation, indicating a very close relationship between the proposed model and the CM calculation. At approximately 4s, 3000RPM in the main graph, it is visible when the torque converter from both the CM and the proposed vehicle dynamics models locks, enabling the full transference of the torque, between 4s and 5 seconds the torque being transferred to the wheels is bigger in the proposed model, most probably due to the simplification applied for a perfect coupling between engine and transmission.
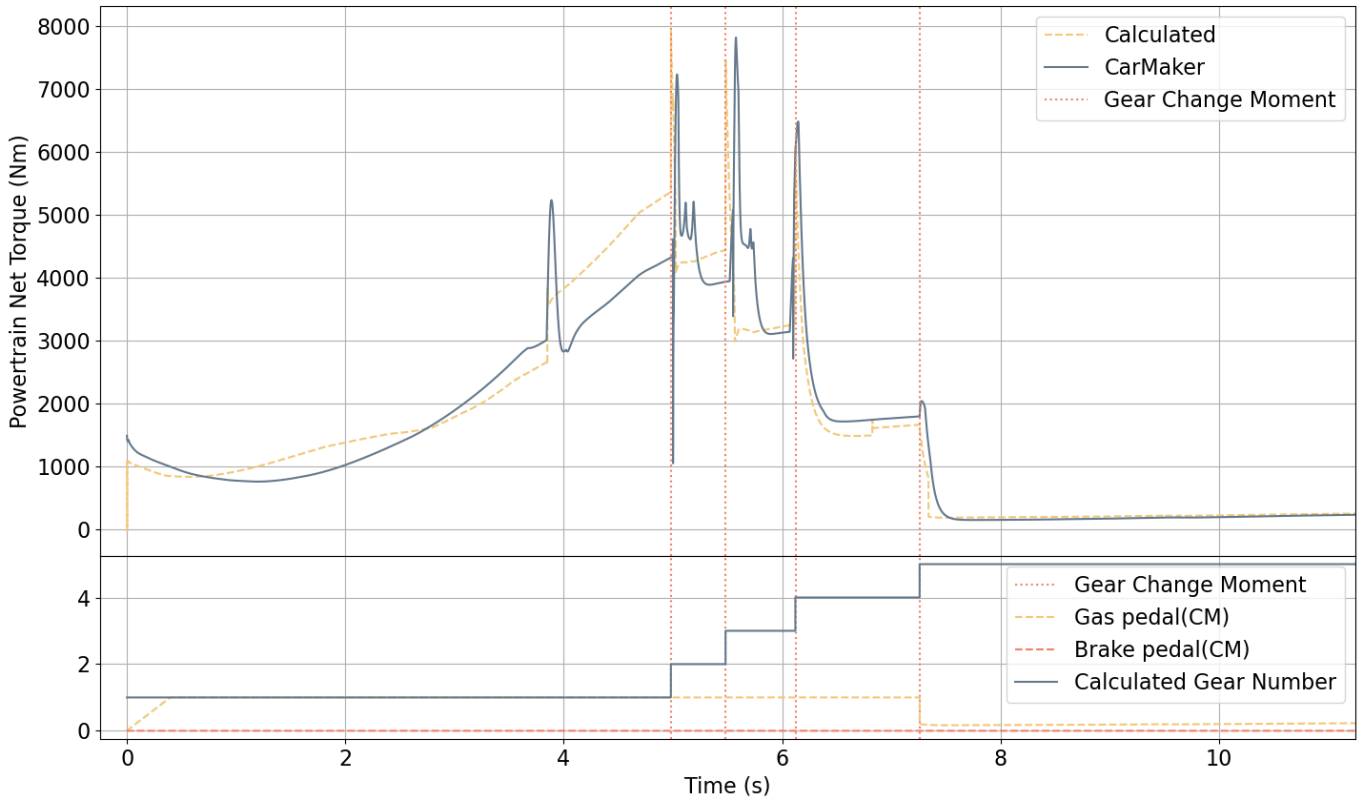
Figure 32. Powertrain torque - CM and ROADVIEW vehicle dynamics model.

Figure 32 also shows the gas pedal (yellow) and the brake pedal (red) in the auxiliary graph, and the powertrain net torque (in yellow – calculated from the proposed model, in blue - calculated from CM) in the main graph. Again, a similar behaviour is observed in the proposed vehicle dynamics model and the CM model.

6.1.2 Wheels module

The wheels module uses the torque generated by the engine as input and based on the wheel angles and velocity calculates the forces being induced on the ground. The inputs required from CM include:

- Orientation states (roll, pitch, yaw)
- Velocities (x, y, z)
- Yaw rate
- Powertrain torque
- Steering wheel angle

The first step on the wheels module is to calculate the longitudinal slip, the obtained results are shown in Figure 33. All graphics presented in this report consider the car from a bird's eye view with the car pointing up. The wheel position is determined as Front Right (FR), Front Left (FL), Rear Right (RR) and Rear Left (RL).
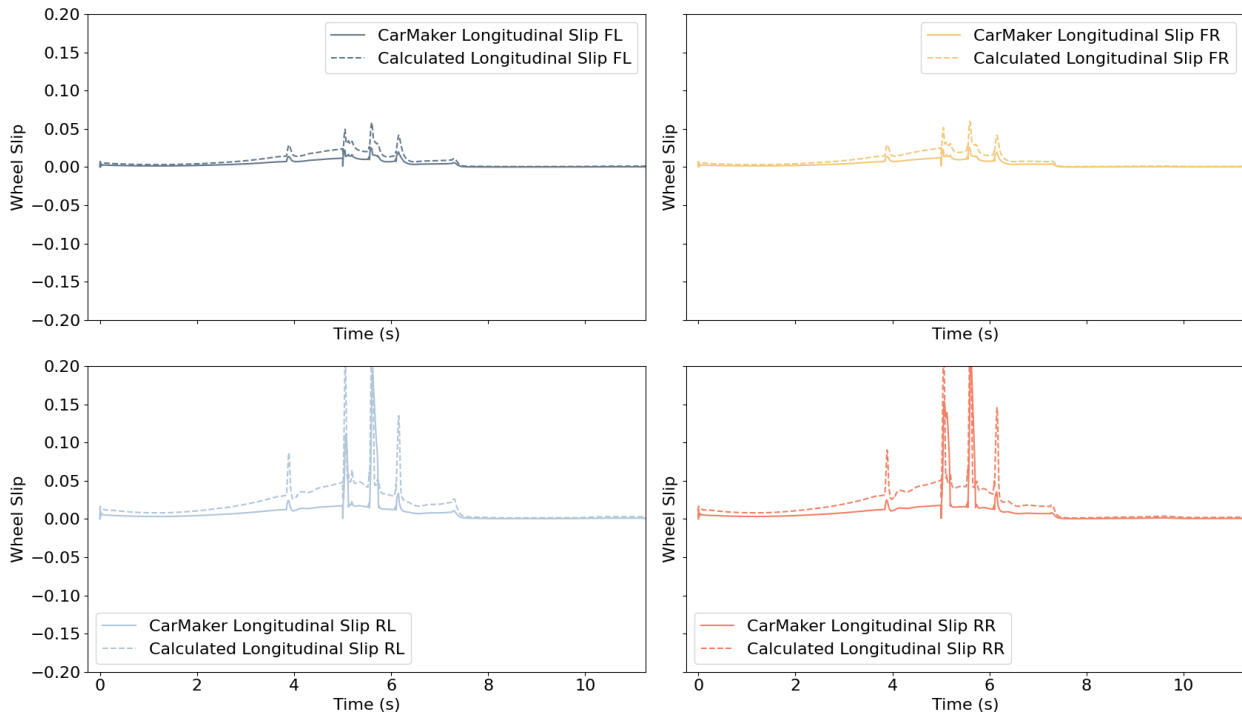
Figure 33. Longitudinal tire slip - CM and ROADVIEW vehicle dynamics model.

Figure 33 shows the longitudinal slip of the four wheels of the car, the dotted line is from the proposed vehicle dynamics model and the solid line is from the CM. It is interesting to note that the behaviour of the slip calculated by the proposed vehicle dynamics model is very similar to that of CM at the front wheels. Note that the rear wheels are not as well aligned as the front wheels but follow the desired behaviour. This can be caused by different torque distributions on CarMaker and the proposed vehicle dynamics model.

The next step is to calculate the lateral slip, which is shown in Figure 34.
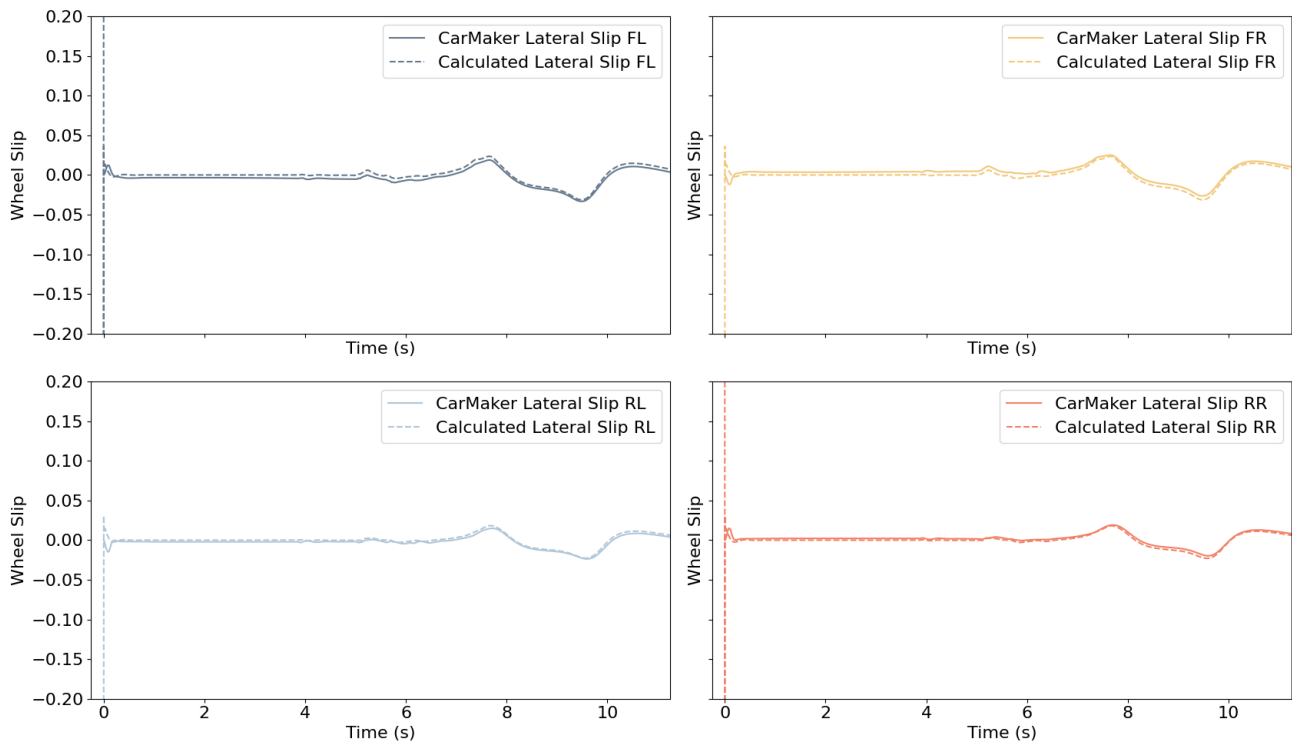
Figure 34. Lateral tire slip.

Deliverable No. D3.6
Version 02
Project no. 101069576

Title
Vehicle dynamics modelling methodology

ROADVIEW

It also follows the colour convention from Figure 33, and the lateral slip matches the slip angles calculated by CM very well. The initial high values obtained in the proposed model are result of the wheel known instability of the slip calculation in very low velocities. With both lateral and longitudinal slips, it is possible to calculate the wheel velocity, shown in Figure 35.
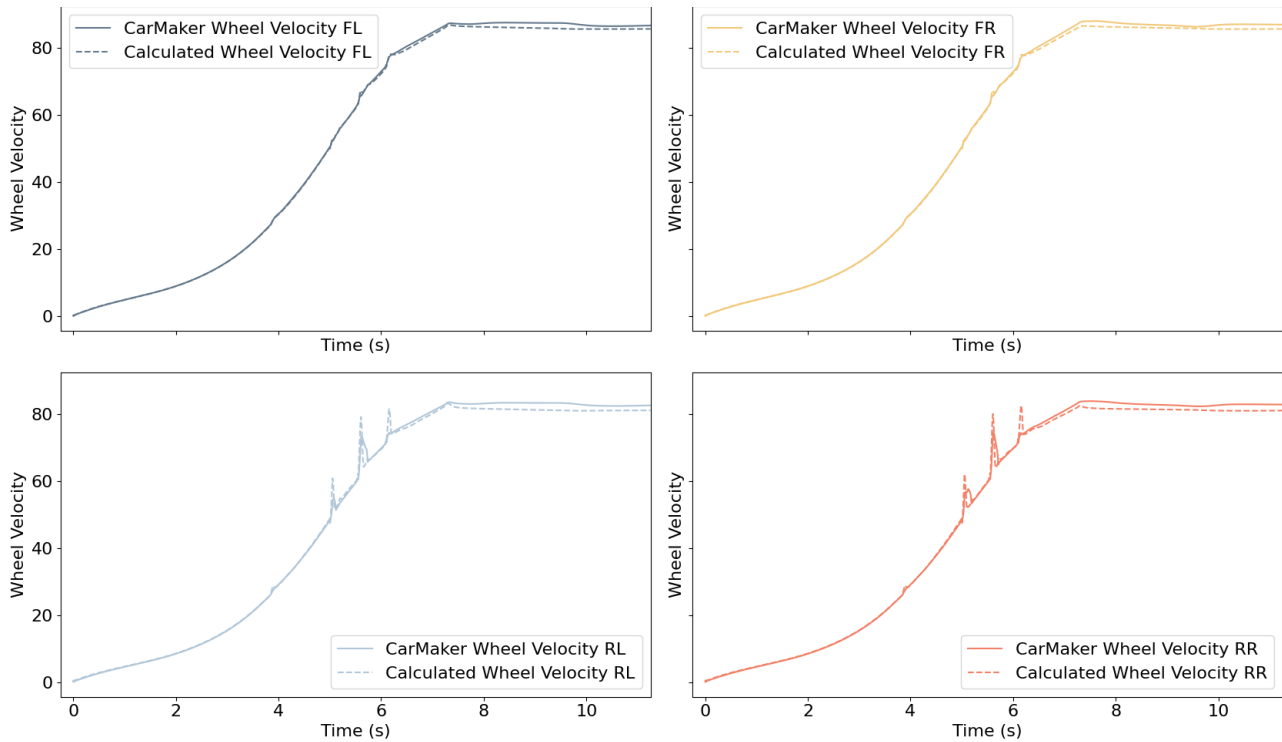
Figure 35. Wheel Velocity - CM and ROADVIEW vehicle dynamics model.

Figure 35 also follows the colour convention from Figure 33, and denotes a close relationship between the calculated wheel velocities and the wheel velocity exported from CM. Finally, the wheel forces can be calculated, the comparison with CM for the longitudinal tire forces is shown in Figure 36.
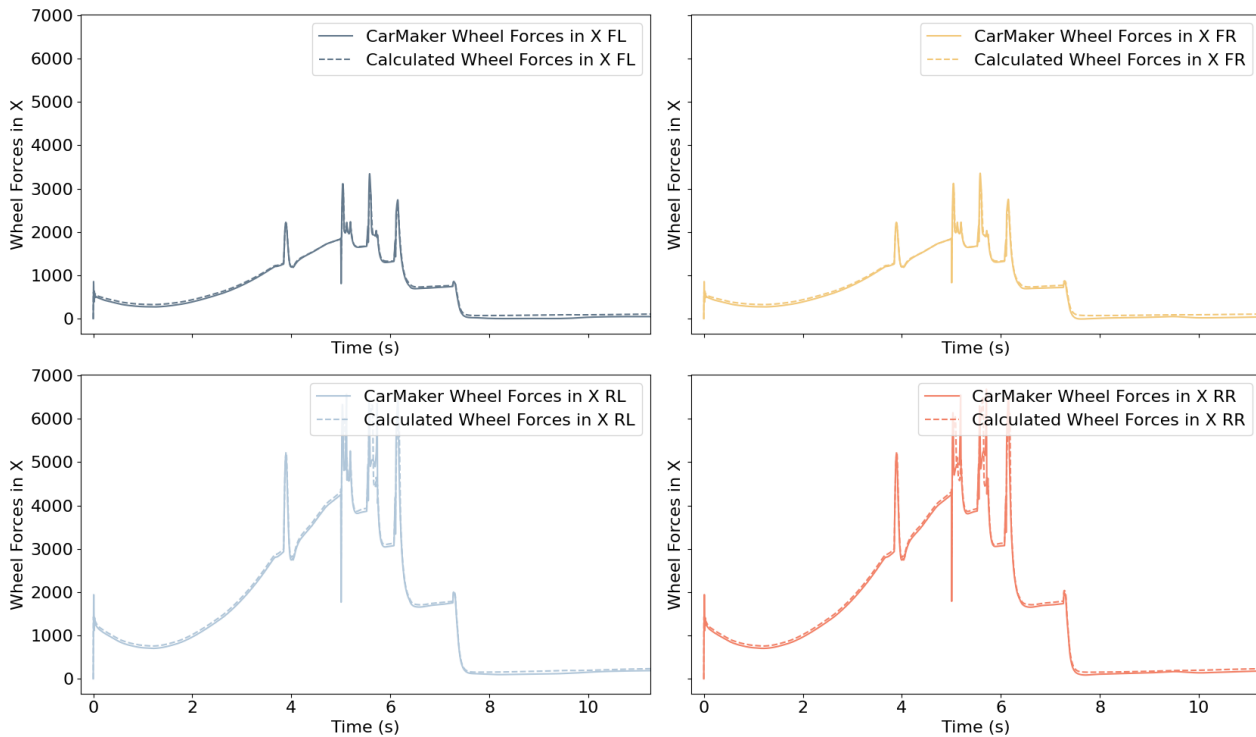
Figure 36. Longitudinal wheel forces - CM and ROADVIEW vehicle dynamics model.

The results from Figure 36 show a correct behaviour of the tire models and slip calculation, generating similar force on the wheels when comparing the implemented model with CM. This result confirms the validity of the implemented model, even when comparing with a more complex model as the CM implementation.

6.1.3 Body module

The body module calculates the full movement of the body based on the longitudinal and lateral forces from the wheels. Figure 37 shows the vertical forces calculated by the model based on the longitudinal and lateral wheel forces in comparison to the results from CM.

Deliverable No. D3.6
Version 02
Project no. 101069576

Title
Vehicle dynamics modelling methodology
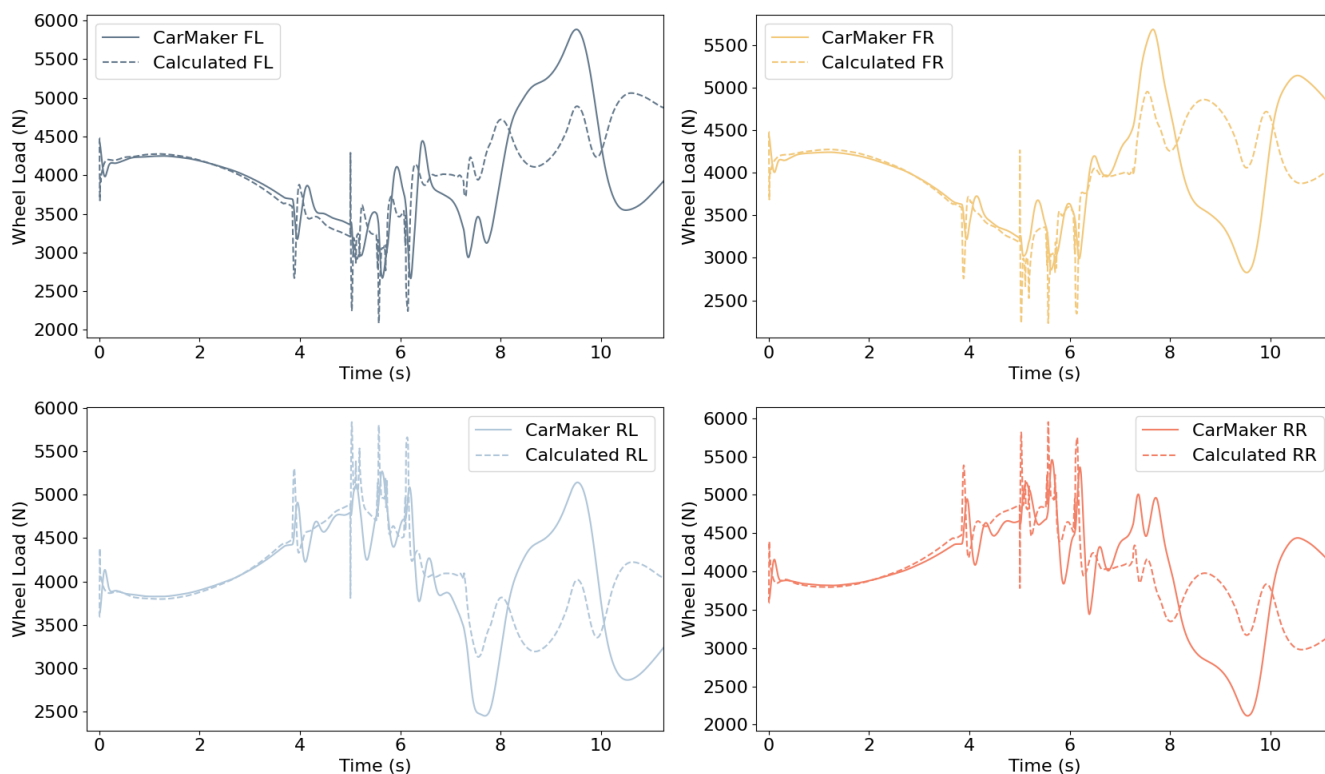
ROADVIEW

Figure 37. Vertical wheel loads - CM and ROADVIEW vehicle dynamics model.

Figure 37 shows each vertical wheel force from a top view of the car. The forces exported from CM are shown in solid lines while the doted lines are the values calculated by the ROADVIEW vehicle dynamics model. It is possible to highlight a limitation of the implemented model in describing the lateral load transference which shall be investigated and improved during the integration process. The longitudinal behaviour on the other hand fits perfectly the behaviour from the CM vehicle.

Based on the available forces the body module calculates the resulting acceleration of the chassis, which is shown in Figure 38. The dotted line shows the accelerations calculated in the ROADVIEW model and the solid lines are the values exported from CM, in dark blue – the X acceleration, in light blue – the Y acceleration, and in yellow – the Z acceleration. Noticeably, the X are spot on while the acceleration in Y has small deviations. The Z acceleration is in the implemented model simplified and described in a limited way the vertical movement.

Deliverable No. D3.6
Version 02
Project no. 101069576

Title
Vehicle dynamics modelling methodology
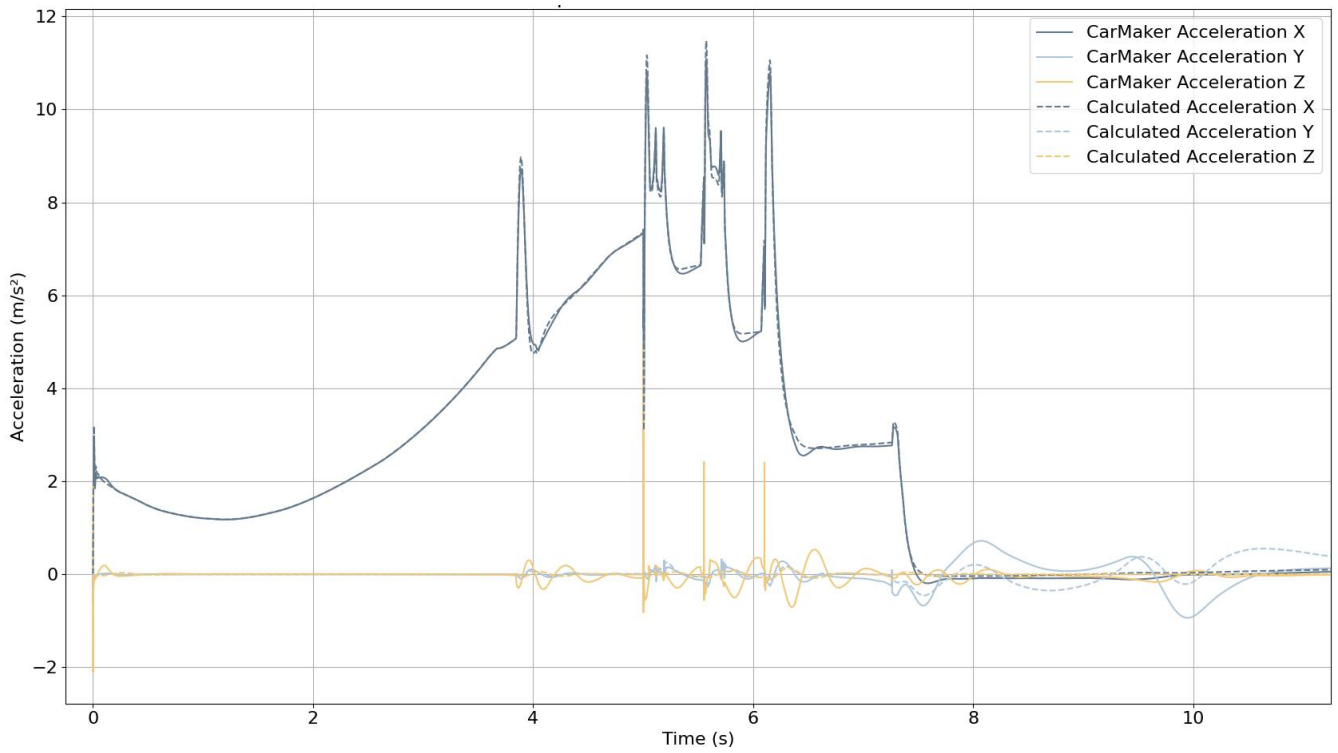
ROADVIEW

Figure 38 Body linear acceleration - CM and ROADVIEW vehicle dynamics model.
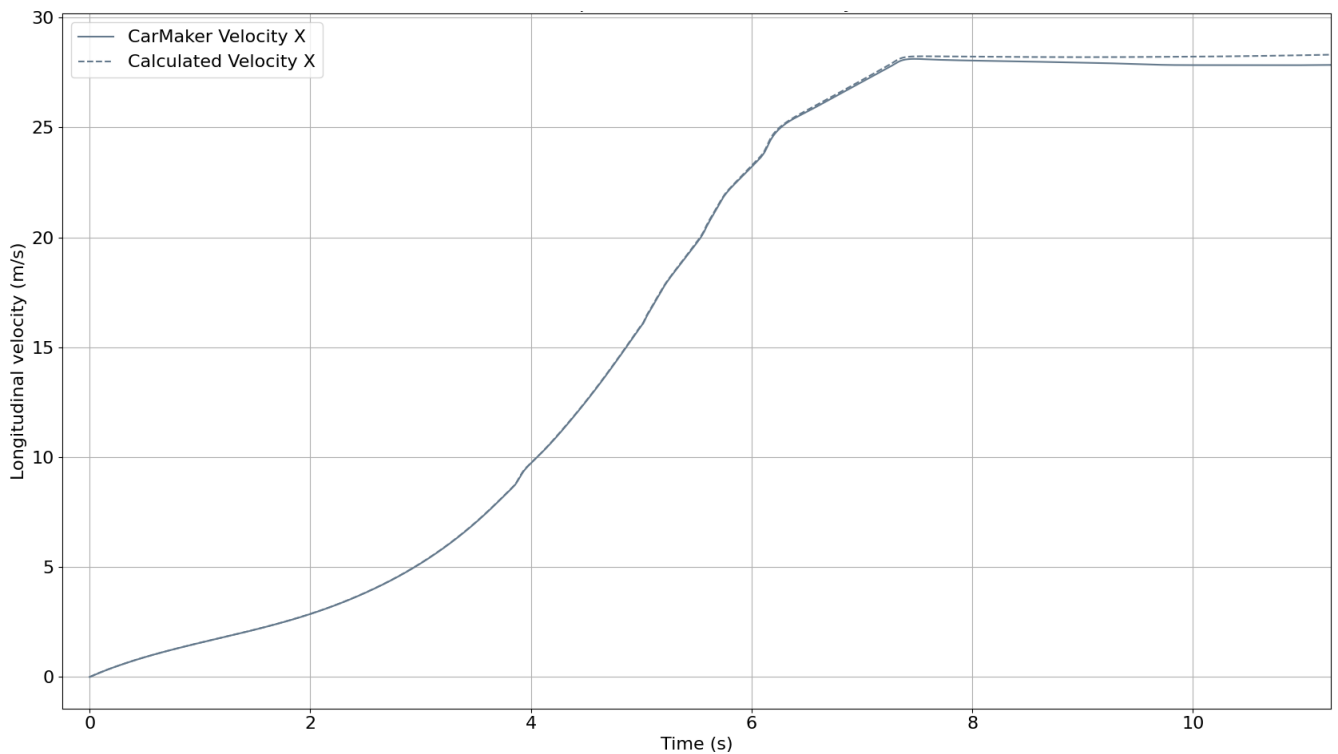
Figure 39. Body linear velocity - CM and ROADVIEW vehicle dynamics model.

The longitudinal velocity is demonstrated in Figure 39. Important to notice the similarity between the calculated velocities and the CM calculation.

Deliverable No. D3.6
Version 02
Project no. 101069576

Title
Vehicle dynamics modelling methodology
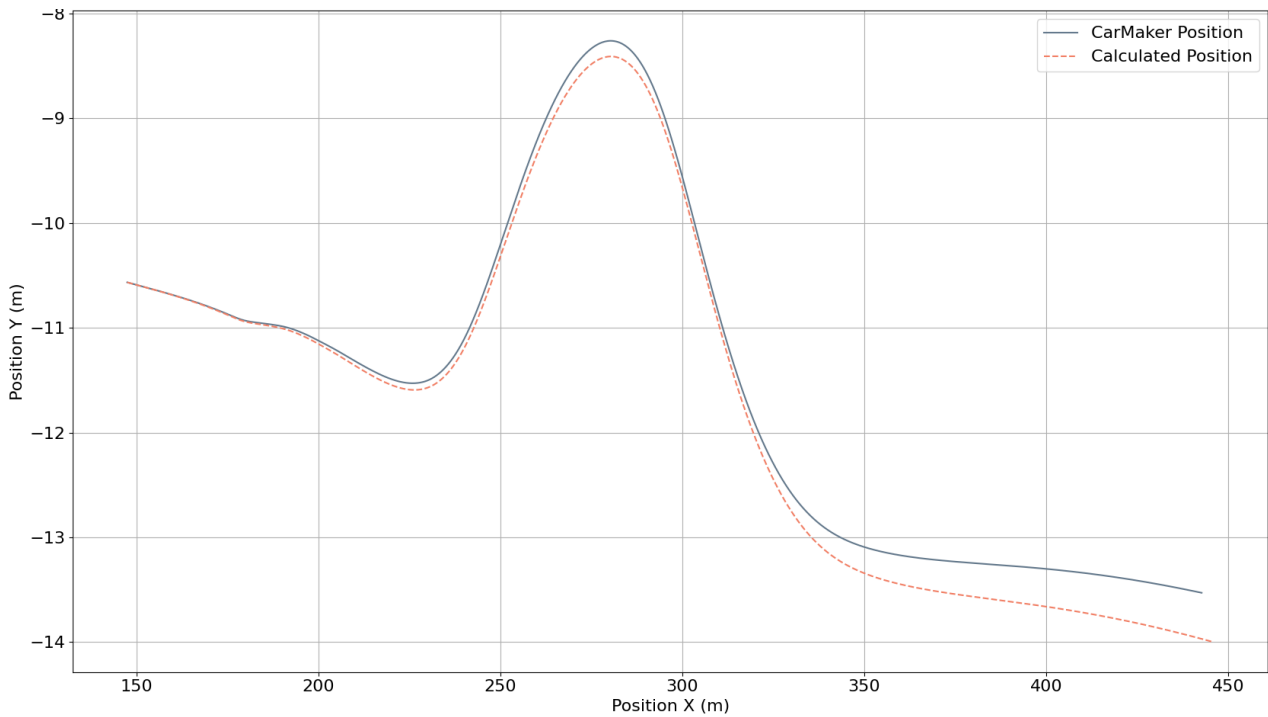
ROADVIEW

Figure 40. Vehicle positioning - CM and ROADVIEW vehicle dynamics model.

Lastly, the final integral from the acceleration is the position, shown in Figure 40, which shows the vehicle position in the global XY coordinates. A very important point is that the presence of minor errors in the acceleration compounds to a larger error in the position (second integral). So, it can be concluded that there is a rather good match between the vehicle positions calculated by the CM and the proposed vehicle dynamics model.
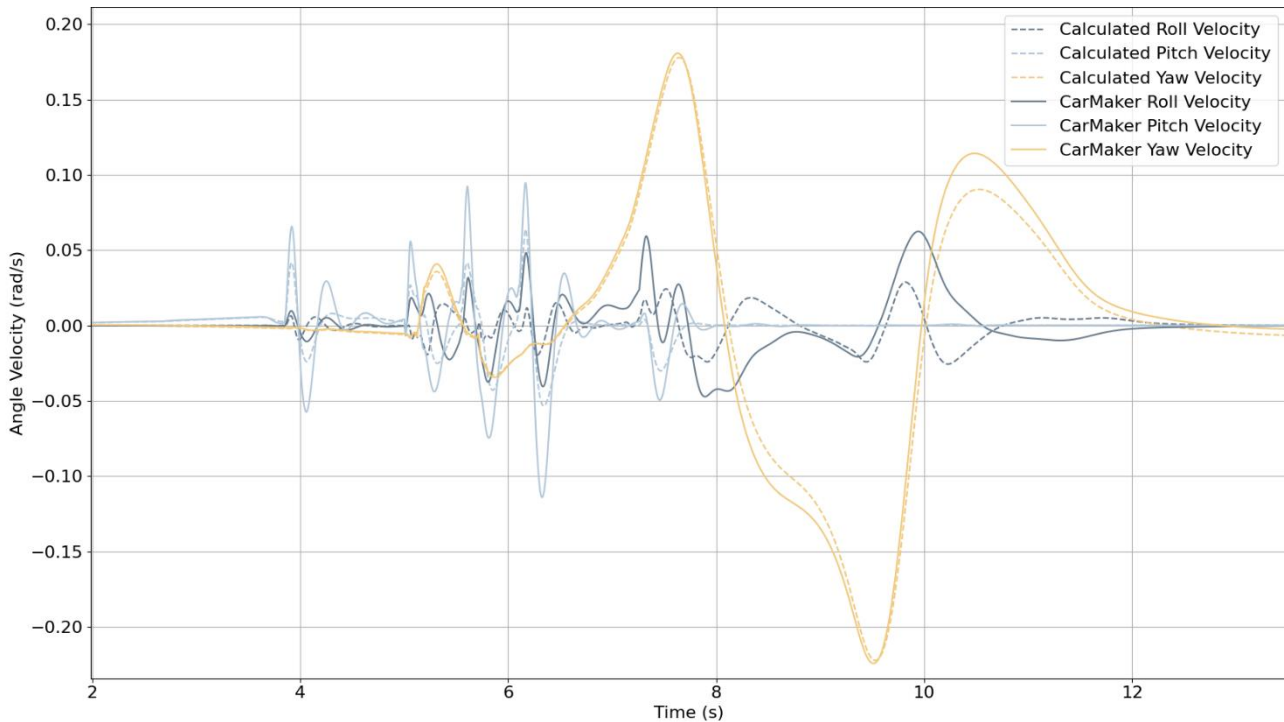
Figure 41. Body orientation rate - CM and ROADVIEW vehicle dynamics model.

Deliverable No. D3.6
Version 02
Project no. 101069576

Title
Vehicle dynamics modelling methodology

ROADVIEW

The body movement could be separated into two parts, the linear position and the orientation, the focus is now shifted from the positional to the rotational part. However, here the comparison starts with the rotational velocities, see Figure 41.

Figure 41 shows the vehicle rotational velocities calculated by the proposed vehicle dynamics model in dotted lines, and the corresponding values from the CM model in dotted lines. In light blue the roll, in dark blue the pitch, and in yellow the yaw. Important to notice that the behaviour from all angles closely follows the data exported from CM. Finally, the body orientation is obtained by integration as shown in Figure 42.
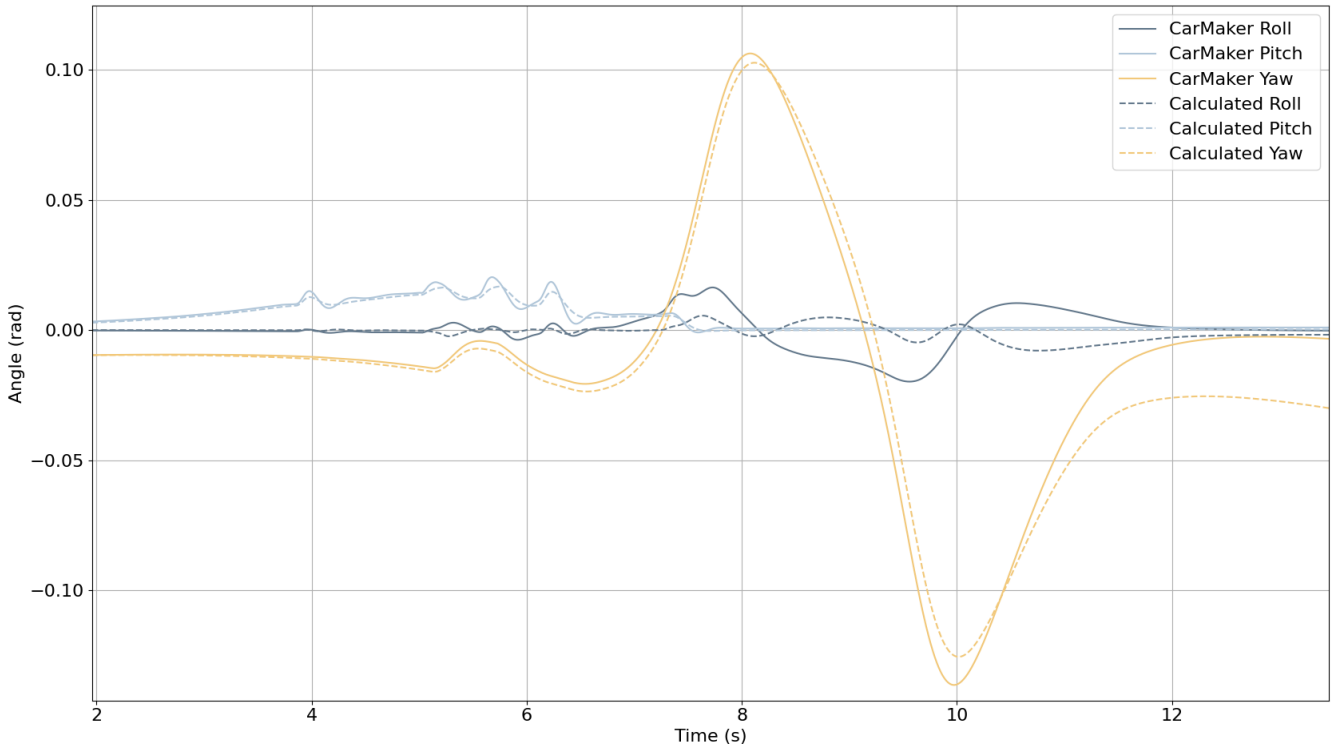
Figure 42. Body orientation - CM and ROADVIEW vehicle dynamics model.

It is possible to directly calculate the angles in Figure 42, which follows the same colour coding from Figure 41. The orientation also closely follows the CM results. It is possible to observe however a small deviation on the vehicle yaw as well as a bigger deviation on the roll of the vehicle.

Overall, the implemented model corresponds the behaviour of the CM models, despite the simplifications conducted to improve the performance of the vehicle. A small improvement can be conducted in the lateral behaviour of the model, including the improvement of lateral acceleration, yaw and roll movements. This improvement will be conducted during the integration in WP7.

6.2   Parameters estimation – CARISSMA DEMO Vehicle

The results of the parameter estimation are shown in the next subchapters, with the deliverable also a ".yaml" file including all the parameters obtained will be made available.

Several parameters from the vehicle dynamics are not made available by the OEM and need to be measured or estimated. Despite that the estimation of the parameters could be directly conducted by an optimization algorithm, parameters that can be measured or calculated are evaluated separately to accelerate the optimization of the model.

6.2.1   Documentation research

The required parameters available on the technical data from the OEM are directly obtained from the documentation [28] . The parameters obtained for the current use case are shown in Table 7.

Deliverable No. D3.6
Version 02
Project no. 101069576

Title
Vehicle dynamics modelling methodology

ROADVIEW

Table 7. Parameters obtained from the official documentation - BMW M8 Competition [28].

Gear Ratio (1st gear)	5.000
Gear Ratio (2nd gear)	3.200
Gear Ratio (3rd gear)	2.143
Gear Ratio (4th gear)	1.720
Gear Ratio (5th gear)	1.313
Gear Ratio (6th gear)	1.000
Gear Ratio (7th gear)	0.823
Gear Ratio (8th gear)	0.640
Gear Ratio Differential	3.154
Steering Ratio	14.3 : 1
Wheel Base	2.827 m
Track Width Front	1.627 m
Track Width Rear	1.632
Drag Coefficient	0.33
Drag Area	2.25

Furthermore, the torque curve is obtained from the automobile-catalog website [29], which is based on the factory data. Figure 43 shows the maximum engine torque obtained for the BMW M8 competition and used in this model.
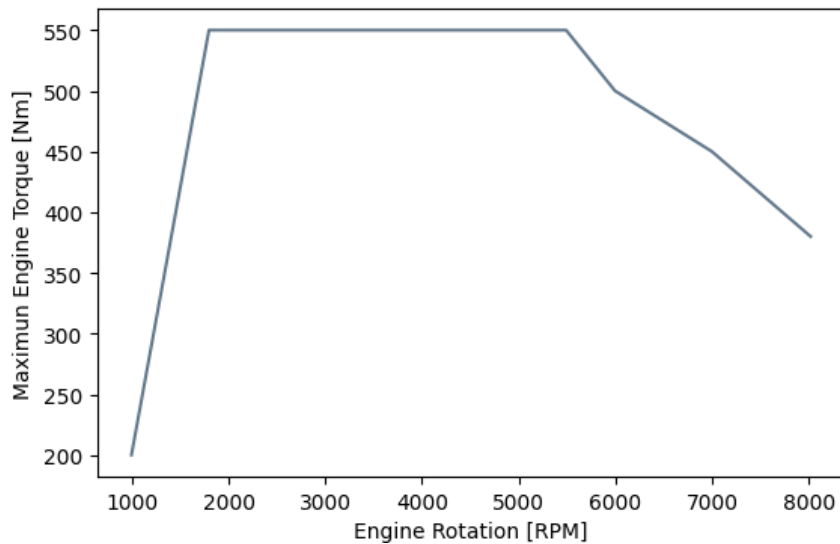
Figure 43. Maximum engine torque - BMW M8 Competition [29].

6.2.2 Static measurements

The results obtained from the measurement of the vehicle weight are shown in Table 8.

Deliverable No. D3.6
Version 02
Project no. 101069576

Title
Vehicle dynamics modelling methodology

ROADVIEW

Table 8. Parameters obtained from static measurements - BMW M8 Competition.

Total mass	2047.4 kg
Distance CG to rear axle	1.496 m
Lateral position CG	0.011 m
Height of the CG from centre of the wheel	-0.078 m

The results obtained by the measurements shown a centred CG slightly positioned on the front of the vehicle. Furthermore, the measurement indicates that the CG of the vehicle is below the wheel centre. Since the vehicle has a combustion engine, and most of the components are above the wheel centre, there is a low probability that this value is correct. A new round of measurements shall be conducted in the future to confirm the results.

6.2.3   Calculated parameters

Based on the dynamics data collected, some parameters can be directly calculated, facilitating the optimization of the parameters in a second step.

6.2.3.1   Torque Converter

Figure 44 shows the data obtained from the turbine and impeller as well as the calculated parameters. The gradient indicates the manoeuvre time. Analysing the turbine and impeller velocity at the superior graph at the left side, it is possible to identify that the system reached the lock point in the end of the manoeuvre when turbine and impeller synchronize the velocity. Furthermore, in the top right graph it is possible to confirm the increase of the torque while the system is not locked. The bottom left and right graphs indicate the obtained results for the converter ratio and the converter factor respectively.
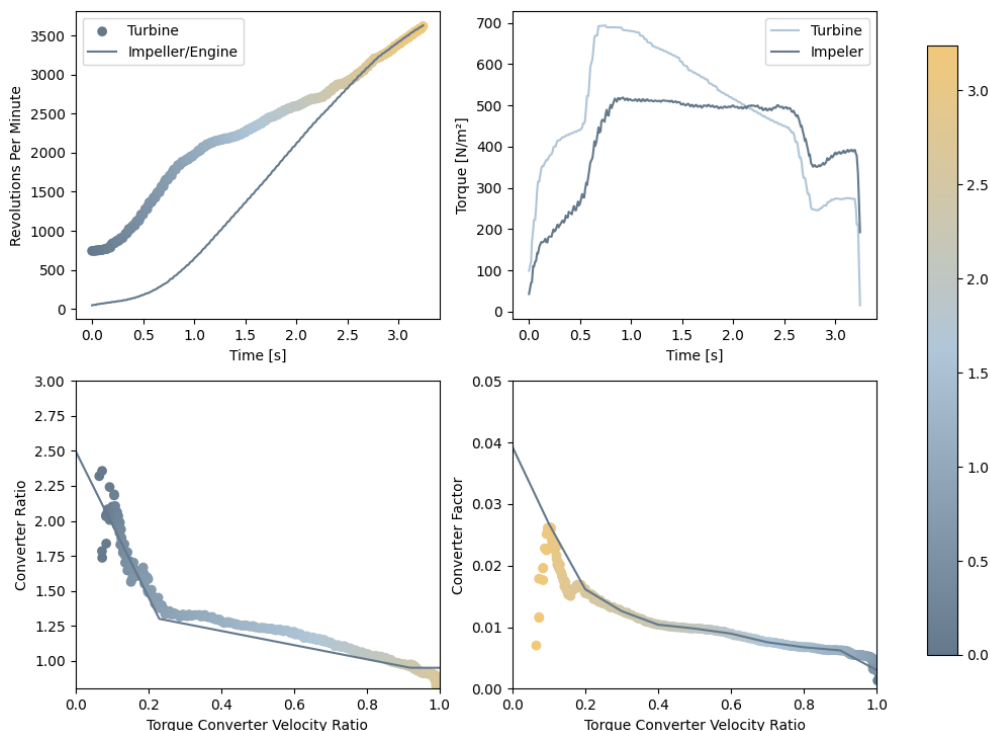
Figure 44. Torque converter parameters - BMW M8 Competition

Deliverable No. D3.6
Version 02
Project no. 101069576

Title
Vehicle dynamics modelling methodology

ROADVIEW

6.2.3.2 Transmission

Based on all the manoeuvres the average engine rotation for the gear change is obtained. The results are shown in the Figure 45a for the up shifting and Figure 45b for down shifting.
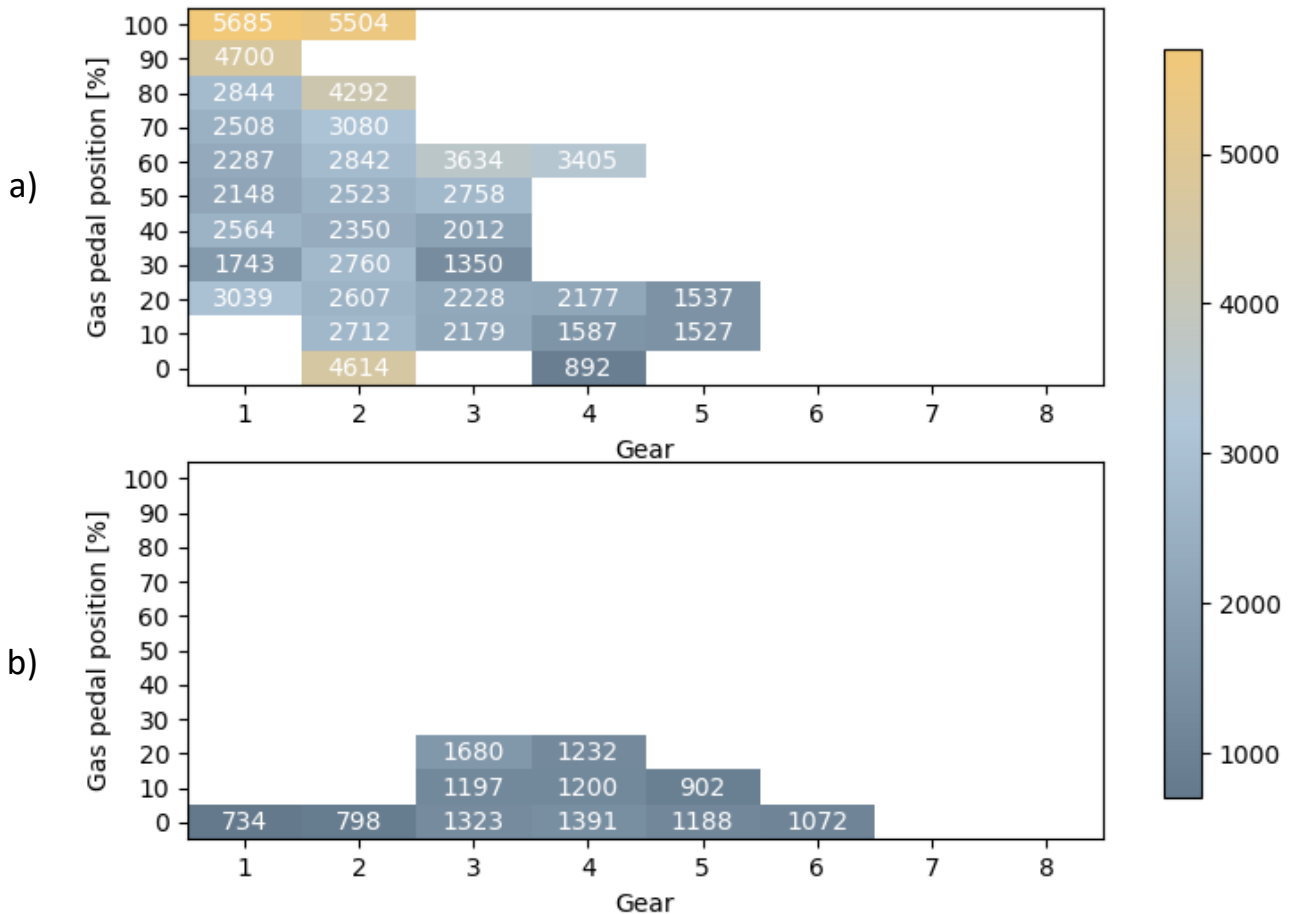
Figure 45. Calculated gear changing table a) up shifting and b) downshifting - BMW M8 Competition

The data shown in Figure 45, is afterwards rounded and the missing points are manually filled in. Furthermore, some specific points of the map are updated using the acceleration and braking manoeuvre with a target speed of 70 km/h to achieve the proper gear changing time. The resulting gear changing table is shown in the Figure 46-a for up shifting and Figure 46b for downshifting. From the obtained results is possible to identify a behaviour in which high values of gap pedal position result in higher engine rotation, benefiting the performance of the vehicle while compromising the consumption and the environment.

Due to the limited area of the test track from C-IAD only gear changes until 6 gears are recorded. Due to that the higher gas pedal position as well as the higher gear should be estimated based on the expertise from THI and VTI. This approximation will not affect the tests conducted in the ROADVIEW project, since only low speed will be applied. However, to have a better description of the gear change logic tests at higher velocities are required.

Deliverable No. D3.6
Version 02
Project no. 101069576

Title
Vehicle dynamics modelling methodology

ROADVIEW
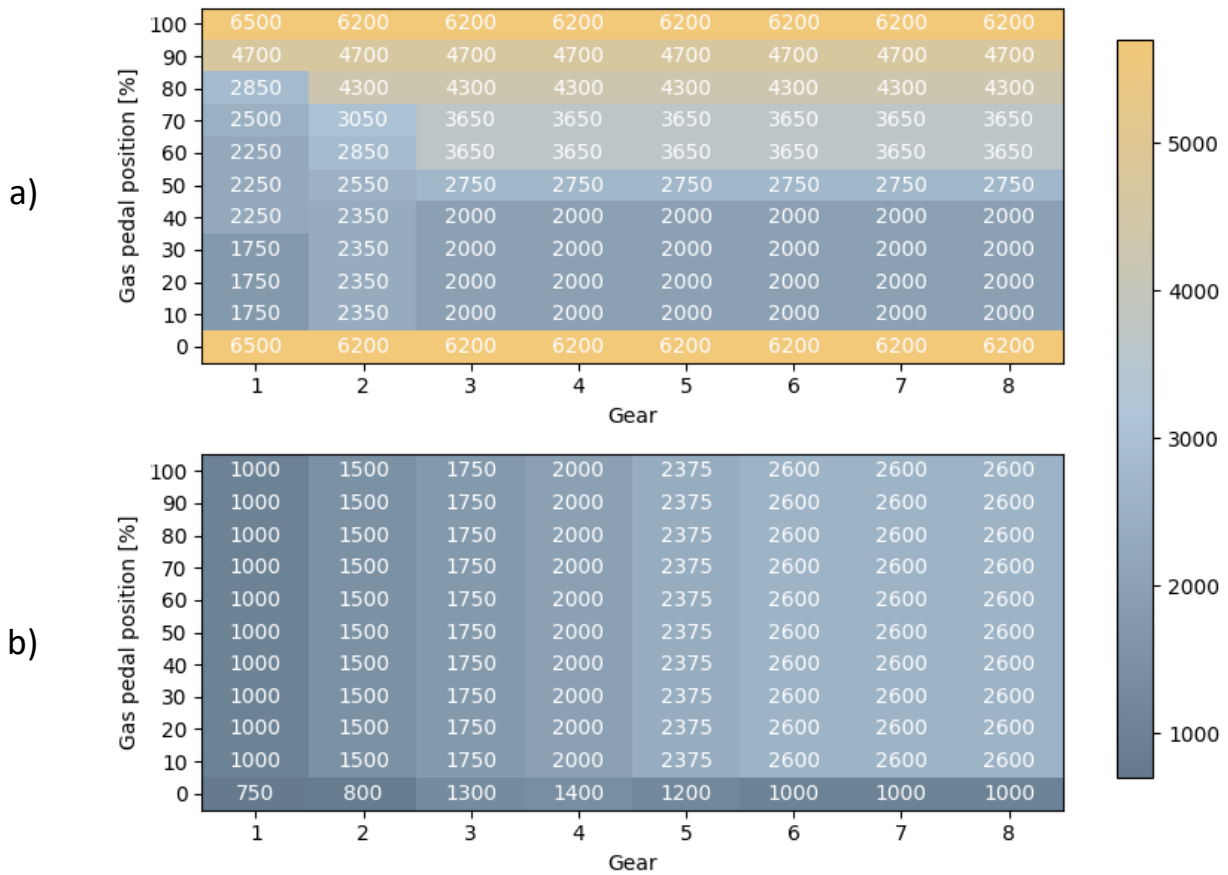
Figure 46. Final gear changing table a) up shifting and b) down shifting - BMW M8 Competition

6.2.3.3 Tires

Lateral force

To measure the cornering coefficient for the front and rear tire a series of measurements in the VTI tire test rig was conducted, as described in section 4.3. The loads, tire temperatures and inflation pressures were chosen according to Table 3. For each condition, individual measurements with three fixed slip angles were conducted. We were aiming for -1, 0, and +1 degrees, which based on previous measurements with other tires on high friction was assumed to be within the tire's linear region. Due to difficulties to properly set a small slip angle after a major upgrade of the rig´s control system, the actually achieved slip angles were -1.1, -0.15 and +0.6 degrees.

For the high wheel load all three slip angles were well within the linear region as evident from the linear fits of Figure 47 and Figure 48. As the wheel load decreases, the linear region also becomes smaller, and the linear fit needs to be done using only the two smaller slip angle values -0.15 and +0.6 degrees. Linear fits using these two slip angle values are indicated with red lines in the figures below, while the black lines are fits with all three slip angle values.

From the outcome from the linear fits of the two smaller slip angle values (red lines) the load dependence of the cornering coefficient for different tire temperatures and inflation pressures could be deduced. The results are summarized in Table 9, and plotted in Figure 49.

Deliverable No. D3.6
Version 02
Project no. 101069576

Title
Vehicle dynamics modelling methodology

ROADVIEW

Tire: Front; Infl. pressure:2.6 bar; Tire temp: cold

Load: 2575 N

Cornering coeff: 38.7 (1/rad)
Red: Cornering coeff: 51.3 (1/rad)
Cornering stiffness: 1738 (N/deg)
Red: Cornering stiffness: 2306 (N/deg)

Load: 5150 N

Cornering coeff: 32.7 (1/rad)
Red: Cornering coeff: 40.2 (1/rad)
Cornering stiffness: 2942 (N/deg)
Red: Cornering stiffness: 3613 (N/deg)

Load: 7725 N

Cornering coeff: 28.1 (1/rad)
Red: Cornering coeff: 27.8 (1/rad)
Cornering stiffness: 3787 (N/deg)
Red: Cornering stiffness: 3744 (N/deg)

Tire: Front; Infl. pressure:3.2 bar; Tire temp: cold

Load: 2575 N

Cornering coeff: 36.5 (1/rad)
Red: Cornering coeff: 46.3 (1/rad)
Cornering stiffness: 1642 (N/deg)
Red: Cornering stiffness: 2083 (N/deg)

Load: 5150 N

Cornering coeff: 35.2 (1/rad)
Red: Cornering coeff: 41.3 (1/rad)
Cornering stiffness: 3159 (N/deg)
Red: Cornering stiffness: 3715 (N/deg)

Load: 7725 N

Cornering coeff: 30.2 (1/rad)
Red: Cornering coeff: 31.2 (1/rad)
Cornering stiffness: 4073 (N/deg)
Red: Cornering stiffness: 4202 (N/deg)

Tire: Front; Infl. pressure:2.6 bar; Tire temp: warm: 50 deg

Load: 2575 N

Cornering coeff: 28.7 (1/rad)
Red: Cornering coeff: 32.4 (1/rad)
Cornering stiffness: 1291 (N/deg)
Red: Cornering stiffness: 1454 (N/deg)

Load: 5150 N

Cornering coeff: 28.9 (1/rad)
Red: Cornering coeff: 29.5 (1/rad)
Cornering stiffness: 2595 (N/deg)
Red: Cornering stiffness: 2652 (N/deg)

Load: 7725 N

Cornering coeff: 23.5 (1/rad)
Red: Cornering coeff: 22.6 (1/rad)
Cornering stiffness: 3173 (N/deg)
Red: Cornering stiffness: 3041 (N/deg)

Figure 47. Measurements and line fits for the front tire.

Deliverable No. D3.6
Version 02
Project no. 101069576

Title
Vehicle dynamics modelling methodology

ROADVIEW

Tire: Rear; Infl. pressure:2.6 bar; Tire temp: cold

Tire: Rear; Infl. pressure:3.2 bar; Tire temp: cold

Tire: Rear; Infl. pressure:2.6 bar; Tire temp: warm: 40 deg
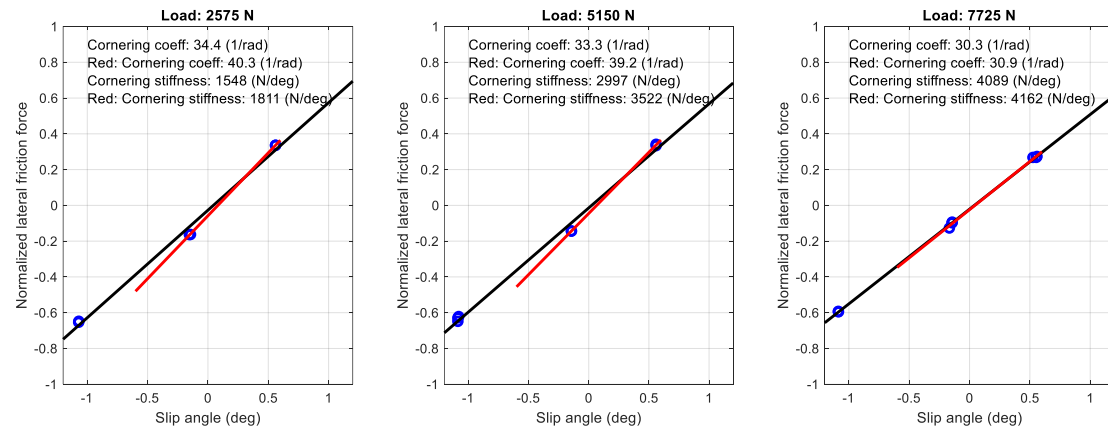
Figure 48. Measurements and line fits for the rear tire.

Deliverable No. D3.6
Version 02
Project no. 101069576

Title
Vehicle dynamics modelling methodology

ROADVIEW
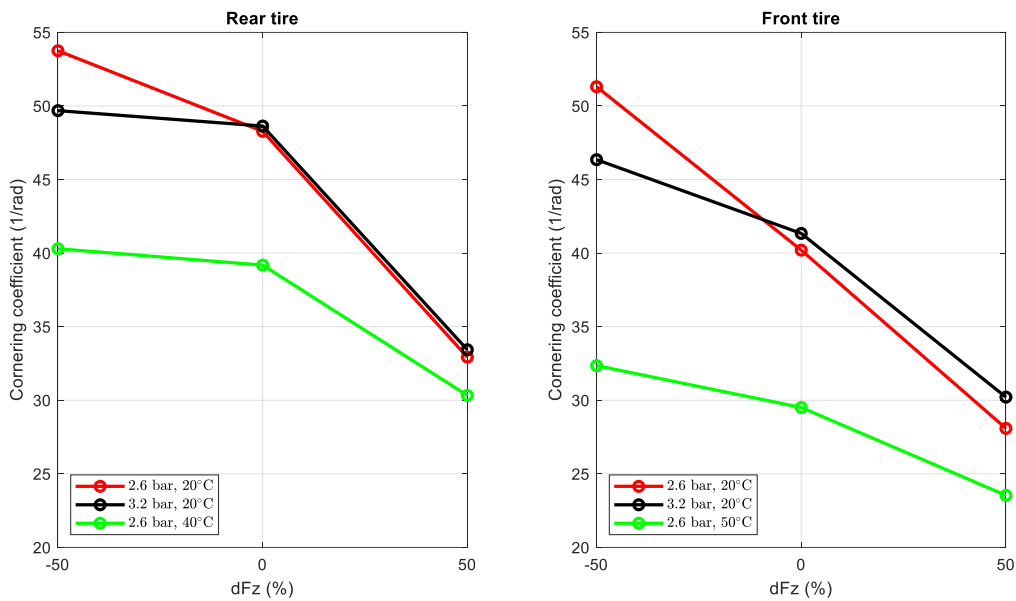
Figure 49. Estimated cornering coefficient for the two tires at different wheel loads, expressed as dFz, the relative wheel load with respect to the nominal load.

Table 9. Estimated Cornering Coefficient (CC) at different wheel loads, expressed as percentage of the nominal load (n.l.)

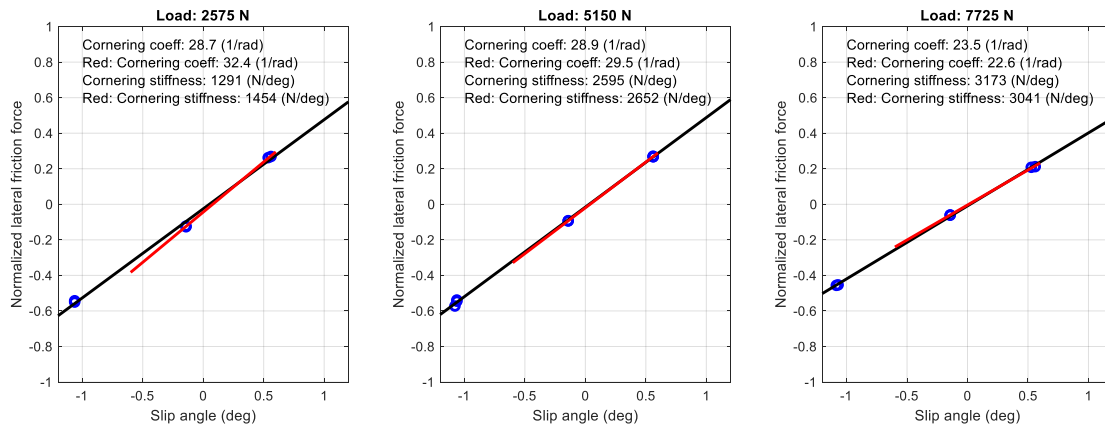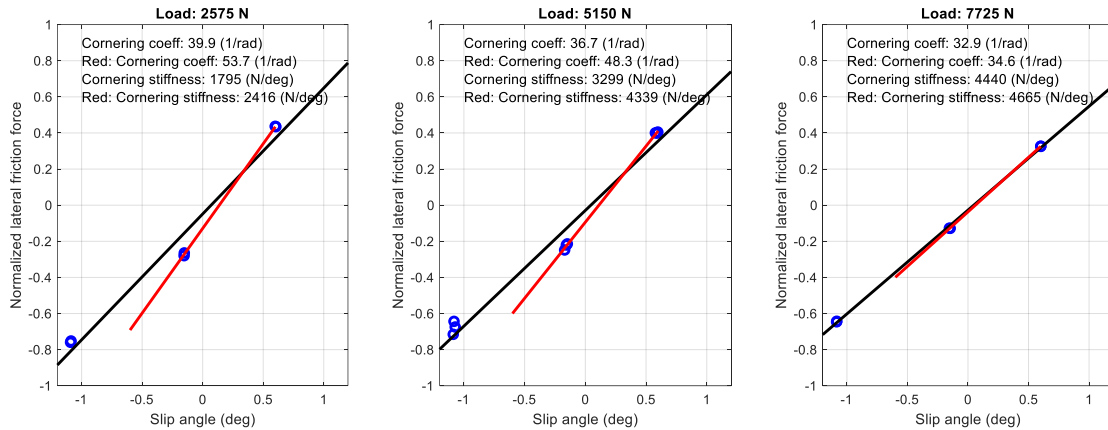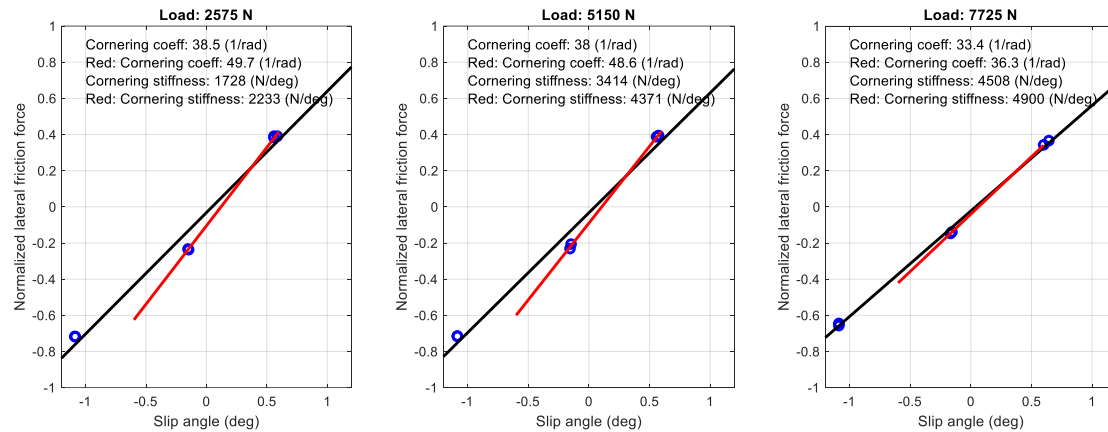| Tire	Inflation pressure (bar)	Tire temp	CC (1/rad) 50% n.l.	CC (1/rad) 100% n.l.	CC (1/rad) 150% n.l.
Front	2.6	Cold	51.3	40.2	28.1
Front	3.2	Cold	46.3	41.3	30.2
Front	2.6	Heated: 50°C	32.4	29.5	23.5
Rear	2.6	Cold	53.7	48.3	32.9
Rear	3.2	Cold	49.7	48.6	33.4
Rear	2.6	Heated: 40°C	40.3	39.2	30.3

It is clear that the cornering coefficient is not linear with respect to wheel load for the entire measured range of wheel loads. However, for simplicity we would like to use the ISO model for describing the tire lateral forces, and therefore would need a linear parameterization with respect to load according to eq. 45. With the assumption that the load dependence is rather linear for loads from and above the nominal, using the results for the two higher loads for the linear parameterization will likely be the best trade-off. The larger forces during load transfer will then be modelled accurately, while the smaller forces will be somewhat overestimated. The parameters from such a parameterization are listed in Table 10.

The load dependent cornering coefficients and the peak friction value obtained from the brake tests (see the section on the longitudinal force below) should be set as fixed tire parameters for dry and wet asphalt conditions. Other parameters of the tire model could then be obtained from the general parameter optimization scheme of the vehicle dynamics model from the field test data.

Deliverable No. D3.6
Version 02
Project no. 101069576

Title
Vehicle dynamics modelling methodology

ROADVIEW

Table 10. Parameters for the linear model in Eq. 45

Tire	Inflation pressure (bar)	Tire temp	CCy0 (1/rad)	CCyg
Front	2.6	Cold	40.2	-0.60
Front	3.2	Cold	41.3	-0.54
Front	2.6	Heated: 50°C	29.5	-0.40
Rear	2.6	Cold	48.3	-0.64
Rear	3.2	Cold	48.6	-0.63
Rear	2.6	Heated: 40°C	39.2	-0.45

A few other tire properties were also measured in the VTI tire test rig. These were the vertical stiffness, the loaded wheel radius and the effective rolling radius. The measured data is presented in Table 11. The loaded wheel radius was measured both for a stand still tire and rolling at 30 km/h, and the results where more or less identical. The effective rolling radius was measured at 1 km/h. As seen in the table, the loaded wheel radius is approximately 10 mm smaller than the effective rolling radius. While the effective rolling radius is quite insensitive to load changes, the loaded wheel radius is quite sensitive to load variations.

Increasing the inflation pressure will lead to an increase of the vertical stiffness, while the effect on loaded wheel radius and the effective rolling radius is very minor.

In the vehicle dynamics model, the so-called dynamic rolling radius will be used instead of separate values for the loaded wheel radius and the effective rolling radius. It is determined from the field test with the car by comparing the GPS-based vehicle speed and the measured rotational speeds of the tyres.

Table 11. Measured vertical stiffness, loaded wheel radius (R), and effective rolling radius (R_e) for cold tires.

Tire	Inflation pressure (bar)	Vertical stiffness (kN)	R 50% n.l. (mm)	R_e 50 %n.l. (mm)	R 100% n.l. (mm)	R_e 100 %n.l. (mm)	R 150% n.l. (mm)	R_e 150 %n.l. (mm)
Front	2.6	355	341	345	333	344	325	343
Front	3.2	405	343	346	335	345	329	344
Rear	2.6	400	345	349	337	348	331	346
Rear	3.2	455	346	349	339	348	333	347

Longitudinal force

Figure 50 indicates the longitudinal slip stiffness obtained from the real data collected. The colormap indicates the time of the manoeuvre and the red line the fit of the linear function on the real data. It is possible to identify that the stiffness on the rear wheels is bigger than the longitudinal stiffness of the front wheels. Since both tires are modelled with the same parameters in the ROADVIEW model, an average value of 22 Nm is applied for the front and rear tires.

Figure 51 on the other hand shows the results obtained for the peak friction values. The graphs on the top show the speed profile and the orange points limit the areas in which the deceleration is calculated. Similarly, the acceleration profile is shown on the bottom graph. The results obtained on the dry asphalt (left graph) show a peak friction of 1.1

while the values for the wet asphalt (right graph) are 0.9. Both values are aligned with the literature, proving the applicability of the estimation method for the harsh weather conditions.
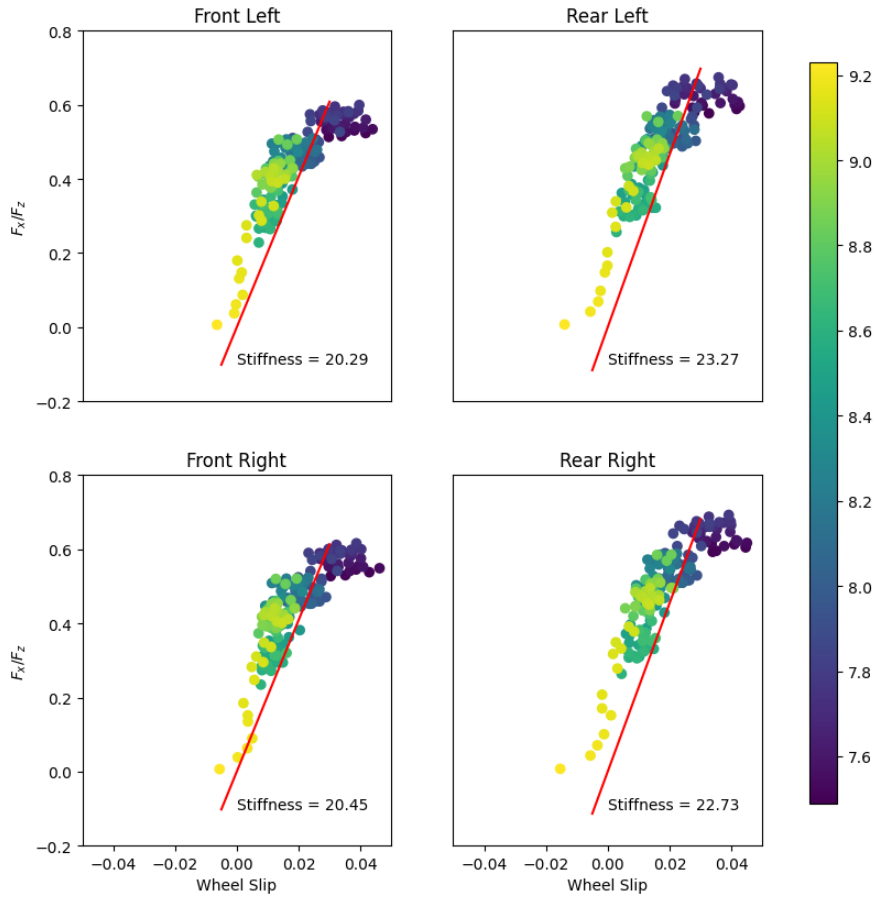

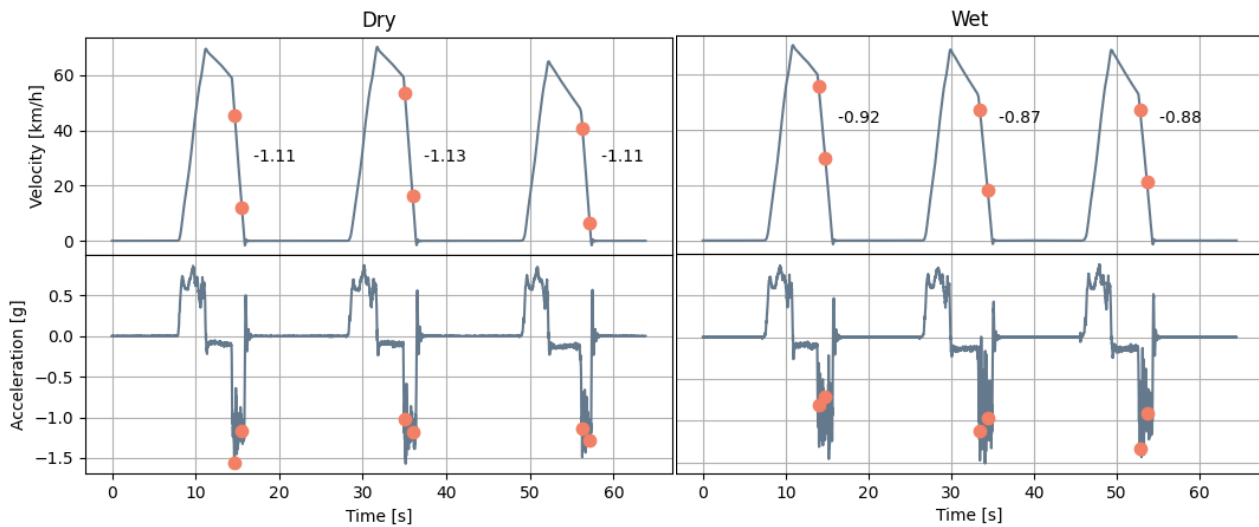**Figure 50. Tire longitudinal stiffness - BMW M8 Competition**

Deliverable No. D3.6
Version 02
Project no. 101069576

Title
Vehicle dynamics modelling methodology

ROADVIEW

Figure 51. Braking profiles used for estimation of peak friction on dry and wet asphalt - BMW M8 Competition

6.2.4   Optimized Parameters

This chapter shows the parameters obtained by applying the proposed optimization method. It is important to highlight that these parameters may not correspond with the physical values, since they can be adapted by the optimization algorithm to overcome simplifications of the implemented model. However, with the obtained parameters a high fidelity of the results can be obtained considering the limitations of the implemented model. The results are divided into the three implemented routines:

6.2.4.1   Powertrain optimization routine

Applying the optimization method proposed in this report the parameters from Table 12 are obtained.

Table 12. Optimized powertrain parameters - BMW M8 Competition

Parameter	Optimized Value
Engine Inertia	0.1 Kgm²
Gearbox Efficiency	0.75 %
Gearbox Inertia	0.19 Kgm²
Front tire inertia	1.85 Kgm²
Rear tire inertia	2.67 Kgm²

Based on the expertise on the vehicle dynamics model parametrization the obtained values of engine Inertia are small, lying on the inferior limit of the optimization, while the Gearbox inertia present higher values than expected. Since both are correlated in the system, there is a high possibility that the Inertia that is neglected in the engine is considered in the transmission. Similarly, despite being an all-wheels drive vehicle the efficiency of the gearbox presents low values, which can support the simplicity of the model or even correct the error of other parameters. The values of the tire inertia are coherent with the literature.

Figure 52 and Figure 53 show the comparison of the real data measured on the test track with the simulated results for engine torque and velocity respectively. Analysing the data is possible to verify that the obtained torque values as well as the velocity of the engine properly represent the behaviour of the engine. In Figure 53 the engine velocity

Deliverable No. D3.6
Version 02
Project no. 101069576

Title
Vehicle dynamics modelling methodology

ROADVIEW

is aligned with the real values and the gear change happens on the proper instant of time, indicating a good correlation between the model and the real data.
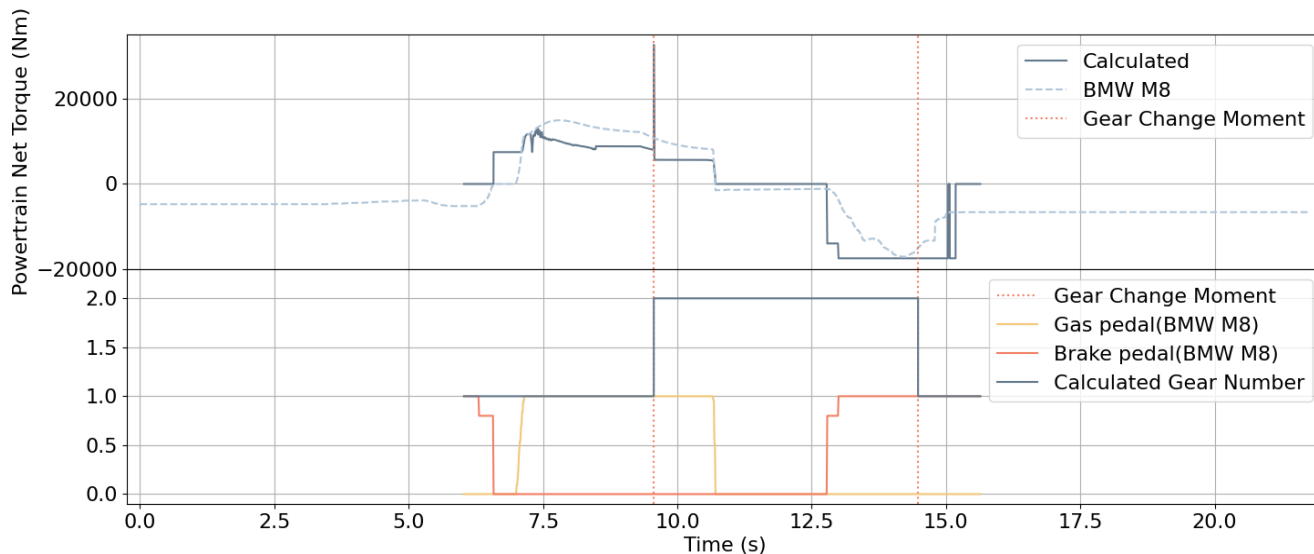

Figure 52. Optimized Powertrain Torque - BMW M8 Competition
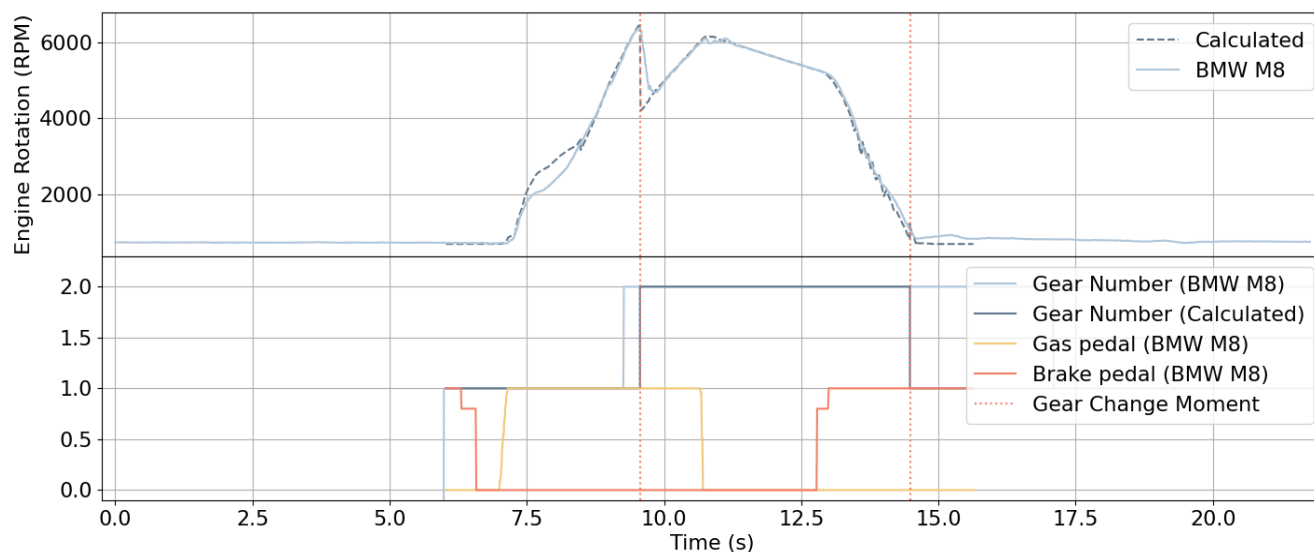
Figure 53 Optimized Powertrain Engine Velocity - BMW M8 Competition

6.2.4.2   Longitudinal effect optimization routine

The results obtained by the optimization of the longitudinal routine are shown in Table 13. The results obtained are coherent, mainly for a sport vehicle.

Deliverable No. D3.6
Version 02
Project no. 101069576

Title
Vehicle dynamics modelling methodology

ROADVIEW

Table 13. Optimized longitudinal parameters - BMW M8 Competition

Parameter	Optimized Value
Front Spring Rate	18795.0 N/m
Rear Spring Rate	14184.0 N/m
Front Damping Rate	5026.0 Ns/m
Rear Damping Rate	5249.0 Ns/m
Pitch Centre height	0.26 m
Pitch Inertia	2638.0 Kgm²
Front Unsprung mass	100.0 Kg
Rear Unspring mass	99.0 Kg

The results shown in Figure 54 indicate the velocity of all the wheels in a comparison between the data collected from the CAN-bus from the BMW M8 and the calculated values. The absence of the ABS during the braking phase is clear due to the complete locking of the wheels. Furthermore, a limitation of the torque sent to the wheels is implemented to emulate a traction control, avoiding the car from accelerating more than the required values.

Figure 55 shows the longitudinal acceleration, velocity, and pitch of the real vehicle and the vehicle model developed in the ROAVIEW project. It is possible to identify that high frequency disturbances measured on the real vehicle cannot be identified in the simulation, the overall shape and behaviour of the vehicle is well reproduced by the model implemented and by the chosen parameters.

Figure 54. Wheel Velocity - BMW M8 and ROADVIEW vehicle dynamics model.

Deliverable No. D3.6
Version 02
Project no. 101069576

Title
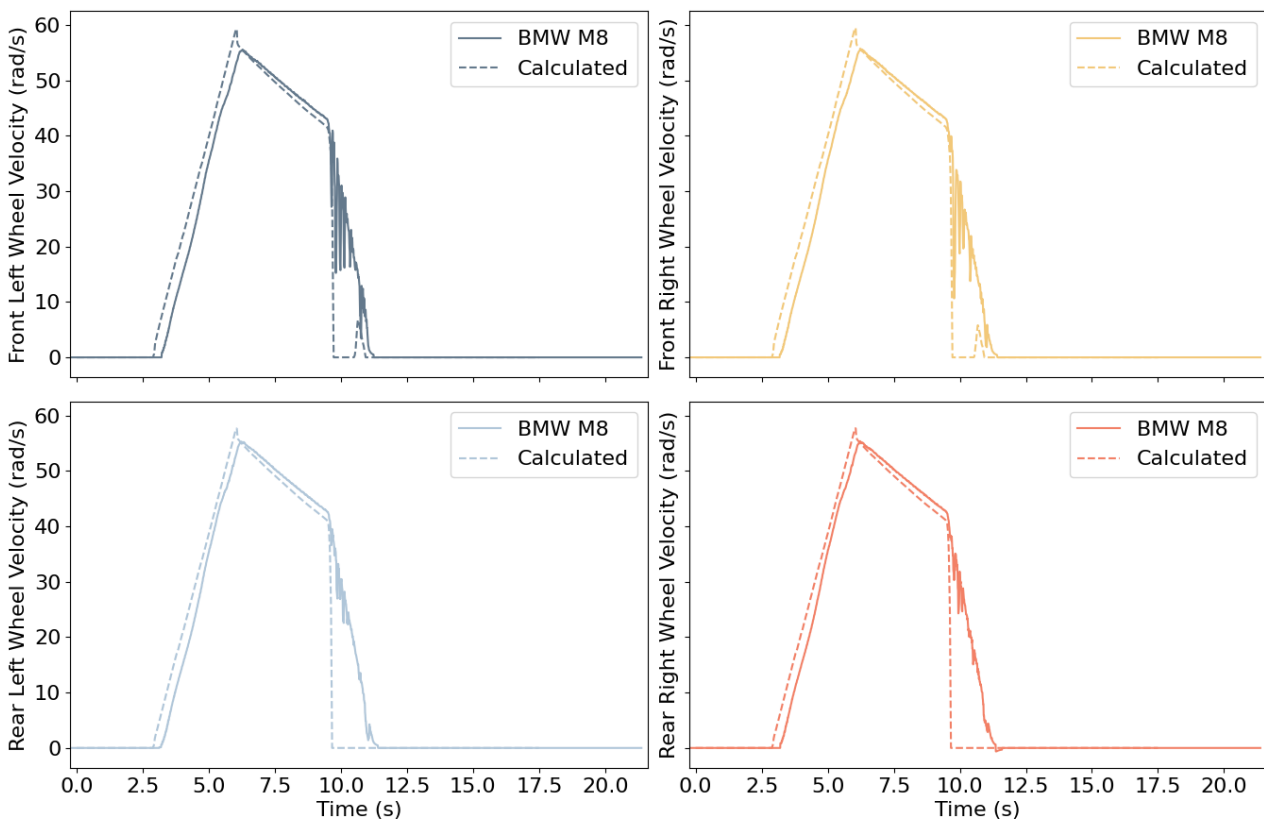Vehicle dynamics modelling methodology
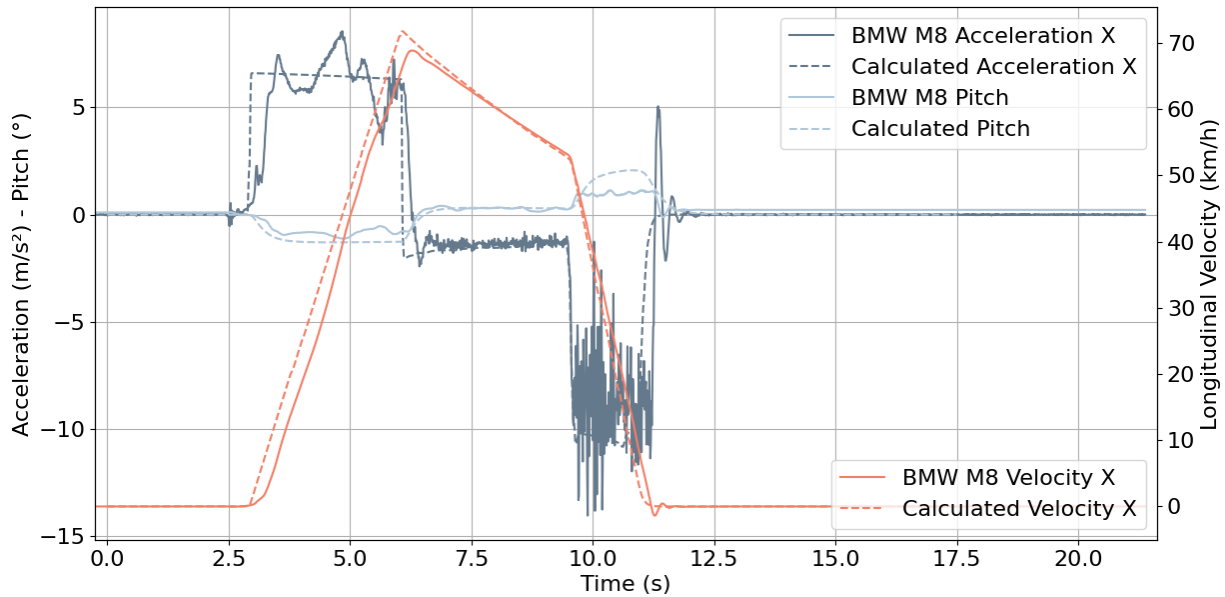
ROADVIEW

Figure 55. Longitudinal variables - BMW M8 and ROADVIEW vehicle dynamics model.

6.2.4.3 Lateral effect optimization routine

The results obtained for the lateral effect optimization are shown in Table 14.

Table 14. Optimized lateral parameters - BMW M8 Competition

Parameter	Optimized Value
Roll Bar Stiffness	10546.58 N/m
Roll Centre Height	0.36 m
Roll Inertia	2701.0 Kgm²
Yaw Inertia	4983.0 Kgm²

The results show in Table 14 indicate high values of Inertias, which can be achieved to correct possible simplifications on the model. The results of roll and yaw for double lane change manoeuvre at 70 km/h are shown in the Figure 56, together with the steering wheel angle input. The yaw behaviour shows an adequate behaviour for high steering wheel angle inputs, however while driving straight deviations between the real vehicle and the model are noticed. This behaviour can be explained by the missing hysteresis of the steering wheel system as well by the simplification of the road inclination. Furthermore, possible misalignments of the real vehicle steering system are not considered on the vehicle dynamics model nor in the data processing. The roll behaviour is satisfactory, mainly at the first lane change, while during the second lane change higher values are obtained on the vehicle model. The implementation of the lateral relaxation length shown in Eq. (20) can improve the final lateral behaviour of the model.

Figure 57 shows the combined longitudinal and lateral behaviour of the vehicle for the double lane change manoeuvre at 70 km/h. Despite of the deviations on the yaw caused by the differences while the vehicle is driving straight, the

whole manoeuvre has an adequate correspondence with the real vehicle behaviour in both longitudinal and lateral movements.
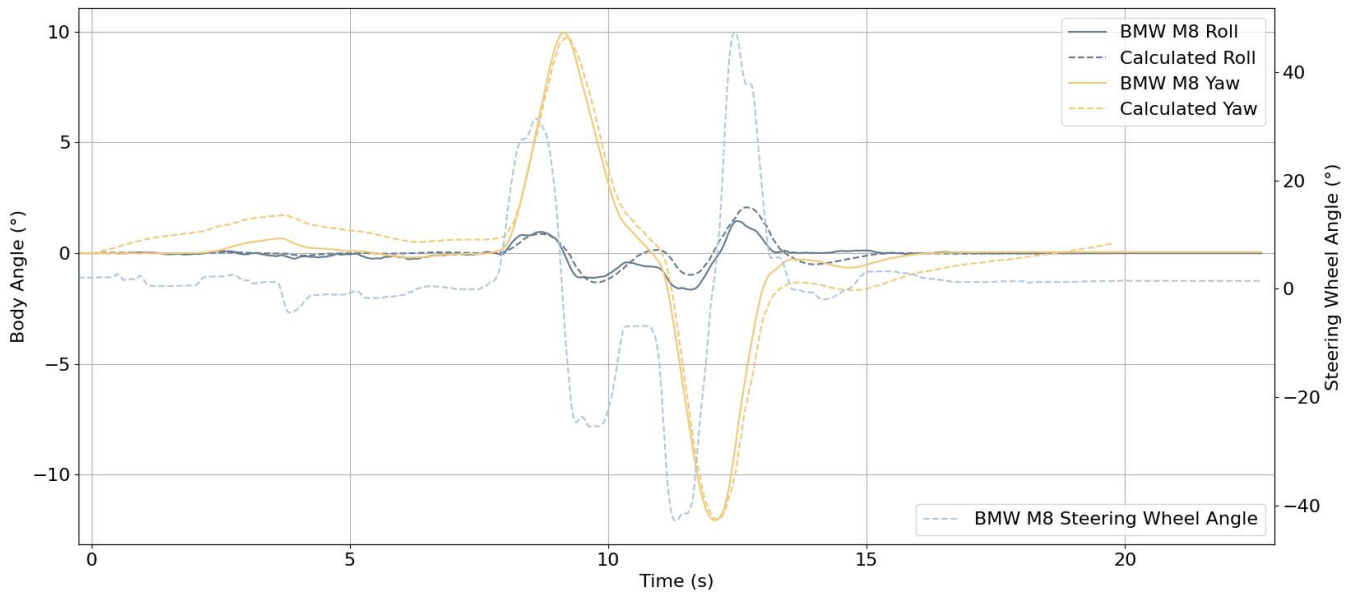
Figure 56. Lateral Variables - BMW M8 and ROADVIEW vehicle dynamics model.
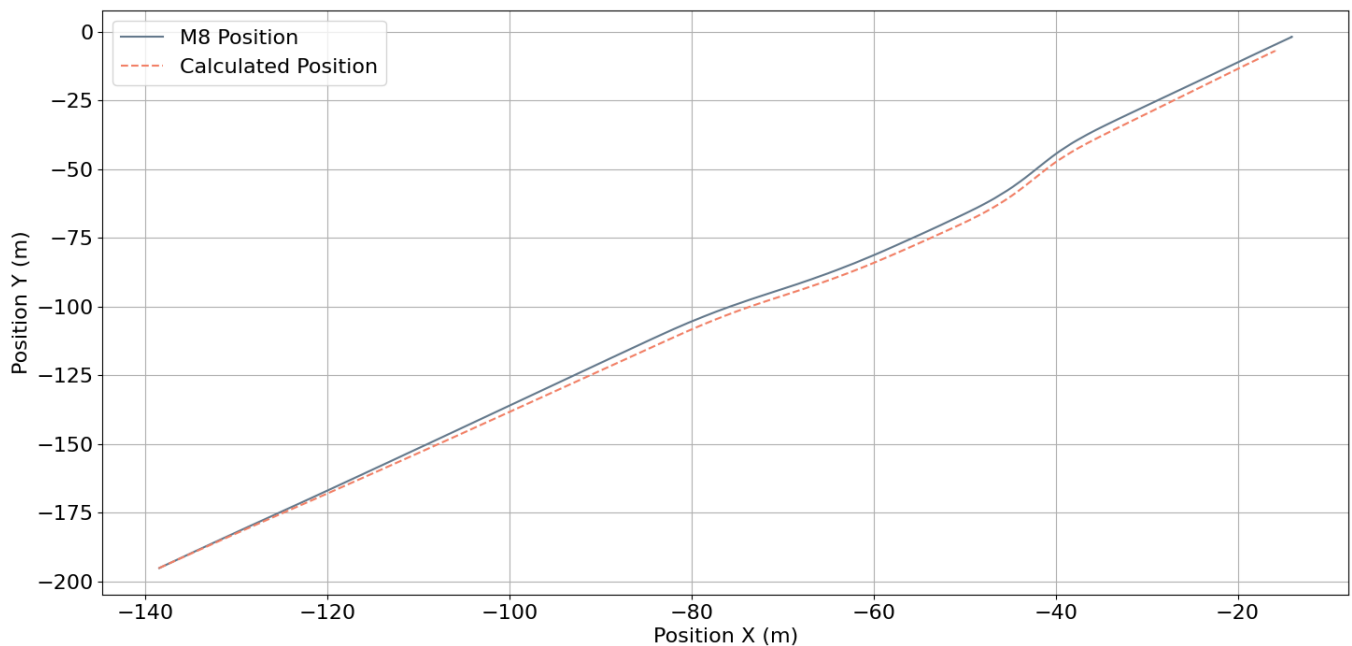
Figure 57. Combined Longitudinal and Lateral behaviour - BMW M8 and ROADVIEW vehicle dynamics model.

6.2.4.4   Vehicle behaviour on wet asphalt

The behaviour of the vehicle on the wet conditions is shown in Figure 58, Figure 59 and Figure 60. The longitudinal behaviour shown in Figure 58 indicates an adequate acceleration and braking conditions, similar to the real vehicle. Despite that the maximal torque was reduced to match the traction control limitations, it is possible to notice that in

Deliverable No. D3.6
Version 02
Project no. 101069576

Title
Vehicle dynamics modelling methodology

ROADVIEW

low velocities the traction control acts more strongly than modelled, adding a delay on the initial acceleration of the vehicle. These limitations shall be minimized by the integration of a traction control on the model.
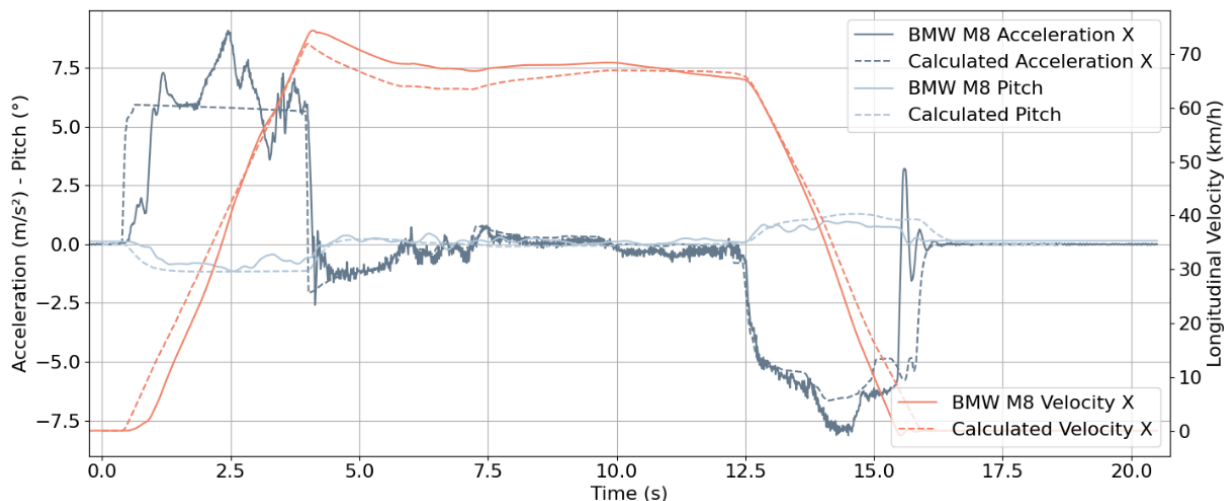
Figure 58. Longitudinal variables - BMW M8 and ROADVIEW vehicle dynamics model on wet surface.

On the lateral behaviour shown in the Figure 59, the yaw deviations during the straight driving are again visible. However, it is important to highlight that the driver finished the manoeuvre with the steering wheel at -60°, since the model took longer to reach the stand still it generates a meaningful value according to the input, but with divergence from the real behaviour. During the acceleration phase it is also possible to identify the when the car drives straight a steering wheel angle of 2° is recorded, reinforcing the possibility of misalignment or sensor limitation from the real vehicle.
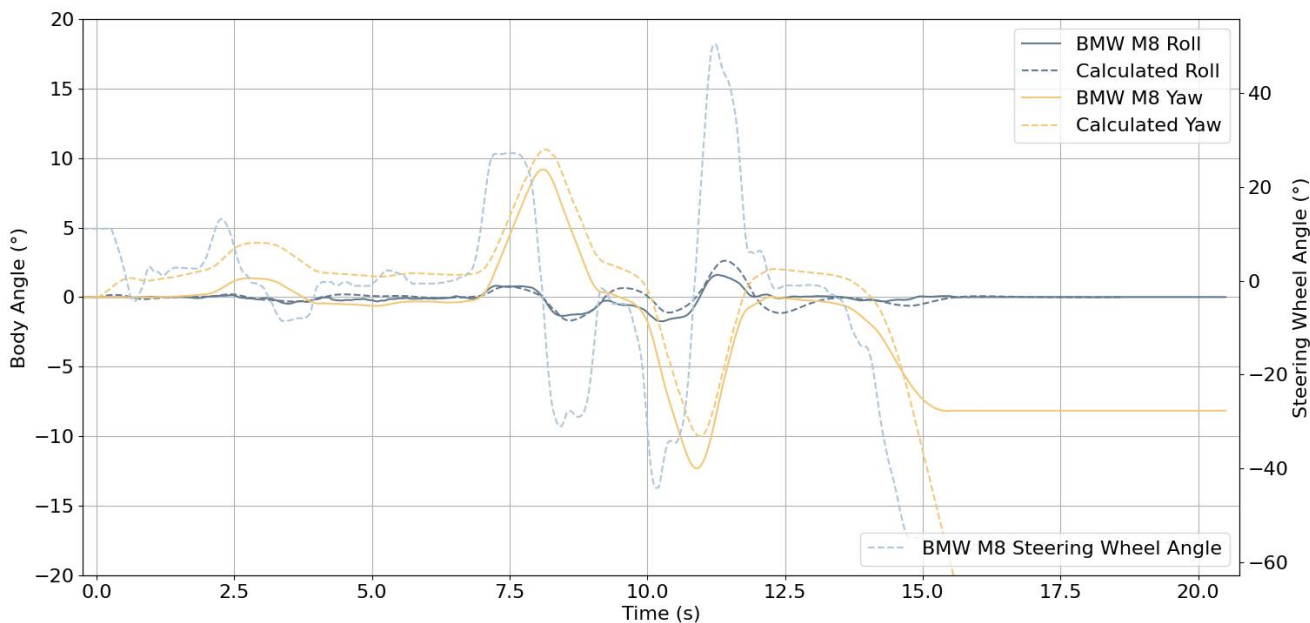
Figure 59. Lateral Variables - BMW M8 and ROADVIEW vehicle dynamics model on wet surface.

Finally, the combination of the longitudinal and lateral movements is shown in Figure 60. The result indicates an adequate behaviour of the modelled vehicle even on wet road conditions. It reinforces the applicability of the proposed method for the estimation of the parameters from real vehicles on different weather conditions. Further data collection shall be conducted on snowy and icy test tracks to estimate the parameters of the vehicle model for more extreme road conditions.
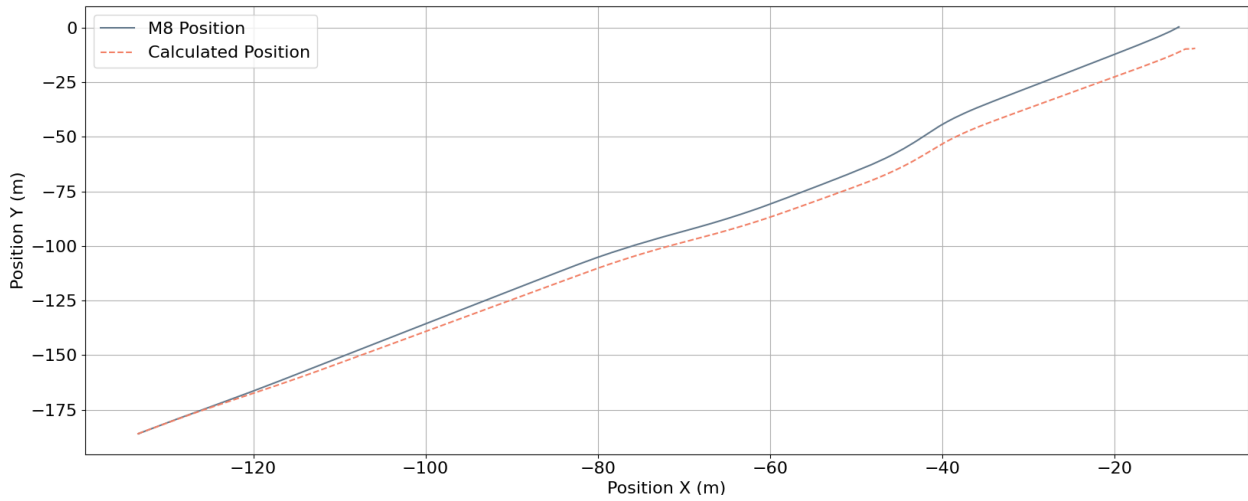
Figure 60. Combined Longitudinal and Lateral behaviour - BMW M8 and ROADVIEW vehicle dynamics model on wet surface.

Deliverable No. D3.6
Version 02
Project no. 101069576

Title
Vehicle dynamics modelling methodology

ROADVIEW

6.3 Tire models for ice and snow

No measurements were carried out in the Roadview project to create tire model parameterizations for slippery road conditions like ice and snow. Since the tire forces on ice and snow largely depend on the road conditions, which could be extremely varying and could change significantly during a very short time period, it would be an impossible task to conduct measurements that would cover the needed range of road conditions. However, it would be possible to create some useful parameterizations based on measurements and observations carried out by VTI previously on ice and snow test tracks.

For a vehicle dynamics model without explicit ABS system the linear braking model of eq. 5 would be used. This model only requires knowledge of the longitudinal slip stiffness and the peak friction. Preferably, the effect of varying wheel load should be included, which is assumed to be linear. For low friction, and especially so on ice, the load shift during braking and steering will however be small, which makes load effects less important than for high friction. Therefore, a parameterization that does not include the load effect can still be useful.

The tire model for steering is a bit more complicated since it will be nonlinear with respect to slip angle.

In 2015 VTI conducted a very large study on tire friction of new and worn tires on ice and snow, as well as on wet asphalt. In total 78 different winter tires were measured on ice and snow, and on cold wet salted asphalt (road temperature around zero degrees Celsius) all winter tires and 8 summer tires were measured as well. Measurements were made with both a passenger car and a mobile tire test rig (see Figure 61), providing both braking distances and longitudinal and lateral slip curves. Part of the results have been published in [30], while other data so far has not been published. Unpublished data from these measurements have been analysed within the Roadview project to provide some useful tire parameterizations on snow and ice. The study included the three main types of winter tires used in the Nordic counties: studded tires, studless winter tires of Nordic type and studless winter tires of central European type. The two studless winter tire types are referred to as Nordic and European in this report. All-season tires are not common in the Nordic countries but are popular in other parts of Europe. VTI has recently conducted a study comparing winter grip of All-season tires compared to traditional studless winter tires [x].

Figure 61. The VTI mobile tire test rig BV12.

6.3.1 Snow:

Snow is easier to model than ice since the maximum friction typically is for very high slip values, with no marked peak in the slip curve. Thus, for steering only the cornering coefficient and the peak friction value would be the needed information. The peak friction can be assumed to be the same for braking and steering. During the VTI 2015 study 70 separate lateral slip curve measurements were made on packed snow with the reference tire, a studless winter tire of Nordic type, during two weeks of time. The peak lateral friction for this tire on the test track snow surface during that time was between 0.45 – 0.56. The cornering coefficient typically varied between 0.1 – 0.2, and as can be seen

Deliverable No. D3.6
Version 02
Project no. 101069576

Title
Vehicle dynamics modelling methodology

ROADVIEW

in Figure 62, there is essentially no correlation between peak friction and cornering coefficient on snow for this kind of packed snow surface.
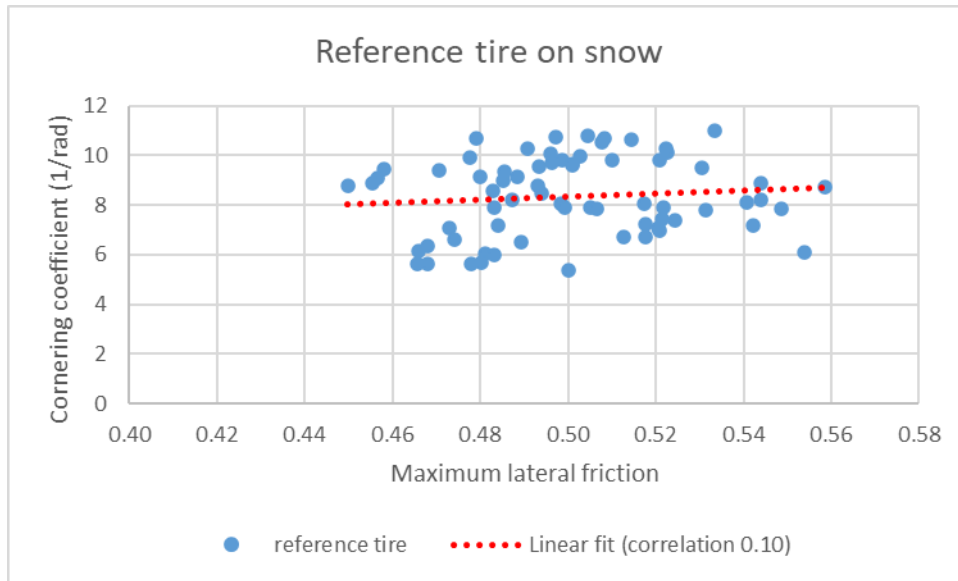
Figure 62. Correlation between peak friction and cornering coefficient on snow for the same tire. Unpublished data from the study published in [30].

A similar investigation for measurements with the 78 different winter tires on snow is shown in Figure 63. Due to the wide spread performance between the different winter tires the peak friction range is larger than for the reference tire, approximately from 0.3 – 0.55. The cornering coefficient (CC) is typically in the same range as for the reference tire, and there is no correlation with peak friction. For wet asphalt, on the other hand, the correlation is quite pronounced where a tire with a high cornering coefficient in general also produces a high peak friction. The same conclusion is made from comparing the performance of different types of winter tires. In Table 15 the average values of the peak friction and CC for each tire type is listed. For new tires an increase of CC on wet asphalt is coincides with an increase of peak friction. On snow there is a difference in peak friction between the tire types, but no difference in CC. When the tire is worn the effective area of the contact patch increases, and the rubber is also generally harder due to aging effects. Both these changes in tire properties leads to increased CC on wet asphalt for worn tires compared to new. No such effect is seen on peak friction, which is essentially unchanged for each tire type. On snow, the increased contact area and harder rubber of the worn tires only leads to a slight increase of CC, while the peak friction on the other hand is reduced for the worn tires compared to new.
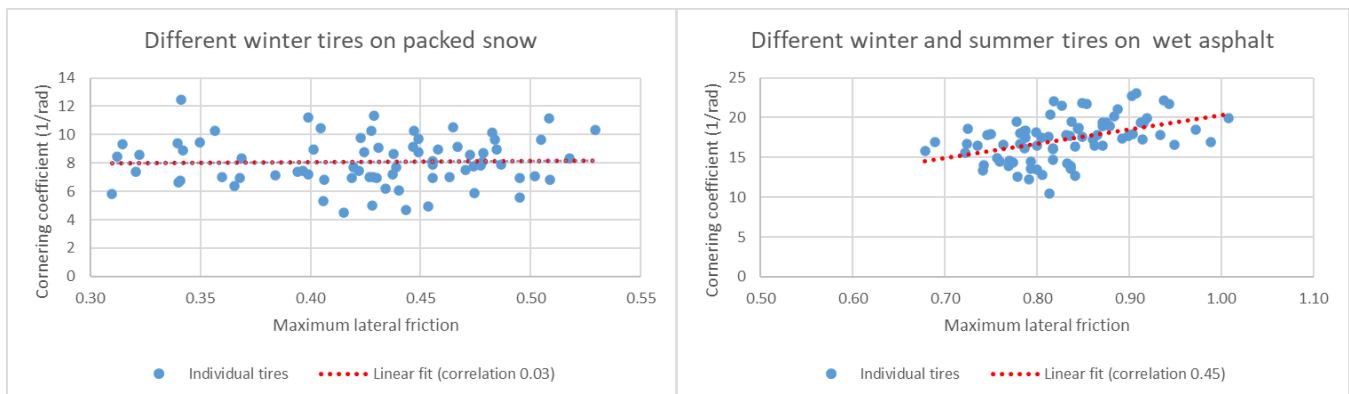

Figure 63 Correlation between peak friction and cornering coefficient for different tires on snow and on wet asphalt. Unpublished data from the study published in [30].

Deliverable No. D3.6
Version 02
Project no. 101069576

Title
Vehicle dynamics modelling methodology

ROADVIEW

Table 15. Cornering coefficient on snow compared to wet asphalt. VTI unpublished data from [30].

Tire type	Number of tires	Wet asphalt		Snow	
		Cornering coefficient	Peak friction	Cornering coefficient	Peak friction
New studded	9	12.9	0.79	7.4	0.47
New Nordic unstudded	9	14.5	0.81	7.6	0.49
New European unstudded	9	16.7	0.87	7.6	0.46
New summer	4	17.6	0.93		
Used studded	18	17.0	0.80	8.3	0.42
Used Nordic unstudded	16	17.5	0.79	8.5	0.43
Used European unstudded	16	20.2	0.87	8.3	0.35
Used summer	4	21.5	0.89		

Thus, it seems like the cornering coefficient on snow is primarily determined by the snow properties. For new tires the CC on snow was 45 – 55% of the CC on wet asphalt. For worn tires the CC on snow was 40 – 45% of the CC on wet asphalt.

It should be stressed that only one tire size, 205/55R16, was used in this study. It is possible that a change of tire dimension, and thus also the contact patch area, would affect the CC. In lack of such data, a simple assumption for packed snow within the peak friction range 0.3 – 0.5 is that CC is 50% of that on asphalt (dry or wet), independent of the peak friction value.

The effect of varying wheel load on longitudinal peak friction has recently been investigated by VTI in a parallel project [31]. Slip curve measurements with the mobile tire test rig on packed snow for a winter tire of central European type did not indicate any significant changes of the peak brake friction for a ± 30% of the wheel load. Hence, assuming no load dependence on peak friction does not seem to be a severe simplification.

Typical lateral slip curves on snow from the 2015 study is shown in Figure 64. As seen, some tires have already reached their peak friction at 15 degrees slip angle, while others have their peak at larger slip angles. Generating slip curves with a similar shape, using the ISO formulation can be achieved from equation 43 with an assumed value of the peak friction slip angle. By letting the peak friction occur at a slip angle of 25 degrees seems to generate curves with a similar shape as the measured data. This is illustrated in Figure 65, for the two different values of the cornering coefficient. The left figure has CC = 10 rad^{-1}, which is similar to the tires measured in the 2015 study. The right figure has CC = 20 rad^{-1}, what we expect for the BMW test vehicle tires on snow, considering that their cornering stiffness on asphalt is around 40 rad^{-1}. The corresponding values ISO tire parameters for load independent model is listed in Table 16, making it easy to implement a lateral snow model for various friction levels of packed snow.

For braking on snow, the same model as for asphalt can be used, which is described by eq. 5. Since a sharp braking will almost immediately trigger the ABS system, the value of the longitudinal slip stiffness in such a model will not have much impact. It is the set peak friction value that will dictate the braking behaviour. Thus, assuming a longitudinal slip stiffness on snow to be 50% of that on asphalt, analogous to the assumption for cornering coefficient, seems reasonable.

The snow parameterization can be used regardless of whether tire is a studded or studless winter tire. The only information needed is the cornering coefficient of the tire and the peak friction level. The latter can be deduced from a brake test with full ABS braking.

Deliverable No. D3.6
Version 02
Project no. 101069576

Title
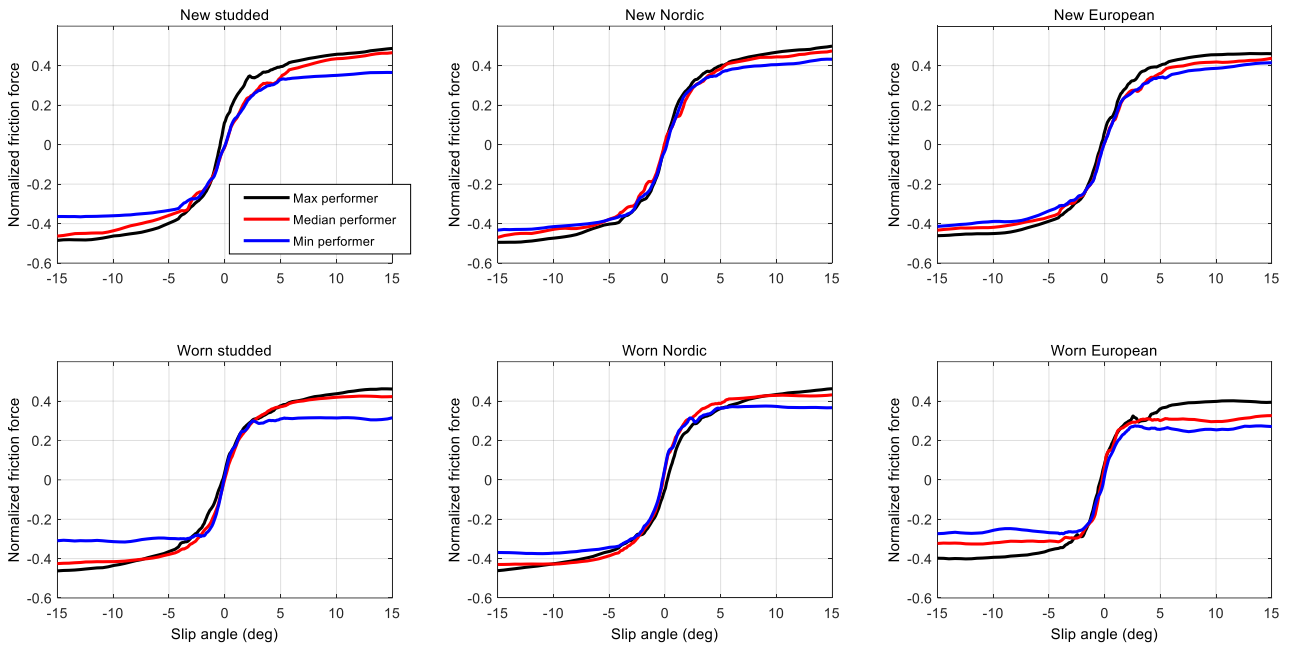Vehicle dynamics modelling methodology

ROADVIEW

Steer tests on snow

Figure 64. Typical lateral slip curves on snow. From [30].
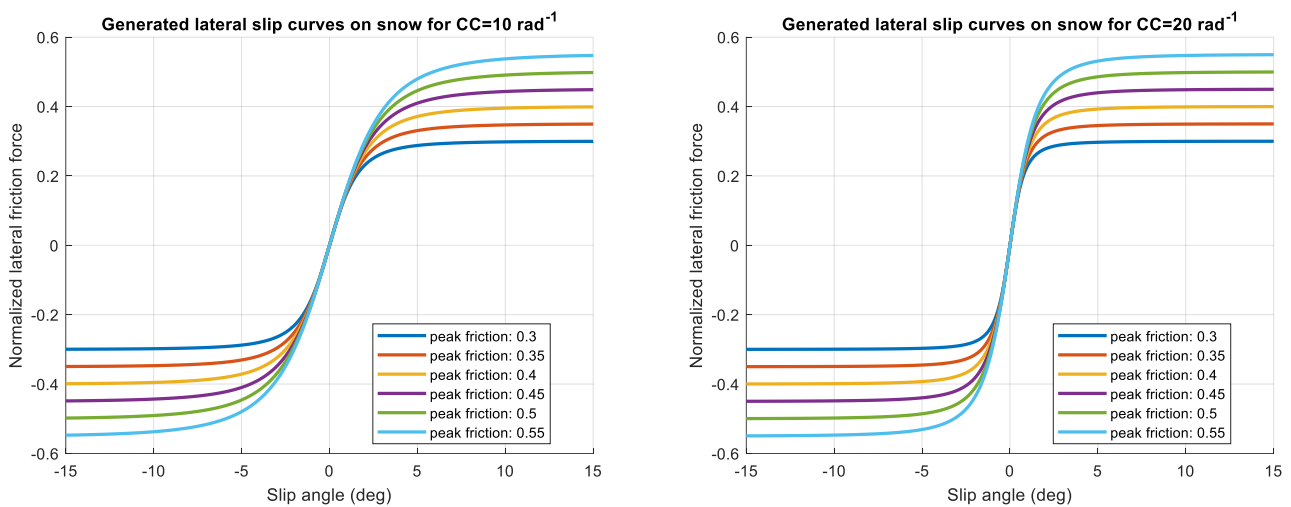
Figure 65. Generated lateral slip curves on snow using the ISO formulation.

Deliverable No. D3.6
Version 02
Project no. 101069576

Title
Vehicle dynamics modelling methodology

ROADVIEW

Table 16. Generated ISO parameters for snow assuming peak friction at 25 degree slip angle

CC (1/rad)	Peak friction	C	μ_{y0}	μ_{yg}	CC_{y0}	CC_{yg}
10	0.30	1.0480	0.30	0	10	0
10	0.35	1.0569	0.35	0	10	0
10	0.40	1.0661	0.40	0	10	0
10	0.45	1.0757	0.45	0	10	0
10	0.50	1.0855	0.50	0	10	0
10	0.55	1.0957	0.55	0	10	0
20	0.30	1.0229	0.30	0	20	0
20	0.35	1.0269	0.35	0	20	0
20	0.40	1.0310	0.40	0	20	0
20	0.45	1.0351	0.45	0	20	0
20	0.50	1.0394	0.50	0	20	0
20	0.55	1.0436	0.55	0	20	0

6.3.2 Ice:

Compared to snow, the relative friction range on ice is much larger. Typically, the peak friction with a studless winter tire varies between 0.05 (wet ice) to 0.35 (cold, rough ice). Thus, the braking distance on wet ice may be 7 times longer than on rough ice. The slipperiness of an ice surface can also vary quite rapidly due to weather changes, sunny or cloudy sky etc, which makes outdoor measurements for tire model parameterization difficult. The difference in ice grip can be very large between different tires, also for tires without studs. VTI recently carried out a study on the performance of all-season tires in comparison with traditional studless winter tires and performed braking tests on Nokian's tent covered ice track in Ivalo, northern Finland. 21 different tires, out of which 14 were all-season tires was tested. Compared to the reference Nordic winter tire, the worst performing all-season tires hade 50% longer braking distance on ice. The worst central European winter tire had 45% longer braking distance than the reference tire [x].

In the 2015 VTI study all 78 winter tires were measured in VTI's tire test rig on smooth ice at four separate occasions. The Nordic reference tire was measured repeatedly in-between. The ice temperature was -3 °C, and the peak friction for the reference tire was within 0.16 – 0.23, which indicates rather high ice friction.

Tire slip curves on ice has two main characteristics that separate them from snow or asphalt:

- The peak friction occurs at very small slip angles.
- The friction at large slip angles drops significantly compared to the peak for studless tires.

The general behaviour is also very different between studded and studless winter tires, and even so between the two studless types of winter tires – the Nordic and the European ones.

Unpublished data from the 2015 study was investigated in the Roadview project in the purpose of providing general tire model parameterizations on ice at different friction levels. First, we study the peak position, i.e. the slip angle where peak friction occurs, for different ice friction levels, and also different tires. The peak position is plotted versus the peak friction for measurements with the reference tire at different levels of ice friction in Figure 66. There is

Deliverable No. D3.6
Version 02
Project no. 101069576

Title
Vehicle dynamics modelling methodology

ROADVIEW

essentially no correlation at all between the peak friction value and peak position, which on average occurs at 3.5 degrees.

Figure 66. Peak position versus peak friction value for the reference tire on ice. Unpublished data from the study published in [30].

The peak position versus peak friction for different tires are shown in Figure 67. Separate plots were made for the different tire types, and data for new and worn tires has been separated in the plots. The studded tires stand out, where the peak position occurs at higher slip angles for tires with better grip. For studless tires in general (Nordic and European combined) the correlation is much weaker, and a model with a constant peak position would be adequate. For most of the tires the peak position is within 2 – 4 degrees, and on average around 3 degrees.

Measurements on smooth ice
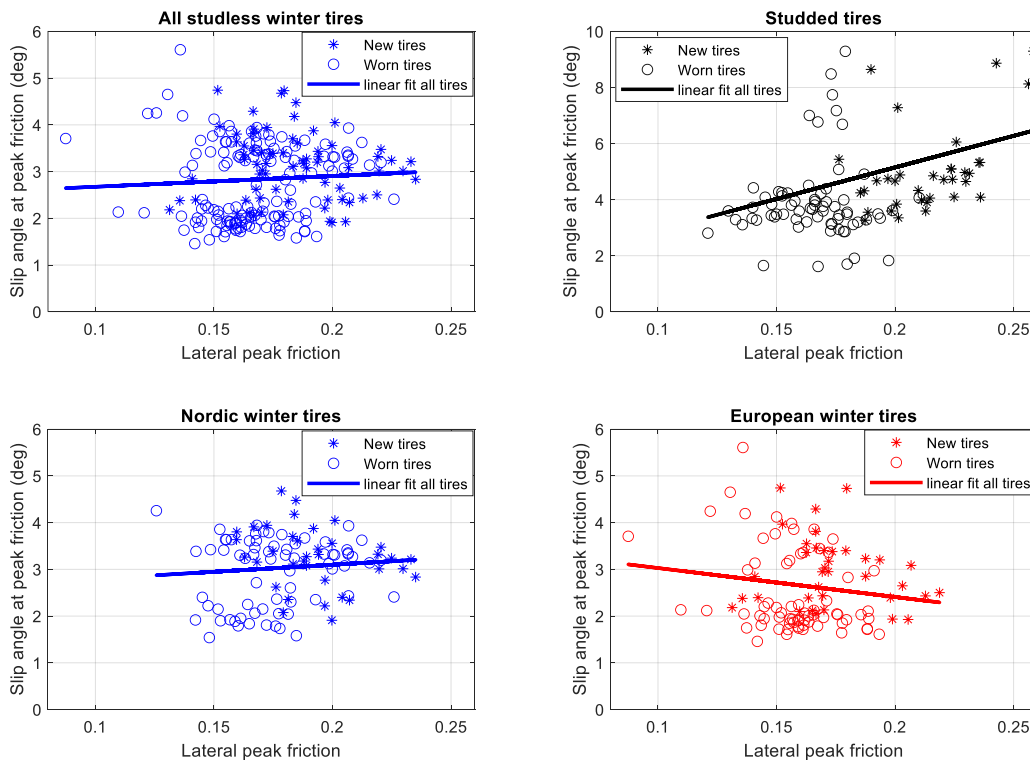
Figure 67 Peak position versus peak friction value for different types of winter tires on ice. Unpublished data from the study published in [30]

Deliverable No. D3.6
Version 02
Project no. 101069576

Title
Vehicle dynamics modelling methodology

ROADVIEW

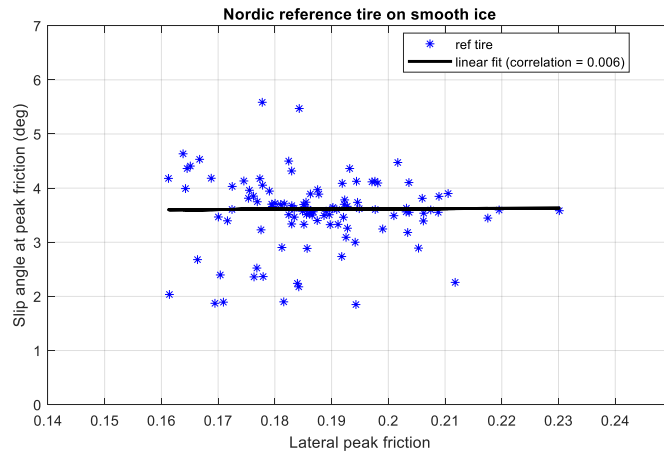**Figure 68. Friction ratio at 15 deg and peak versus peak friction value for the reference tire on ice. Unpublished data from the study published in [30].**

A similar investigation was carried out with respect to the friction drop at large slip angles. As a measure of the friction drop, the ratio between the friction at 15 deg slip angle and the peak friction value was used. The friction ratio is plotted versus the peak friction for measurements with the reference tire at different levels of ice friction in Figure 68. There is a clear correlation where the ratio becomes smaller when the ice friction increases. From the linear fit the ratio is 0.96 – 1.12*(peak friction).
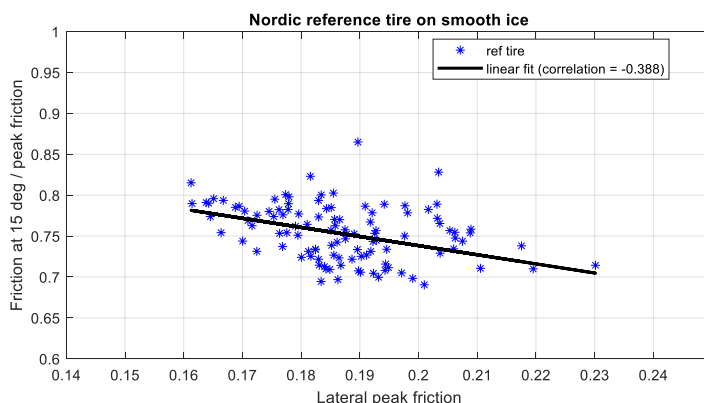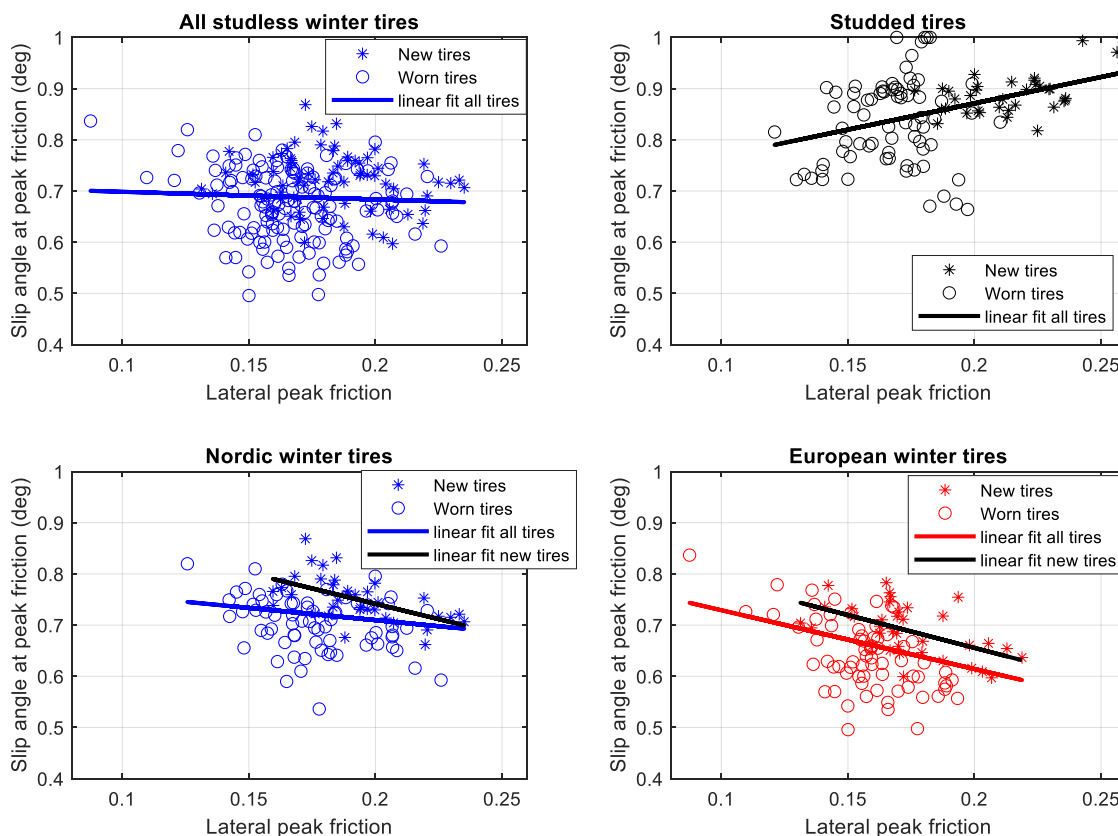
Measurements on smooth ice

Figure 69 Friction ratio at 15 degrees and peak versus peak friction value all tires on ice. Unpublished data from the study published in [30].

Deliverable No. D3.6
Version 02
Project no. 101069576

Title
Vehicle dynamics modelling methodology

ROADVIEW

The friction ratio for different tires are shown in Figure 69. It is clear that worn tires in general suffers from a larger friction drop at large slip angles compared to new tires. The line fits on the new Nordic and European winter tires indicates a similar correlation as for the reference tire.

Thus a generalized parameterization for a new studless winter tire on ice could be made assuming a constant peak position of 3 degrees, coupled with a friction drop at 15 degrees slip angle described by the linear fit from the reference tire. The measurements on ice did not allow for an accurate determination of the cornering coefficient, but a recent study on truck tires indicate that cornering coefficient on ice is essentially the same as on asphalt [16].

For a given cornering coefficient and peak value, the ISO model is not able to model a fix peak position with a specific friction drop off. The additional E-parameter of the MF formulation is needed for this, which makes MF the preferred model to use for ice. But even the MF has limitations with regards to the shape of the slip curve that can be modelled. A very large cornering coefficient combined with a low peak friction value, will lead to peak position values that are extremely small. The E-parameter is able to shift the peak position to higher values, but excessive use of this parameter will lead to weird curve shapes with very flat peaks. This is illustrated in Figure 70, where MF slip curves with different cornering coefficent were created with fixed values of the peak friction (0.25), peak position (3 degrees), and friction ratio at 15 degrees (0.68). The curve shapes can be compared to those from measurements in Figure 71.
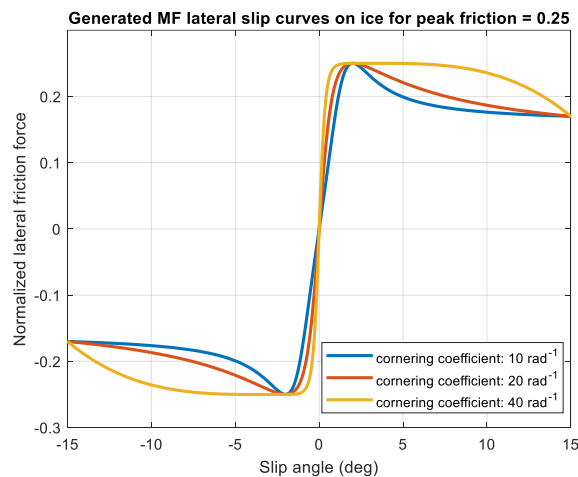

Figure 70. Generated MF slip curves on ice with different cornering coefficient

For lower values of the peak friction the flatness affects also the lower values of cornering coefficient. Thus, there is a practical limit on how high CC values that can be used for tire parameterization on ice. The cornering coefficient value has a large practical implication for the handling properties of a vehicle during steering on asphalt. This is because the linear region is quite large on high friction, so the CC dictates the steering response during normal steer inputs at speeds above parking speeds. For ice however, the linear region of the slip curve is much smaller compared to asphalt, and from a practical point of view the actual value of the cornering coefficient becomes less important. A "practical" cornering coefficient defined as the inclination within a specified slip angle interval, say ± 0.5 degrees, rather than in the very small linear region, would be a more useful characteristic on ice. It would be smaller than the real cornering coefficient, but would therefore also be better for MF tire parameterization on ice.

A MF parameterization for the lateral slip curves on ice were generated using for two different values of the cornering coefficient, 10 and 15 rad^{-1}. The peak position was set at a slip angle of 3 degrees, and the friction ratio at 15 degrees was set according to the linear model: 0.96 – 1.12*(peak friction). The slip curves are shown in Figure 72, and the parameter values are listed in Table 17. Apart from peak friction values 0.15 and 0.20 coupled with a CC of 15 rad^{-1}, which suffer from the flatness problem, the generated parameterization should be useful for vehicle dynamics simulations on ice with a studless winter tire.

For the longitudinal slip, the same model as for asphalt can be used, which is described by eq. 5. Since a sharp braking will almost immediately trigger the ABS system, the value of the longitudinal slip stiffness in such a model will not have much impact. It is the set peak friction value that will dictate the braking behaviour.

Deliverable No. D3.6
Version 02
Project no. 101069576

Title
Vehicle dynamics modelling methodology

ROADVIEW
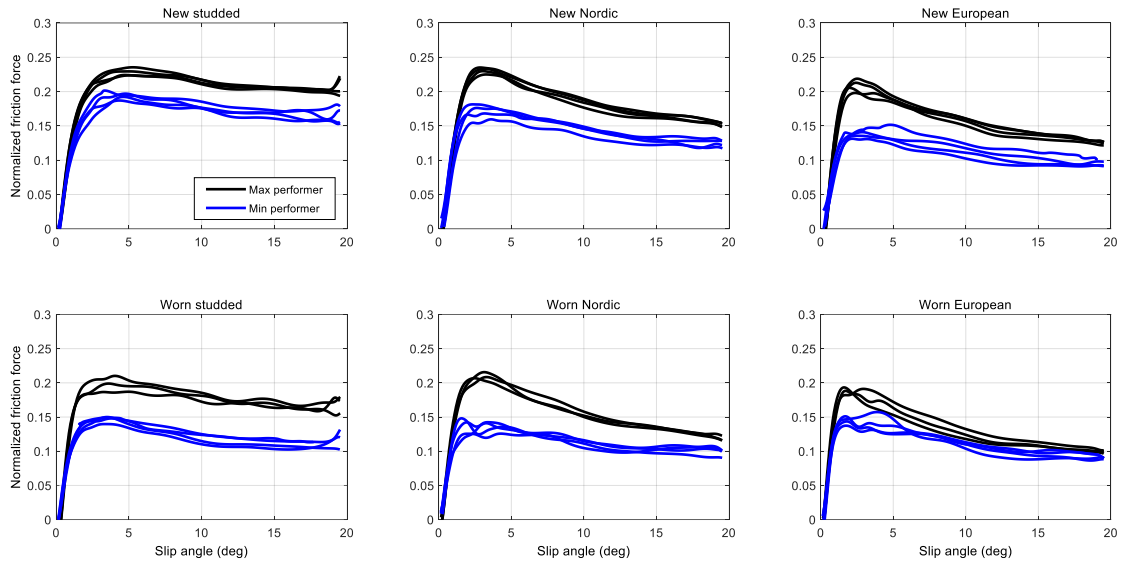
Figure 71 Typical lateral slip curves on ice. From [30]. Four separate measurements with the best and the worst performing tire of each tire type.
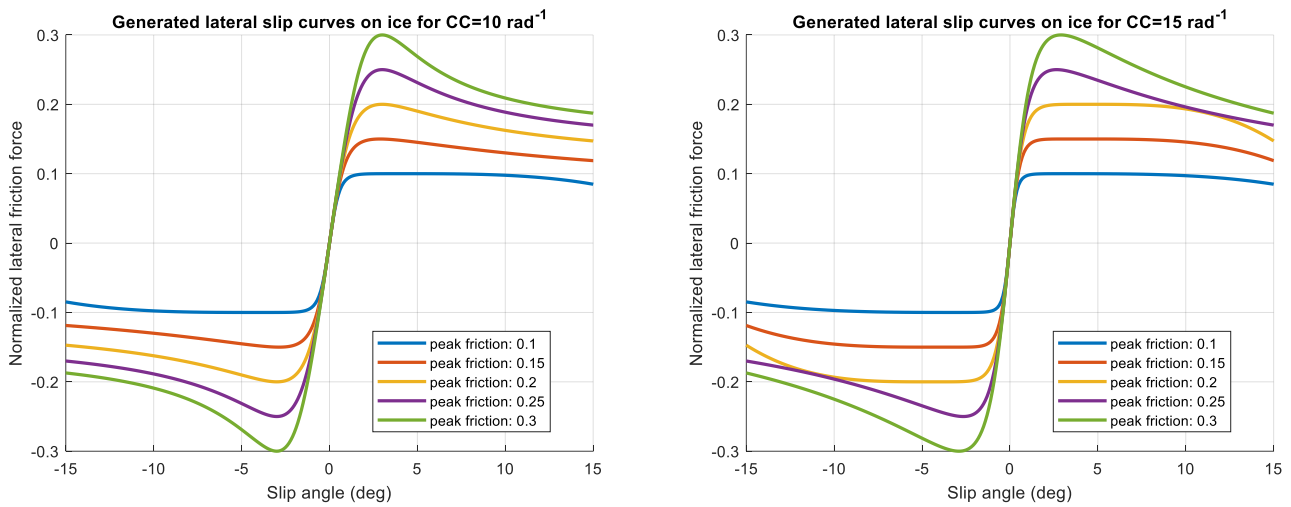
Figure 72. Lateral slip curves on ice generated using the MF formulation for two different values of the cornering coefficient, 10 and 15 rad^{-1}.

Deliverable No. D3.6
Version 02
Project no. 101069576

Title
Vehicle dynamics modelling methodology

ROADVIEW

Table 17. Generated MF parameters for ice assuming peak friction at 3 degree slip angle and friction ratio at 15 deg according to 0.96 – 1.12*(peak friction).

CC (1/rad)	Peak friction	B	C	μ_y	E
10	0.10	54.21	1.84	0.10	1.07
10	0.15	39.30	1.70	0.15	0.74
10	0.20	30.31	1.65	0.20	0.31
10	0.25	24.20	1.65	0.25	-0.37
10	0.30	19.93	1.67	0.30	-1.37
10	0.10	84.90	1.77	0.10	1.04
15	0.15	53.15	1.88	0.15	1.08
15	0.20	38.38	1.95	0.20	1.12
15	0.25	32.69	1.84	0.25	0.69
15	0.30	26.13	1.91	0.30	0.62
15	0.10	54.21	1.84	0.10	1.07
15	0.15	39.30	1.70	0.15	0.74

Parameters for tire data parameterization of heavy vehicle tires are listed in Appendix C.

Deliverable No. D3.6
Version 02
Project no. 101069576

Title
Vehicle dynamics modelling methodology

ROADVIEW

7 Conclusions

The use of virtual testing is quickly gaining space in the automotive branch due to the complexity of the automated driving system under development. Due to that, comprehensive models of the vehicle dynamics need to be provided to support the virtual testing of decision-making and control systems. Despite that the use of vehicle dynamics models is already well known, the definition of the parameter is still a task that involves expensive and time intensive testing in different test benches that are not accessible to all small companies and test centres. The estimation of the parameters from dynamic manoeuvres is a possibility to overcome these limitations.

On this scene, this work proposes a methodology for the parameter estimation applied for vehicle dynamics models on different weather conditions. The development conducted in the project includes the definition of the methodology for the parameter estimation, the implementation and verification of a vehicle dynamics model, the data gathering and the optimisation of the parameters. The implementation is evaluated using the test vehicle from CARISSMA Institute of Automated Driving and the data will be made available together with the vehicle dynamics model.

The obtained results show the applicability of the proposed methodology reaching adequate results relative to the behaviour of the vehicle in relation to the real data gathered from the test vehicle. However, good initial values and coherent boundaries need to be given to the optimization method to obtain coherent results. Since there is a strong correlation between the modules future work should investigate the optimisation of the whole integrated model splitting the optimisation in different conditions such as acceleration, braking and steering in order to separately obtain the desired parameters.

For further tests it is indicated to include different manoeuvres, including highway driving at higher speed to enable the proper estimation of the transmission parameters. Furthermore, tests on snowy and icy grounds shall be conducted to validate the application of this method for any kind of weather conditions, using the derived general tire models for snow and ice. In order to improve the optimisation method a implementation focused on vehicle dynamics can be integrated, which also takes the correlation between the input parameters and the affected variables into account.

The next steps of this work in the ROADVIEW project include the integration of the vehicle dynamics model in the XiL test system from WP7, including the controllers, a simplified traction control system as well as ABS and improvements on the steering modelling. Furthermore, together with WP6 the controls can be tested and other test vehicles from the ROADVIEW project can be modelled to support the testing of the decision-making and control algorithms.

Deliverable No. D3.6
Version 02
Project no. 101069576

Title
Vehicle dynamics modelling methodology

ROADVIEW

8 Dissemination of Resource

8.1 Vehicle dynamics model

The scripts with the implemented vehicle dynamics model as wells as a configuration file with the data of the test vehicle from THI has been made available to the public. The scripts include the core modules implemented in this project (Powertrain, wheels, and body), the required auxiliar scripts, a main code and a yaml file containing the parameters of the vehicle. The scripts and an installation guide can be found in GitHub. The integration of the modules in one common code which can be used to run the complete vehicle model will be finish in WP7 and made available in the same repository.

8.2 Data collection video

A video demonstrating the cada collection process conducted with the test vehicle from the CARISSMA Institute of Automated Driving (THI) on the Outdoor test track is available on Youtube.

Deliverable No. D3.6
Version 02
Project no. 101069576

Title
Vehicle dynamics modelling methodology

ROADVIEW

References

[1] ACEA - European Automobile Manufacturers' Association, "Report - Vehicles in Use, Europe 2023.," ACEA, 17 January 2023. [Online]. Available: www.acea.auto/publication/report-vehicles-in-use-europe-2023/. [Accessed 10 January 2024].

[2] R. Rajamani, Vehicle dynamics and control, Springer Science & Business Media, 2011.

[3] T. D. Gillespie, Fundamentals of Vehicle Dynamics, Warrendale: SAE International, 1992.

[4] S. Yang, Y. Lu and S. Li, "An overview on vehicle dynamics," International Journal of Dynamics and Control, vol. 1, no. 1, pp. 385-395, 2013.

[5] R. N. Jazar, Vehicle dynamics. Vol. 1, New York: Springer, 2008.

[6] D. Schramm, M. Hiller and R. Bardini, Vehicle Dynamics: Modeling and Simulation, Berlin: Springer Nature, 2017.

[7] M. Abe, Vehicle handling dynamics: theory and application, Butterworth-Heinemann, 2015.

[8] J. Katz, Automotive Aerodynamics, John Wiley & Sons, 2016.

[9] M. Heisler, Advanced Vehicle Technology, Butterworth-Heinemann, 2002.

[10] Y. G. A. E. Mehrdad Ehsani, Modern Electric, Hybrid Electric, and Fuel Cell Vehicles: Fundamentals, Theory, and Design, CRC Press, 2010.

[11] D. L. M. William F. Milliken, Race Car Vehicle Dynamics, SAE International, 1995.

[12] J. Y. Wong, Theory of Ground Vehicles, John Wiley & Sons, 2022.

[13] J. C. Dixon, The Shock Absorber Handbook, John Wiley & Sons, 2007.

[14] H. Pacejka, "Tire and Vehicle Dynamics," Elsevier, Oxford, 2021.

[15] H. W. Manfred Mitschke, Dynamik der Kraftfahrzeuge, Springer Vieweg Wiesbaden, 2015.

[16] TNO, "MF- Tire user manual version 5.0," TNO, 1996.

[17] S. Kharrazi and M. Hjort, "Performance Based Standards, Project II - Generic tire models for a PBS scheme, VTI report , to be published in 2024," VTI.

[18] M. Blundell and H. Damian, The Multibody Systems Approach to Vehicle Dynamics, 2015.

[19] International Organization for Standardization, "ISO 8855:2011 Road vehicles: Vehicle dynamics and road-holding ability," ISO, 2011.

[20] Y. Zhang and C. Mi, Automotive Power Transmission Systems, Hoboken: John Wiley and Sons, 2018.

[21] M. Hjort, S. Kharrazi, O. Eriksson and M. Hjälmdahl, "Limit handling in a driving simulator," VTI, Linköping, 2015.

[22] IPG Automotive GmbH, CarMaker, Karlsruhe, 2023.

[23] L. da Costa Machado Leal, E. da Rosa and L. C. Nicolazzi, Uma introdução à modelagem quase-estática de automóveis, Florianópolis: GRANTE - UFSC, 2012.

Deliverable No. D3.6
Version 02
Project no. 101069576

Title
Vehicle dynamics modelling methodology

ROADVIEW

[24] R. Isermann, Automotive Control, Darmstadt: Springer-Verlag GmbH, 2022.

[25] International Organization for Standardization 4138, "Passenger cars Steady-state circular driving behaviour: Open-loop test methods," ISO, 2021.

[26] International Organization for Standardization, "Road vehicles Lateral transient response test methods: Open-loop test methods 7401," ISO, 2011.

[27] I. O. f. Standardization, "Passenger cars Braking in a turn Open-loop test method 7975," ISO, 2019.

[28] International Organization for Standardization, "Passenger cars — Test track for a severe lane-change manoeuvre — Part 2: Obstacle avoidance 3888," ISO, 2011.

[29] R. H. Byrd, L. P and N. J., "A Limited Memory Algorithm for Bound Constrained Optimization," SIAM Journal on Scientific and Statistical Computing 16 (5), pp. 1190-1208, 1995.

[30] C. Zhu, B. R H and N. J, " L-BFGS-B: Algorithm 778: L-BFGS-B, FORTRAN routines for large scale bound constrained optimization," ACM Transactions on Mathematical Software 23 (4, pp. 550-560, 1997.

[31] R. Storn and K. Price, "Differential Evolution - a Simple and Efficient Heuristic for Global Optimization over Continuous Spaces," Journal of Global Optimization, vol. 11, pp. 341-359, 1997.

[32] F. Gerber and R. Furrer, "An R package providing a parallel version of the L-BFGS-B optimization method," The R Journal, pp. 352-358, 2019.

[33] BMW AG, "Technische Daten. BMW M8 Coupé. M8 Competition.," BMW Medien Information, Munich, 2021.

[34] Automobile catalog, "2022 BMW M8 Competition Coupe (aut. 8) engine Horsepower / Torque Curve," [Online]. Available: https://www.automobile-catalog.com/curve/2022/2978510/bmw_m8_coupe_competition.html#gsc.tab=0. [Accessed 22 January 2024].

[35] M. Hjort, O. Eriksson and F. Bruzelius, "Comprehensive Study of the Performance of Winter tires on Ice, Snow and Asphalt Roads: The influence of Tire Type and Wear," Tire Science and Technology, TSTCA, vol. 45, no. 3, pp. 175-199, 2017.

[36] M. Hjort, K. S., F. Bruzelius and D. Yang, "Tyre-road friction correlation to enable autonomous driving at all weather and road conditions.," VTI (in preparation), 2024.

[37] M. Guiggiani, The Science of Vehicle Dynamics, Springer Cham, 2023.

Deliverable No. D3.6
Version 02
Project no. 101069576

Title
Vehicle dynamics modelling methodology

ROADVIEW

Appendix A. CM export Variable List

Table 18. Data exported from IPG CarMaker

Variable Name	Description
brake_pedal	Brake Pedal Position
Brake_trq	Brake Torque Position
clutch	Clutch Pedal Position
engine_rotv	Engine Angular Rotation
gas_pedal	Gas Pedal Position
gear_no	Gear Number
steer_ang	Steering Wheel Angle
Vhcl_Distance	Distance
Vhcl_Pitch	Pitch Angle
Vhcl_PitchAcc	Pitch Acceleration
Vhcl_PitchVel	Pitch Velocity
Vhcl_PoI_Acc_1_x	Vehicle Point of Interest 1 Acceleration in X
Vhcl_PoI_Acc_1_y	Vehicle Point of Interest 1 Acceleration in Y
Vhcl_PoI_Acc_1_z	Vehicle Point of Interest 1 Acceleration in Z
Vhcl_PoI_Acc_x	Vehicle Point of Interest Acceleration in X
Vhcl_PoI_Acc_y	Vehicle Point of Interest Acceleration in Y
Vhcl_PoI_Acc_z	Vehicle Point of Interest Acceleration in Z
Vhcl_PoI_Pos_x	Vehicle Point of interest position in X coordinates
Vhcl_PoI_Pos_y	Vehicle Point of interest position in Y coordinates
Vhcl_PoI_Pos_z	Vehicle Point of interest position in Z coordinates
Vhcl_PoI_Vel_1_x	Vehicle Point of Interest 1 Velocity in X
Vhcl_PoI_Vel_1_y	Vehicle Point of Interest 1 Velocity in Y
Vhcl_PoI_Vel_1_z	Vehicle Point of Interest 1 Velocity in Z
Vhcl_PoI_Vel_x	Vehicle Point of Interest Velocity in X
Vhcl_PoI_Vel_y	Vehicle Point of Interest Velocity in Y
Vhcl_PoI_Vel_z	Vehicle Point of Interest Velocity in Z

Deliverable No. D3.6
Version 02
Project no. 101069576

Title
Vehicle dynamics modelling methodology

ROADVIEW

Variable Name	Description
Vhcl_Roll	Vehicle Roll
Vhcl_RollAcc	Vehicle Roll Acceleration
Vhcl_RollVel	Vehicle Roll Velocity
Vhcl_v	Vehicle Velocity
Vhcl_Wheel_FL_Fx	Vehicle Front Left Wheel Forces X
Vhcl_Wheel_FL_LongSlip	Vehicle Front Left Wheel Longitudinal Slip
Vhcl_Wheel_FL_Sidelip	Vehicle Front Left Wheel Lateral Slip
Vhcl_Wheel_FR_Fx	Vehicle Front Right Wheel Forces X
Vhcl_Wheel_FR_LongSlip	Vehicle Front Right Wheel Longitudinal Slip
Vhcl_Wheel_FR_Sidelip	Vehicle Front Right Wheel Lateral Slip
Vhcl_Wheel_RL_Fx	Vehicle Rear Left Wheel Forces X
Vhcl_Wheel_RL_LongSlip	Vehicle Rear Left Wheel Longitudinal Slip
Vhcl_Wheel_RL_Sidelip	Vehicle Rear Left Wheel Lateral Slip
Vhcl_Wheel_RR_Fx	Vehicle Rear Right Wheel Forces X
Vhcl_Wheel_RR_LongSlip	Vehicle Rear Right Wheel Longitudinal Slip
Vhcl_Wheel_RR_Sidelip	Vehicle Rear Right Wheel Lateral Slip
Vhcl_Yaw	Vehicle Yaw
Vhcl_YawAcc	Vehicle Yaw Acceleration
Vhcl_YawVel	Vehicle Yaw Velocity
wheel_load_x_FR	Vehicle Wheel Load X
wheel_load_y_FR	Vehicle Wheel Load Y
wheel_load_z_FR	Vehicle Wheel Load Z
Wheel_trq	Vehicle Wheel Torque Position

Deliverable No. D3.6
Version 02
Project no. 101069576

Title
Vehicle dynamics modelling methodology

ROADVIEW

Appendix B. Test vehicle measured data

Table 19. Data collected from the test vehicle.

Marwis - road weather information sensor [1 Hz]	Road and environment Temperature [°C]
	Relative Humidity [%]
	Water film height [µm]
	Snow height [µm]
	Friction [%]
	Ice [%]
Vehicle CAN-Bus [100 Hz]	Wheel speed [rad/s]
	Engine Rotation [RPM]
	Longitudinal Acceleration [m/s²]
	Lateral Acceleration [m/s²]
	Velocity [km/h]
	Brake Torque [Nm]
	Steering wheel angle [°]
	Front wheels angle [°]
	Brake pedal position [%]
	Gas pedal position [%]
	Gear [-]
	Torque on the wheels [Nm]
Genesys GNSS and IMU sensor [100 Hz]	Position relative to the test centre coordinate system [m]
	Velocity [m/s]
	Acceleration [m/s²]
	Yaw rate [rad/s]
	Pitch rate [rad/s]
	Roll rate [rad/s]
	Orientation [rad]

Deliverable No. D3.6
Version 02
Project no. 101069576

Title
Vehicle dynamics modelling methodology

ROADVIEW

Appendix C. Tire parameters for heavy vehicles

Tire parameter values for heavy vehicle tires of different types has been developed within working group 6 of the ISO TC 22 / SC 33 and is currently being prepared for becoming and ISO standard. The standard is denoted "Heavy commercial vehicles and buses — Vehicle dynamics simulation and validation — Tire model for lateral estimation of heavy vehicle combinations operated at dry paved road surface". The model is the ISO model described by eq. 38 – 47, together with the MF transient model described by eq. 19 – 20.

If tire data is not available, the standard values in Table 20 can be used to represent a new (not worn) generic tire on dry asphalt. Tire parameters are provided for three tire dimensions, as well as for an all-purpose tire. The latter can be used for tires with other dimensions. The parameters have been derived from tire measurements on multiple truck tires, and the process is described in detail in [16].

Table 20. Standard values for Tire parameters in case tire measurement data is not available.

	Single mounted steer/trailer tire[a]	Twin mounted drive tire[b]	Twin mounted trailer tire[c]	All-purpose tire
Nominal normal force (kN)	45	35,5	27,25	Use rated load
Nominal cornering coefficient (1/rad)	7,60	6,69	6,65	7,0
Cornering coefficient gradient (-)	-0,19	-0,33	-0,12	-0,2
Nominal peak lateral friction (-)	0,84	0,77	0,78	0,8
Peak lateral friction gradient (-)	-0,15	-0.12	-0,30	-0,15
Shape factor (-)	1,41	1,31	1,42	1,4
Nominal lateral relaxation length (m)	0,59	0,52	0,50	0,55
Lateral relaxation length gradient (-)	0,87	0,67	0,91	0,8

[a] Parameters were deduced from measurements on 385/65R22,5 tires.

[b] Parameters were deduced from measurements on 315/70R22,5 tires and should be applied to each individual tire.

[c] Parameters were deduced from measurements on 265/70R19,5 tires and should be applied to each individual tire.

NOTE   Parameters were deduced for specific dimensions as indicated by the footnotes but can also be used for similar dimensions.

Typical ranges of nominal cornering coefficient and nominal lateral relaxation length for both new and worn tires are listed in Table 21. Note that these two parameters are interconnected and cannot be tuned individually; a stiff tire usually has a longer relaxation length. As a rule of thumb, increasing cornering coefficient by one unit, results in an 0,05 m increase in the relaxation length.

Table 21. Typical ranges of cornering coefficient and relaxation length.

	New tires	Worn tires
Nominal cornering coefficient (1/rad)	6,0-10,0	10,0-16,0
Nominal lateral relaxation length (m)	0,5-0,7	0,7-1,0